Fermilab Library
0 1160 0052509 1

SDC-90-00095

SDC
SOLENOIDAL DETECTOR NOTES

REPORT OF THE SOLENOIDAL DETECTOR COLLABORATION
MAGNET TASK FORCE

October 12, 1990

SDC-90-00095

REPORT

of the

Solenoidal Detector Collaboration

Magnet Task Force

October 12, 1990

TABLE OF CONTENTS

	Page
Recommendations	2
Introduction	6
1.1 Task Force Appointment and Charge	
1.2 Composition and Methodology	
1.3 Physics Performance Implications	
1.4 Partons and Detector Systems	
Technical Considerations	12
2.1 Magnet Design Considerations	
2.2 Magnet-Related Calorimetry Considerations	
2.3 Magnet-Related Tracking Considerations	
2.4 Magnet-Related Trigger Considerations	
2.5 Magnet-Related Muon System Considerations	
Cost Considerations	70
3.1 General Remarks	
3.2 Magnet Coil and Cryogenic Support System	
3.3 Calorimeter Costs	
3.4 Other Detector Subsystems	

Appendix A - Task Force Membership

Appendix B - Charge to the Magnet Task Force

Appendix C - Technical Comparisons of Three Design Options for the SDC Solenoid

Appendix D - Ray Tracing Study for Magnet Style Selection

Appendix E - Momentum Resolution for Muons Using the Full Tracking System of SDC

RECOMMENDATIONS

The SDC Magnet Task Force has reached agreement on the following recommendations, which it submits to the SDC Technical Board, the SDC Executive Board and to the SDC membership:

1. We recommend that the Type-S and Type-I coil options be combined in a unified coil design concept (Type-U) and that the resulting Type-U design be the focus of future engineering design and magnet R&D activities.

2. We recommend that the Type-L coil option with the coil extending to a solid iron return yoke be dropped from further consideration.

Our reasoning in brief is given below. First, we note that technical magnet design now indicates that a single, unified coil design could function successfully in both the Type-S and Type-I magnetic configurations. Both magnetic geometries result in calorimeter systems of closely similar size, geometry and absorber thickness. The two options are also estimated to have nearly equal construction costs. Furthermore,we note that the two options, S and I, are virtually interchangeable for most of the SDC detector components except for the endcap calorimeter modules whose design and composition are totally involved with the specific coil options.

Figure 1.1 shows two configurations for the scintillator plate calorimeter approach that illustrate this point. In this figure we see that the geometry is nearly identical for either version. A similar argument cannot be made for the liquid calorimetry option (for which only a coil of Type-S is relevant), or for calorimetry based on ferromagnetic iron (which is demanded by the Type-I option). The concept of pursuing a unified coil design means that most of the rest of the SDC detector design could proceed independently of the coil-type decision. In addition, this recommendation allows time to resolve with appropriate R&D, the open technical questions. These are: compensation and resolution performance of iron-based calorimetry; technical feasibility of a Type-S coil; and performance of tracking and triggering in a non-uniform field. We now elaborate a bit on the specific areas of concern.

The major open technical question associated with the Type-S coil is as follows: The Type-S coil is subject to strong electromagnetic compressive forces in the coil turns. These forces are absent (or much reduced) in the L or I options as noted in Section 2.1 of this report. The method currently assumed for bonding the coil to the bobbin uses epoxy resin, mechanically interlocking shapes or both. Significant R&D must be carried out to demonstrate specific designs. It is estimated that it will take up to two years to resolve this and other design issues.

Two other detector systems (in addition to the coil itself) are closely involved with the S/I choice, namely the central and intermediate tracking systems and the calorimetry. The tracking considerations relevant to the coil choices are discussed in detail in Section 2.3. The calorimetry issues are detailed in Section 2.2.

In summary, from the viewpoint of charged particle tracking, the uniform field of the Type-I magnet is ideal. In the Type-S magnet, the momentum resolution above eta = 1.5 deteriorates by about 20 - 30% relative to Type-I. This will have an effect on the forward muon momentum resolution and on the ability to distinguish the electric charge sign for electrons above 1 TeV. The charged particle tracking, pattern recognition and track fitting will also be somewhat more difficult in the Type-S design. Furthermore, the wire-chamber triggering in the central and intermediate regions will be somewhat more sensitive to the non-uniform Type-S field than other tracking devices.

The situation with calorimetry is more involved as the calorimetry technology is intimately connected to the magnet style. Under the assumption that a single technology is used for both barrel and endcap calorimeters, only warm liquid and tile/fibre technologies are practically compatible with a Type-L coil, while Types S and I can be compatible with any of the calorimeter technologies.

A ray-tracing study indicates that the calorimeter system is more hermetic with the Types S and I options relative to the Type-L, whatever the chosen calorimeter technology. For the case of the Type-I coil design, ferromagnetic iron must be used as the passive absorber in the hadron calorimeter, a choice that may limit the level of e/h compensation that can be achieved. This question is currently under study and will be resolved during the next year.

The performance compromises associated with unifying the Type-S and Type-I coil options are twofold. First, a Type-U coil design employed in a Type-I geometry is approximately 10% thicker than would otherwise be needed. Second, a Type-U coil employed in a Type-S geometry may contain overdesigned coil-end supports. We note that the additional thickness of the Type-U carries with it the benefit of allowing a full-field excitation test prior to installation in the detector.

Pulling all these considerations together, we feel that the best overall strategy for the SDC at this point in time is to adopt the Type-U coil design approach, pursue vigorous engineering design and R&D to resolve the remaining technical issues in the coil and calorimetry areas and thereby refrain from limiting calorimetry and tracking options before full answers to the coil dependent questions have been obtained.

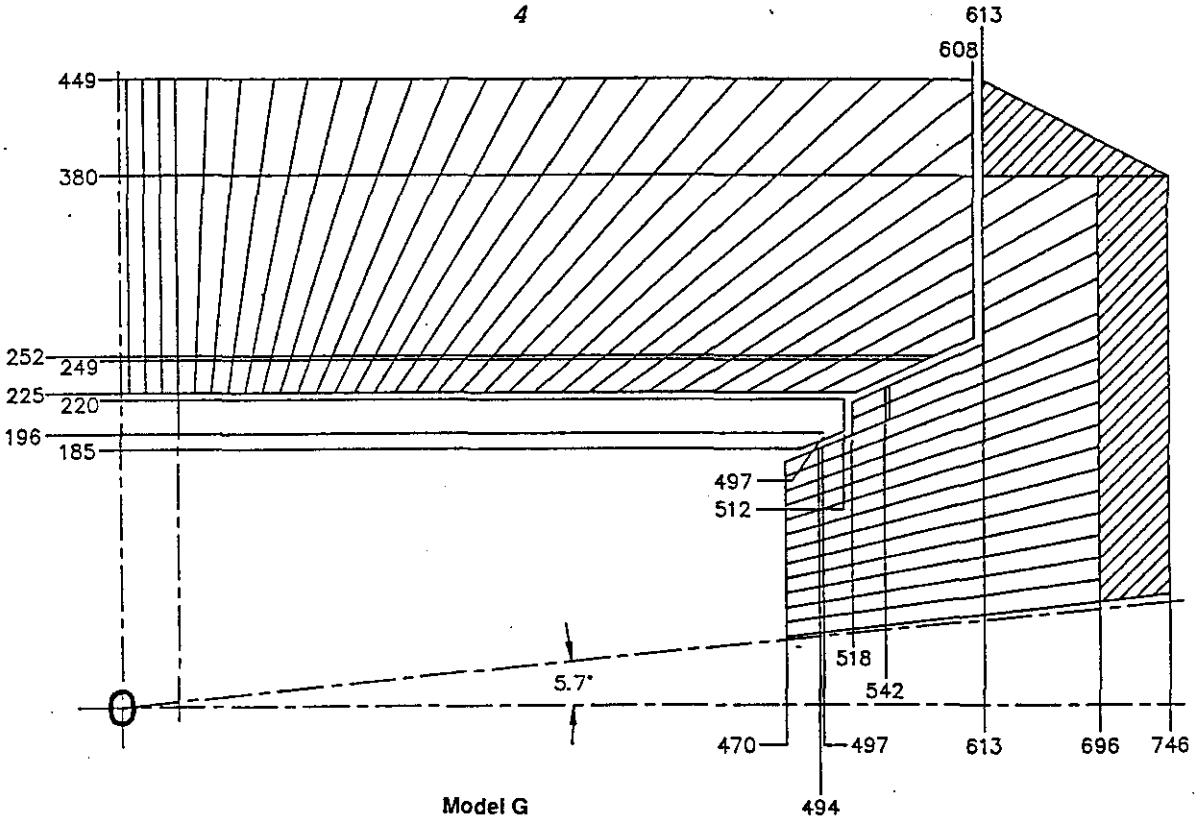

Model G

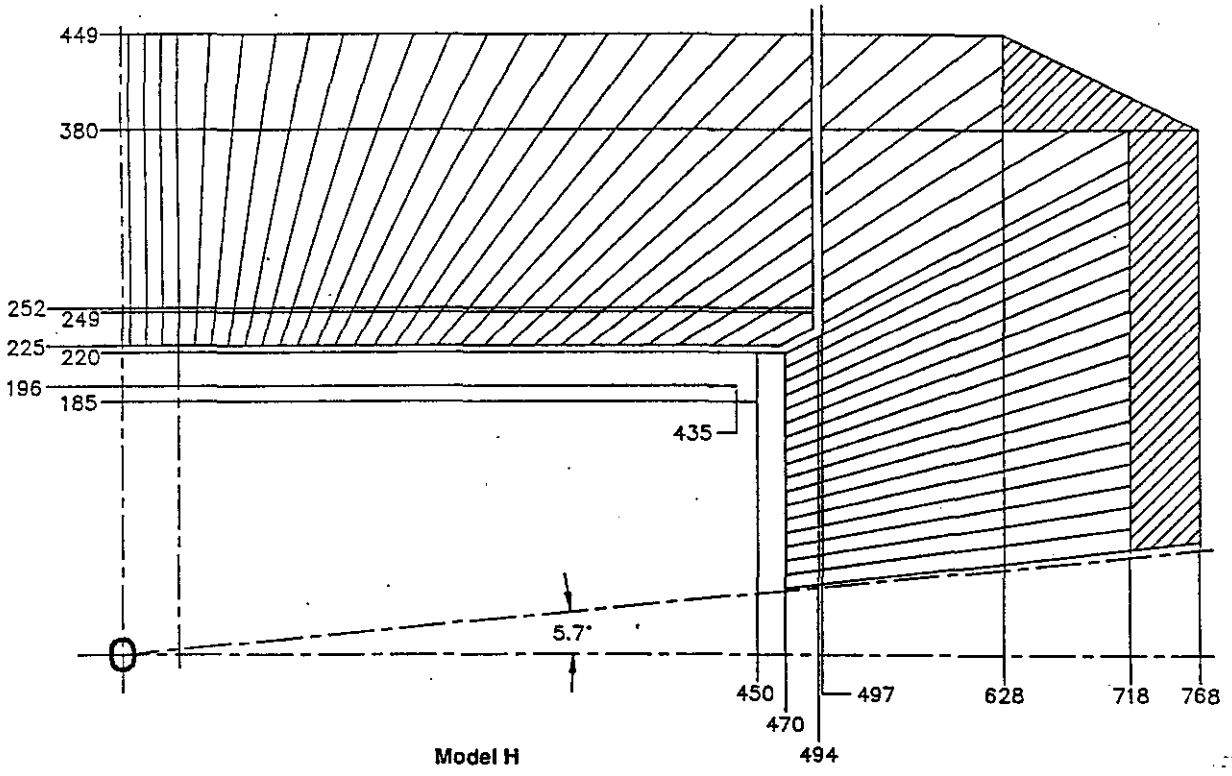

Model H

Figure 1-1 - SDC Calorimeter Models

Model G above has ferromagnetic hadron calorimetry in the endcap, hence maintains nearly uniform field in the solenoid volume; Model H has non-ferromagnetic hadron calorimeter sections behind the EM section, hence has a large fringe field near the end of the tracking volume. Dimensions in Cm.

INTRODUCTION

1.1 Task Force Appointment and Charge

The Solenoid Magnet Task Force was appointed in June 1990 by M. G. D. Gilchriese, SDC Technical Manager, and given the task of assembling relevant technical and cost information, plus organizing this information in an appropriate manner to allow selection of the magnet style to be used in the SDC detector. The material so assembled and organized was to be presented in the form of a written report, submitted to the Technical Manager and directed to the SDC Technical Board. The Task Force membership is included here as Appendix A and the formal charge to the Task Force as Appendix B.

It was further desired that the report include summary statements on the suitability of each magnet style considered for the SDC detector, plus a recommendation to the Board for a preferred magnet style for this application. This document is the final report of the Task Force and is available to all members of the SDC.

1.2 Composition and Methodology

Composition of the Task Force

The Task Force membership was chosen to represent technical expertise relevant to the design and construction of superconducting solenoid magnets of the types considered for use in the SDC. The membership also includes specialized expertise in the technical areas associated with other detector subsystems that will be strongly affected by the choice of magnet style (namely calorimetry, central tracking, and trigger capability). A careful attempt was made to balance the membership of the Task Force to insure that current technical views and approaches in all of these critically related areas would be fairly and adequately represented in the process of evaluation and in formulating of Task Force recommendations.

Methodology

Recognizing that any finite-sized Task Force could not encompass all the needed technical expertise, the Task Force sought wide consultation within the SDC and actively solicited contributions by collaborators relevant to the work. Input in either written or oral form was allowed. At the SDC Collaboration Meeting held on July 7, 1990 in Snowmass, Colorado, a schedule for Task Force Meetings was announced and input to the Task Force was publicly solicited. It was stated that the fourth day of the SDC Group Meeting in August would be devoted to an interim report by the Task Force and to general oral presentations on this subject (provided the presentations were scheduled prior to the day of the Task Force session on August 16). The announcement and charge to the Task Force was also circulated to SDC Contact Persons by electronic mail on July 20.

The Task Force further agreed that it would do most of its work outside the context of full Task Force meetings. Toward this end, a report outline and division of labor were agreed to at the first meeting held on July 6, 1990. There, the members agreed to work independently, communicating with each other as needed and soliciting input as necessary. Draft report language was circulated by electronic mail.

The final report was assembled and edited by the full Task Force. The conclusions represent a consensus of this group and the report contents, including the recommendations have been concurred in by all Task Force members. This report was supplied in final written form to the SDC Technical Manager on September 28, 1990; preliminary results were presented orally to the full Collaboration on September 20.

1.3 Background and Physics-Related Issues

Magnet Models

The basis for collaboration by the SDC is the member's recognition that a large central solenoid magnet containing a high resolution tracker with a hermetic calorimetry system and an outer muon tracking detector, constitutes the best conceptual basis for a powerful, general-purpose SSC detector. Three design options have been explored. We call these Type-L, Type-I, and Type-S. Each has advantages and disadvantages, but there are many common design features.

In the Type-L magnet design, the coil is located as close as possible to a ferromagnetic flux return yoke. This results in a very uniform magnetic field in the bore and negligible fringe fields. The radial field components are small, as is the resulting compressive force on the coil. However, the proximity of the coil to the iron yoke results in axial and radial decentering forces that must be resisted by supports from the 4.5 K coil to the room temperature yoke. In addition, since the coil penetrates the calorimetry, care must be taken to ensure that the calorimetry performance in the coil end region is not compromised.

The Type-I magnet is very similar to Type-L except that ferromagnetic calorimetry replaces the flux return yoke near the ends of the coil. This type also has a uniform internal field, a negligible fringe field, and compressive and decentering forces on the coil similar to that of Type-L. However, since the coil does not penetrate the calorimetry, the detector hermiticity is potentially better than Type-L provided that the thickness of material in the coil ends remains sufficiently small and that suitable ferromagnetic calorimetry can be developed.

The Type-S magnet does not have an iron flux return near the end of the coil. This allows the calorimetry to wrap around the end of the coil in a more hermetic way than the Type-L design, without the requirement of carrying flux as in Type-I. However, the magnetic field in this coil is much less uniform than in the Type-L or Type-I designs, especially near the ends of the winding, and large fringe fields extend into the volume occupied by

calorimetry and other external detectors. The large radial component of the magnetic field that penetrates the coil produces a very large magnetic compressive force on the winding that must be resisted with a structure adequate to prevent quenches induced by coil motion. Because of the large distance to the ferromagnetic return yoke, the axial and radial decentering forces are negligible and supports must carry essentially only the coil cold mass.

All three magnetic geometries have advantages and disadvantages. The principal goal of this report will be to identify, to quantify (to the extent possible) and to compare their relative merits. We also identify and recommend a best overall style of magnet for the physics goals of the collaboration.

In order to make the most incisive comparisons among the models, the ground rules for the present exercise specified that the magnetic volume for the central tracker as well as the value of the central magnetic field would be common to all models. The specifications for these parameters were taken from the SDC Expression of Interest (EoI). The same principles apply to the other main detector systems as they were brought into the comparative magnet study. Thus, parameters characterizing the depth and segmentation of calorimetry, its rapidity coverage, as well as characteristics of specific technologies for tracking and calorimetry were all to be set nominally equal and specified as in the EoI when used to compare the attributes of each magnet geometry studied.

1.4 Physics Performance Implications

The physics performance characteristics of the Solenoidal Detector are the primary reason for its existence, hence these must play the strongest overall role in the decision process. This role, however, is largely expressed implicitly and indirectly in the present study through the detector subsystems and their mutual interactions and especially by their interactions with the various magnet styles. This circumstance results from the specific method of technology comparison chosen for this study.

To clarify this aspect of the comparison method the present section has been included. Its goal is to make explicit some of the direct connections between physics capabilities and detector technology. Elaborations of these comments can be found in the many physics/detector simulation studies carried out by members of the SDC.

The 'high mass' physics of the SSC is our primary experimental priority. It is essentially of two basic types: 1) searches for high-mass particle states by means of the reconstruction of effective mass peaks (or characteristic effective mass distributions such as H°, $H^{\pm}$, top, Z'/W', Technicolor, etc.); 2) searches for new interactions or parton substructure by or levels of parton structure as revealed through continuum scattering distributions (compositeness, QCD breakdown, Higgs strong interactions, etc.). In these physics processes, we are limited in signal detection sensitivity by two general aspects of the problem: a) high effective mass

states are produced at intrinsically low rates (in general scaling as the product of a $1/m^2$ dependence, a coupling constant squared and a branching ratio); b) signal-to-background ratios which vary on a process-to-process basis (these ratios are normally related directly to our ability to reconstruct parton four-momenta). All other aspects of the problem are really elaborations of these fundamental properties.

High Masses - Let us consider the first basic problem, that of low rates for high masses. There is no effective way to offset the general $1/m^2$ problem except by raising the luminosity of the machine. It is pretty clear by now that masses at the 1-TeV scale and above will demand that we accept luminosities of up to 10^{34} cm^{-2} sec^{-1} (an order of magnitude above the nominal SSC design) in order to achieve statistically significant results. So far, we have no guidance as to whether the 1 TeV mass scale will be the required one for success, but we do know that a definitive result on the Higgs question requires that we be potentially able to reach this energy scale.

Actually, independent of the specific Higgs question, it is inevitable that, if we can function experimentally at the level of 10^{34} cm^{-2} sec^{-1}, we will eventually want to explore the few-TeV mass scale, regardless of what we find at lower masses. It's the very nature of our science to keep pushing at the high energy frontier!

Four-Momenta - The second basic problem to be addressed involves the measurement of parton four-momenta. Partons (as used here) comprise leptons and photons as well as primary process quarks and gluons. The leptons consist of electrons, muons, taus, and their neutrinos. The first two leptons are long-lived and distinctive in their interaction behavior. As a direct consequence, they are easily and well measured by electromagnetic calorimetry and by magnetic deflection, respectively.

Electrons and Muons - Experimental resolution for four-momentum determination of electrons and muons is typically at the 2-3% level except for the highest energy muons (~ 1 TeV) where the resolution degrades to about 20% and then deteriorates as 1/P as the energy increases further. For most of the measurement range, the resolution for electrons and muons as well as photons, is limited by systematic errors of myriad types which can be reduced to (possibly) as low as 1% by Herculean efforts. Practical resolutions in real systems, however, generally wind up in the 2-3% range and are systematics limited.

Neutrinos and Taus - All neutrinos produced in primary interactions or through cascade decays are undetectable and can only be inferred by balancing the transverse momentum of detected particles. Because the missing transverse momentum is related to the measurement of the other (detected) partons, the neutrino four-momentum resolution is not unique for a particular neutrino (or neutrinos) in an event but is derived from properties of the specific physics process in question. In general, the quality of calorimetric measurements (resolution in angle and energy) and the hermiticity (solid angle coverage) are key determinants of the missing transverse momentum resolution for the neutrinos.

Tau leptons decay rapidly into quarks and leptons (or pure leptons) and therefore, cannot be measured with the precision of electrons and muons; they behave more like quarks and gluons and can be considered for momentum resolution purposes essentially as low multiplicity quarks or gluons.

Quarks and Gluons - The four momentum measurement of scattered quarks and gluons is much more difficult than for electrons and muons but equally important. These strongly interacting partons can never emerge as free entities in the laboratory and we are left with measuring their fragmentation products. Parton fragmentation is a statistical process and results in showers of mesons, photons and leptons; the shower composition fluctuates strongly on an event-to-event basis.

The (generally limited) numerical values of decay fragment momenta about the primary parton direction in the fragmentation of high energy quarks and gluons gives rise to the phenomenon of 'jets'. In a jet, a primary-process quark or gluon with laboratory momentum of several hundred GeV and up to several TeV appears as a well-collimated jet of ordinary particles. Typically, about 90% of the energy in the jet is contained within a cone of radius 0.7 radians about the original parton direction in azimuth/rapidity space. In general, quark jets and gluon jets cannot be distinguished from one another on an event-to-event basis, regardless of the completeness of the information available from their fragmentation products.

Nevertheless, it is highly desirable to achieve good resolution in the measurement of quark/gluon four momenta. The achievable resolution can, in principle, approach the intrinsic limit imposed by fluctuations of the neutrino decay products in the fragmentation chain. This neutrino fluctuation-limited resolution occurs at the 4-5% level. Assuming that good quark and gluon four-momentum measurements reach this resolution, a number of important physics objectives are attained: 1) effective mass distributions can be formulated which reflect the natural decay widths of their parent states (thereby maximizing signal/background rejection); 2) exponentially falling continuum transverse momentum distributions for single and multiple primary partons (jets) can be directly measured (without large corrections for curve flattening due to jet energy resolution); 3) missing transverse momentum for neutrinos (or light SUSY particles) can be inferred on an event-to-event basis (enhancing signal-to-background ratios for processes in which these non-interacting neutrals play a decisive role).

1.5 Partons and Detector Systems

We need to link the luminosity and four-momentum resolution issues raised above to the implications for the SDC detector. Electrons, taus, neutrinos, photons, quarks, and gluons all rely on calorimetry for measurement of four momenta, while muons depend upon magnetic tracking (plus their own penetrating power through thick absorbers). The rate capabilities of all the detectors are vitally connected to the overall achievable luminosity of the experiment (intrinsic accelerator limitations are now set in the regime of 10^{35} cm^{-2} sec^{-1} or above!) Both resolution and rate capability are, therefore, very important detector subsystem attributes.

Before plunging into the technical details of the solenoid magnet models and those of the other detector subsystems, a few more words on the functional aspects of calorimetry need to be made. These considerations derive from the fact that calorimetry measures both electromagnetic (e, γ) and hadronic (mesons, nucleons, nuclei) showers and is therefore of extreme importance to the detector performance. Different systematic errors result from each type of energy measurement.

Electrons and photons create intense showers that are very limited in spatial extent and, in consequence, have extremely steep gradients of energy deposition transverse to the shower axis; these showers are quite limited in their longitudinal penetration as well. EM showers are fast processes and involve little or no excitation of nuclei in the absorber material. Very little energy is lost from these showers (some low energy photons are escape through albedo).

Hadron showers on the other hand, are naturally larger in spatial extent (both longitudinally and transversely) and extensively involve inelastic nucleon collisions in the shower absorber. As a result of the nuclear breakup that occurs, free neutrons are created which can escape the calorimeter; nuclear binding energy is also released.

The calorimetric effects of the nuclear phenomena in hadron showers are very complex and result in both energy-flow and time-dependence (tens to hundreds of nanoseconds) effects in the resulting measurements of hadron energy. On top of these basic considerations (all of which obtain for single hadrons incident), there are the combinatoric complications induced by jets of hadrons which represent the quark and gluon primaries whose four momenta are to be determined. These present a complex and difficult challenge for the calorimeter design.

The resulting output signals from calorimeters are typically different for the two types of showers. The resolution for hadronic measurements is always poorer than for the electromagnetic ones. In general, the mean value of measured energy is also different (typically lower) for hadronic showers relative to electromagnetic showers of the same actual energy. The ratio of mean energy measured for electrons incident to hadrons incident is called the 'e/h' characteristic.

The numerical value for e/h depends on all the details of the calorimeter including active and passive materials, as well as time processing of the shower signal. In an ideal calorimeter, e/h =1.0; in some of the least good combinations, it can be as poor as 1.3 and be energy and fragmentation-dependent. As noted above, the e/h characteristic for each calorimeter technology is key aspect of its physics performance. This particular aspect of calorimetry is particularly noted in the discussions of calorimeter technologies below.

TECHNICAL CONSIDERATIONS

2.1 Magnet Design Considerations

The SDC Magnet Working Group is growing, is quite active and is making steady progress. The working group consists primarily of two subgroups, one at Fermilab and one at KEK.

Technical differences and opinions do exist, but all efforts have been directed toward the three magnet types described in the EoI. The group is developing good working relationships with each other and with the calorimetry, simulation and integration working groups.

This section addresses various magnet issues and summarizes the present technical status of each. It outlines the similarities and differences among the three magnet types and points out the strong points and problems of each.

2.1.1 Basic Magnet Design

The following design characteristics were taken in common for all the magnet styles studied:

Coil type:	Single layer helix
Support cylinder:	External to winding
Winding scheme:	Inside winding
Cooling scheme:	Indirectly cooled by 2-phase LHe*

The actual cooling scheme might be force flow LHe, thermosiphon or pumped LHe, but the choice is not coupled to any particular magnet style.

The quench protection scheme assumes the following:

Rapid discharge:	All styles into external dump resistor
Quench Back effect:	All styles due to eddy currents in external cylinder
High purity Aℓ strips:	Under discussion for all types.

Other relevant design characteristics were assumed as follows:

Radiation shields:	Aluminum, trace cooled by LN_2	All styles
Vacuum vessel shells: (inner and outer)	Aluminum honey-comb material (if possible)	All styles
Refrigeration:	Approx. the same for all styles	

The magnet heat load is dominated by the 8000 A current lead He usage (25 L/h) in steady state conditions. The radiation loads and support loads differ somewhat between designs, but these differences are not significant. The most

important difference is related to the cold mass (30-60 tonnes) which determines the cooldown time of the magnet. Many items of the design are approximately the same for all three styles, and all working group members agree on how to proceed with these.

The superconductor was specified as follows:

NB/Ti stabilized with high-purity aluminum
Coextruded with Cu/NbTi (0.5/0.5) superconductor
Operating point = 50% of short sample on the load line

The remaining operating parameters were taken from the SDC EoI:

EOI parameters	Type-S	Type-I	Type-L
Operating current (A)	8000	8000	8000
Cross section width × thickness (mm x mm)	4.4 × 50	4.8 × 42	4.8 × 54
Current density (amps/square meter)	36.4	39.4	30.6

The operating current characteristics chosen took account of the following considerations:

Advantages of high current: Lower temperature following a quench, lower discharge voltage, lower conductor aspect ratio.

Advantages of low current: Cheaper power supply and DC switch gear, smaller room temperature bus, lower heat leak from vapor cooled leads. The final parameters, including operating current, may differ from these as a result of further optimization.

There is basic agreement on the style of conductor for all three coil types. The radial thickness of the conductor depends on the type; this introduces small variations in the overall coil thickness in radiation lengths, but basically the conductor does not influence the choice of magnet type.

Tables 1 and 2 of Appendix C shows the design details of all three types of solenoids.

2.1.2 Magnetic Field Uniformity, Field Integral and Tracking Issues

The magnetic field uniformity and field integral relate to the performance of the tracking system. These issues are discussed at length in section 2.3, but are summarized here for convenience.

Overall Comparison

a) Type-I and Type-L both have very uniform magnetic fields inside the tracking volume, well approximated by Bz = 2.0 T.

b) Type-S has a non-uniform magnetic field in the z direction with large radial field components near the ends. The field integral varies with ε.

Specific Tracking Effects

a) A detailed field map is required for Type-S. Lookup tables are required in software or hardware track processors; these are doable with some effort.

b) Track resolution will be degraded at η greater than 1.5 by a factor of 1.2 with the working silicon detector (this becomes worse by a factor of 2-3 if we do not depend on the vertex constraint and use only an intermediate tracker).

c) Computer time for pattern recognition with a Type-S solenoid is shown to be similar to that for a Type-I.

d) There are $E \times B$ effects that could impact gaseous tracking.

e) The spiraling of soft particles in non-uniform field needs to be understood; is it better for a Type-S or worse?

2.1.3 Forces on the Coil

The three types of coil and flux return have significant differences in where the magnetic forces occur and what their magnitudes are. In particular, the short coil experiences all the magnetic forces as internal stresses within the coil and has only relatively weak forces acting between the coil and the yoke iron. The long and intermediate coils experience small forces in the coils, but have strong forces pulling on the iron yokes from the coil's field.

Both the Fermilab and KEK Group have done an extensive investigation of these forces and the resultant magnetic stresses. Results from the KEK Group are included as Appendix A of this report, similar results are available as Fermilab engineering notes for this and other designs.

A brief table of forces from the EoI on this subject consists of:

Force	Type-S	Type I	Type-L
Axial compressive (tonnes)	2200	285	91
Axial decentering (tonf/cm)	4	37	64
Weight of cold mass (tonnes)	33	24	48
Radial decentering (tonf/cm)	Small compared to weight for all styles		

Approximately 2200 tonnes of axial force has to be carried by some structure in any of the three styles. For a Type-S coil, essentially the entire EM compressive force is carried by the coil winding. For a Type-I coil, 2200 - 285 = 1915 tonnes of EM compressive force acts on the iron calorimeter modules. For a Type-L coil 2200 - 91 = 2109 tonnes acts on the endplug steel and is then carried by the solid steel return yoke.

Force Reacting Member	Type-S	Type-I	Type-L
Coil (tonnes)	2200	285	91
Yoke (tonnes)	negligible	NA	2109
Endplug/Calorimetry (tonnes)	0	1915	0

Some detailed design considerations for the coil types under consideration are given here:

Type-S

In a Type-S coil the 2200 ton load is carried from the conductor to the support cylinder through a glue joint between them or by a new mechanical locking technique which interlocks the conductors to the support cylinder. The reliability of this joint is a major issue. Very small conductor motions at this interface could quench the coil and prevent it from working at useful fields. Type-S relies on the integrity of the coil-to-support cylinder bond. It must work reliably for the life of the magnet at SSC. In principle the bonding technique using epoxy should be reliable since the calculated shear load on that bond, 0.5 kg/mm^2 (700 psi), is smaller by factor > 3 than that obtained in small test samples. However the bonding technique is vulnerable to major failures due to:

(a) improper surface preparation, formulation, application, or curing of the epoxy,

(b) long term (> 10 yrs) deterioration of the bond due to chemical action,
radiation, corrosion, humidity, etc. whatever,

(c) cracking or peeling during cooldown or warmup of the magnet, heat exposure, etc.

Considerable effort must be committed to the engineering study of the mechanically interlocking bond as well since this method could be very effective. Obviously, the coil to bobbin bond must be very well understood before committing to a Type-S design. This mandates a vigorous R&D program, including a full diameter prototype with its associated costs.

Type-I

Type-I employs ferromagnetic calorimetry as the flux return. We need to understand if this material can satisfy the requirements for SDC hadron calorimetry. Plausible mechanical schemes exist for tile/WS solution and perhaps SCIFI, but is e/h and resolution acceptable? These issues are expanded in Section 2.2, but the answers are not yet clearly known. The questions will be addressed vigorously by R&D work in the coming year.

Most of the axial compressive loads are carried through the endcap calorimetry. This circumstance places additional design constraints on the structure of the calorimeter. The forces on the coil are small enough that mechanically preloading the coil against the external support cylinder should

insure that there will be no conductor motion even without an epoxy bond. The CDF coil was preloaded and bonded to the support cylinder.

Type-L

The axial force is carried almost entirely by the solid iron return yoke. As with the Type-I coil, the Type-L coil would be preloaded against the external support cylinder. The endcap hadronic calorimetry is either ferromagnetic or is immersed in a 2T field (plug configuration). If it is ferromagnetic, it must be designed to withstand the electromagnetic forces on it.

2.1.4 Coil Testing and Detector Commissioning Issues

The SDC solenoid is sufficiently small that it is likely that the coil will be wound and assembled into the cryostat at a vendor's facility remote from the SSCL and shipped to the site.

A Type-S coil could be tested to full field by the vendor before shipping to the SSCL. This is important for the Type-S because of the necessity to bond the coil to the support cylinder and the uncertainties associated with the reliability of this bond, as described in Appendix C.

A Type-I or Type-L solenoid could also be tested to full field without the iron components if the conductor and outer support cylinder were sized for the greater forces encountered when operating without them. This implies that the coil would be bonded to the support cylinder as in a Type-S coil, although the bond would have to withstand only the ironless test. We estimate that the magnet would be about 10% thicker if it were designed for this test than if it were not. However, because the compressive forces during the test are X10 larger than a Type-I or Type-L coil are expected to normally experience in operation, such a test might be ill advised. This subject will need continued study.

2.1.5 Field Mapping and Fringe Field Issues

It is unlikely that a Type-S magnet could be mapped adequately without the return yoke in place at the vendor's. However, it could be mapped with no calorimetry in place. Because of the nonuniformity of the field, a good field map is important. In order to field-map a Type-I magnet, the steel of the end calorimeter (instrumented or not) must be in place. This complicates the calorimetry assembly sequence somewhat, although this was done at CDF with the end plugs and end wall calorimeters.

Only the passive return yoke must be in place to map a Type-L magnet, so the mapping could occur early in the assembly sequence. The fringe field around a Type-S magnet is large, about 1 kG at the outer surface of the calorimeter. It is negligible for a Type-I or Type-L magnet. These fringe fields have implications both for calorimetry and for safety as follows:

a) Operational effects on calorimeters:

Photomultipliers require heavy shielding. The gain shifts are a function of field, tube orientation, etc. Fan motors, source drive motors, etc may not work. Transformers in power supplies may saturate. There may be inductive noise picked up by the electronics. CRTS (oscilloscopes, terminals, etc) will have trouble. In addition calorimetry immersed in non-uniform fields may have subtle position-dependent and depth-dependent effects that could affect their performance. (See Section 2.8.)

b) Safety considerations

Gates, interlocks, lights, keys and non magnetic tools will be required. Because of the potential for damaging detector components from magnetic objects left near calorimeter, a magnetic material search and secure procedure must be followed after each access. We will have to follow DOE personnel exposure limits for magnetic fields. This probably means there will be limited or no access to electronics on the detector with the field on.

2.1.6 Calorimeter Hermeticity Issues

The existence of cracks, support structures and other sources of imperfection in a real coil/calorimeter structure introduce appreciable degradation of the calorimeter hermeticity and resolution. Some of the mechanisms include:

a) Loss of EM energy in coil material which degrades calorimeter resolution and worsens jet and missing E_t resolutions.

b) The complete loss of energy at cracks, holes and boundaries in causes similar degradation. This can also generate missing E_t ``Zoo'' events.

c) The spreading of EM energy due to interaction of electrons in the coil
material can degrade the electron identification efficiency.

A large, perfectly-hermetic, uniform-field calorimeter, with a coil and cryostat of nearly zero thickness which has low technical risk simply is not possible; all solutions under consideration are compromises involving predictability and reliability tradeoffs. These tradeoffs are just now being studied quantitatively.

These effects can be compared in the three types of coil geometry considered in this report as follows:

a) All three styles have thicknesses at 90 degrees of 1.15 ± 0.2 radiation lengths. The thickness at eta = 0 is not, therefore, a major factor. Type-S tends to be about 10% thicker than Types-I or -L.

b) The material at the coil ends in Type-I or -S is in front of the EM calorimeter. There are many mechanical support and connection items present in the end region that are not at 90 degrees. We must carefully consider these items and calculate the thickness versus eta for Type-S and -I to understand whether the performance of the EM calorimeter is acceptable in this region. A partial list of these items at the end(s) of the magnet includes: axial supports, radial supports, support attachment blocks, chimney adaptor, end ring of vacuum shell, end ring of radiation shield, structural material for coil termination, liquid nitrogen intercepts and plumbing, liquid helium intercepts and plumbing, the coil to yoke/calorimeter mount and the tracking chamber mount.

c) Type-L attempts to solve this end problem by placing all this hardware behind both the EM and hadronic calorimeters. This is the prime motivation for considering the Type-L design. Magnet builders, ignoring calorimetry considerations, would rather build a Type-I solenoid, which provides a uniform field with less total stored energy. Partial solutions in which a Type-I or Type-S is lengthened by one meter, so that the ends are placed behind the EM section only may be a possible solution.

The cryogenic connections to the solenoid coil present very specific problems for the calorimeter (but problems that ocur only at one azimuthal position). We estimate a penetration of about one square foot through the detector will be required for the superconducting current leads, cryogenic piping, and to provide adequate vacuum pumping speed and pressure relief. A vertical penetration to the top of the detector is being discussed with the systems integration group.

For Type-S and Type-I magnets, the cryogenic penetration passes through both the EM and hadronic calorimetry and crosses several tower boundaries. Projective chimneys are possible but are more complicated. It is possible that a Type-L coil with a projective chimney could avoid penetrating the EM calorimeter

2.1.7 Cryostat Mounting Requirements and Issues

The cryostat for the solenoid imposes particular constraints also. We summarize its properties and characteristics here.

Forces

a) Weight of coil/cryostat: Type-S, 40 tonnes; Type-I, 31 tonnes; Type-L, 60 tonnes

b) Electromagnetic forces between coil and steel:

	Type-S	Type-I	Type-L
Axial decentering (lbf/cm)	3.8	37	64
Radial decentering	small << weight of cold mass for all three designs		
Weight of the tracking system			6 to 8 tons

c) These loads must be carried from the coil/cryostat package to the steel yoke/calorimetry supports in a way that does not interfere with the other requirements that follow.

Other Requirements and Considerations

a) For Type-I and Type-S coils, the cryostat supports must either penetrate the calorimetry or the calorimetry itself must provide sufficient mechanical strength and have attachment points to carry the loads.

b) The material at the ends of the cryostat is in front of the EM calorimeter for Types-I and -S and therefore the amount of material in the supports must be minimized to avoid degrading the resolution of it.

c) Type-S has small axial forces compared to Type-I and -L so the support technique could be different. However, Type-S requires non-magnetic supports because of the fringe fields.

d) Type-L supports are completely hidden behind the EM calorimetry and so material is not an issue. The CDF support system would be acceptable.

e) For all three magnet types, the support system must permit access to the tracker and be consistent with calorimetry assembly and service procedures.

Alignment and stability

a) It is likely that the central tracking chamber will be mounted to the cryostat vacuum shell, as is the case at CDF.

b) Absolute positioning of the tracker with respect to the beam line is important for triggering purposes, but stability is more important. The main considerations here are:

- Beam alignment reference from the tunnel to bedrock.
- SDC tracking system reference: tracker to cryostat to yoke/calorimeter support to collision hall to bedrock.

- Tracking system alignment should not be time (temperature) dependent at least not with a short time constant. The coil mount must be a part of this overall system.

  Example: For SDC, if the beam line is 10 m from the floor of the detector hall and the support structure is 1020 steel (6.7 x 10-6 in/degree F) then we expect 120 microns of detector motion with respect to beam line/degree C.

c) The coil mount must allow for differential motion between the cryostat and the calorimeter/steel support to handle such failures as loss of insulating vacuum in the cryostat.

2.1.8 Cost and Schedule; R&D Needs

There is now a large experience base with thin solenoids. The cost and schedule of a Type-I or -L solenoid can be well estimated. A Type-L magnet would be more expensive (about 20%) than a Type-I because of its length and stored energy. The materials cost for a Type-S would be similar to Type-I but the additional R & D to reduce the technical risk will drive up the total cost.

All coil types require an R&D program to back up the engineering design decisions such as the honeycomb vacuum shell, and to develop the outside-in winding fixture and assembly procedure. The Type-S will require a significant additional R&D effort to build and test a large prototype coil to verify the quality and reliability of the coil to support cylinder bonding technique. The cost of the R&D effort is estimated to be in the range of 10-30% of the total cost of the coil/cryostat package and is estimated to require a 1 to 2 year effort.

The history of construction and operation of large superconducting magnets (dipoles, solenoids, toroids) teaches us that:

a) Large SC magnets are complex and must be well engineered.

b) Many coils have had problems of various sorts:

- Electrical problems; shorts, current lead failures, inability to reverse polarity, etc.
- Mechanical problems; support failures due to design errors and larger than expected EM forces.
- Materials problems; defects in superconductor, inappropriate choice of materials.
- Miscellaneous problems; insulating vacuum leaks, excessive heat loads, coil hot spots, refrigerator capacity and reliability, etc.

These problems are usually not fundamental and they eventually get solved, but they can effect the schedule and cost. We conclude that superconducting magnet technology is mature enough to be `up to the task' of building the SDC solenoid successfully, but that reliability and predictability should be a major design consideration.

2.1.9 Conclusions

From the considerations above, we draw the following general conclusions:

a) All three thin solenoid geometries described in the EOI are receiving serious engineering design attention at this time.

b) All three designs share many common features so that up to now, much of the engineering has proceeded with different groups working in parallel; a lot of progress has been made.

c) The principle geometric differences among the three styles are a result of how the flux-return at end of the coil is handled and how this return interacts with the nature of the calorimetry.

d) The geometric differences among styles affect coil forces, field uniformity, hermeticity, etc., which in turn cause significant effects on other parts of the detector; the physics performance of the detector is impacted in turn.

Detailed engineering and system studies are in process aimed at understanding both the physics and engineering tradeoffs for each design. Hopefully these will lead us to pick the best detector geometry for doing physics at the SSC. The collaboration needs to compare self consistent versions of the overall detector to make this choice wisely. The coil, detector geometry, calorimetry choice, tracking system etc. are all involved in the choice of coil style to a greater or lesser extent, hence the inclusion of the subsequent sections of this report to explore these connections.

2.2 Magnet-Related Calorimetry Considerations

2.2.1 Introduction

One of the principal concepts of the SDC detector is to locate the superconducting solenoid inside the calorimeter in order to keep the dimensions of the coil manageable. The solenoid can be made sufficiently thin that calorimeter performance and electron identification are not degraded. The coil, however, has a finite dimension and mass. The approximate dimension and mass are:

Coil thickness:	35 cm
Coil weight:	50 tons
Transverse radiation thickness:	1.2 X_0
Cransverse interaction length:	0.25 lambda

Some of these parameters depend slightly on the magnet type. It is important to evaluate the effects of these dimensions and mass on the calorimeter performance (and ultimately on the physics capability of the SDC). Three types of solenoids, Type-S, I and L were proposed in EoI and are similar in their main features to the coil mentioned above. Therefore the ultimate physics performance is expected to be comparable whatever type of magnet is selected to the first order. However, as we describe in the following, there exist non-negligible differences among three types in various detailed aspects. We categorize these into:

1. calorimeter geometry
2. passive materials in front of and in the middle of the calorimeter,
3. magnetic field return path in the calorimetry.

There are five different calorimeter technologies proposed in SDC. Some of the magnet styles affect these strongly depending on the specific calorimeter technology. In fact, the magnet and the calorimeter are tightly coupled. For example, Type-I is coupled to an iron-loaded scintillator calorimeter. At the present stage of SDC, the technology is yet to be chosen, and all we can do at this time is to point out such technology-dependent effects as needed in our evaluation. In addition, calorimeter-related engineering designs are still in a primitive stage and, consequently, it is inevitable to make assumptions in various places based on past experience. We hope these assumptions are not far from reality.

2.2.2 Geometry Related Effects

1. Calorimeter geometry.

The largest difference in calorimeters of Type-L (long coil) and Type-S/I (short coil) are found in its geometry. There are, in fact, essentially two types of calorimeters as far as their geometrical configuration are

concerned. With a liquid argon calorimeter, non-negligible amounts of space and material are necessary in front of the active region to accommodate the liquid argon cryostat. It is not clear how much material and space are necessary in the case of other calorimeter types at present. We assume no space and zero materials in front of the active region as an extreme case. In consequence, we have to consider four different configurations depending on calorimeter type and magnet style:

Solenoid Style	Calorimeter Type
Case-1 long coil	non-LA
Case-2 long coil	LA
Case-3 short coil	non-LA
Case-4 short coil	LA

where LA stands for a liquid argon calorimeter and non-LA includes the rest of the calorimeter types: warm-liquid; scintillating plate; and scintillating fiber calorimeters.

We made a drawing for each case according to the following guidelines:

1. inner tracking volume: r = 1.85 m, half z length = 4.5 m;
2. coil thickness: 35 cm physical and 1.15 radiation length;
3. calorimeter depth: > 25 X_0 for EM and > 9 lambda for total;
4. space for cabling and/or tracker support:
   10 cm for long coil; 20 cm for short coil;
5. calorimeter material and density based on currently going designs;
6. thickness and density of liquid argon cryostat:
   Case-2: 10 cm
   Case-4: 10 cm (barrel inner face)
   12 cm (barrel endplates)
   17 cm (endcap front face).

More details are described in Appendix C[2.1]. Figures 2-1, 2, 3, 4 show the cross sections of the detector quadrant in the z-r plane. It is clear from these figures that there is a distinct difference in calorimeter shape.

2. Calorimeter Weight and Shape

In the case of the long solenoid, the barrel calorimeter must be stretched out to > 8.5 m in half length in order to maintain the required calorimeter depth; the endcap calorimeter can be compact and small. The length of the barrel calorimeter has an impact on the dimensions of the muon system as well as on service accessibility inside.

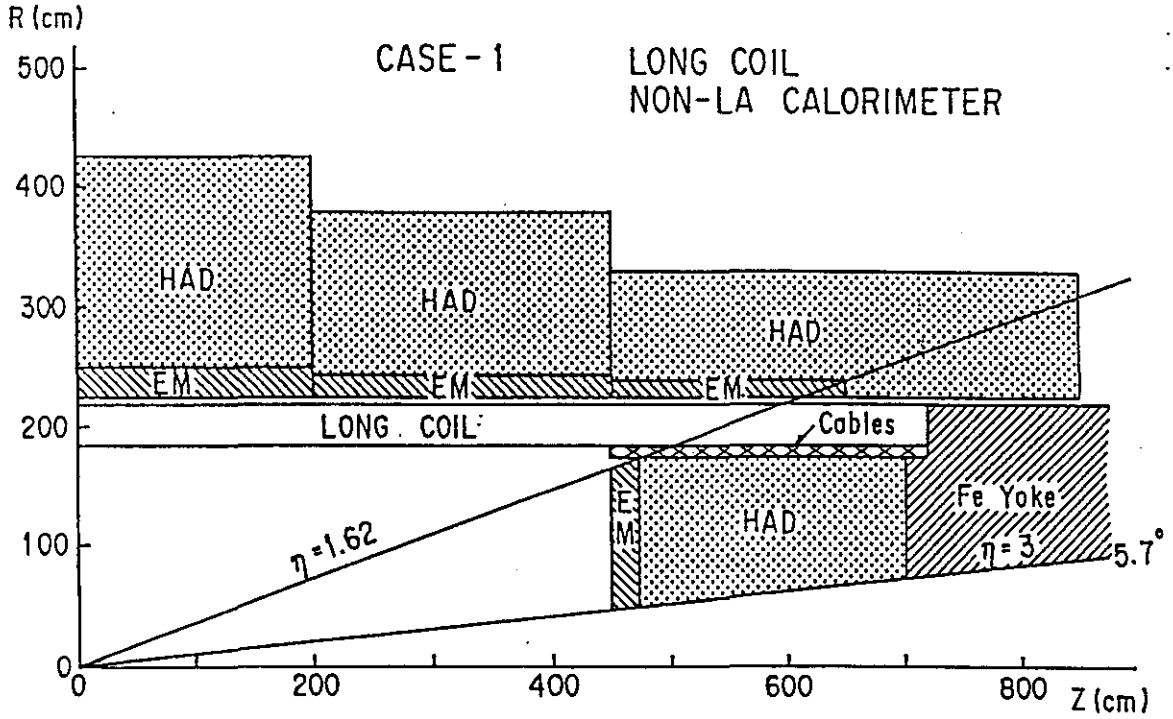

Fig.2-1 Configuration case-1 : long coil and non-liquid argon calorimeter.

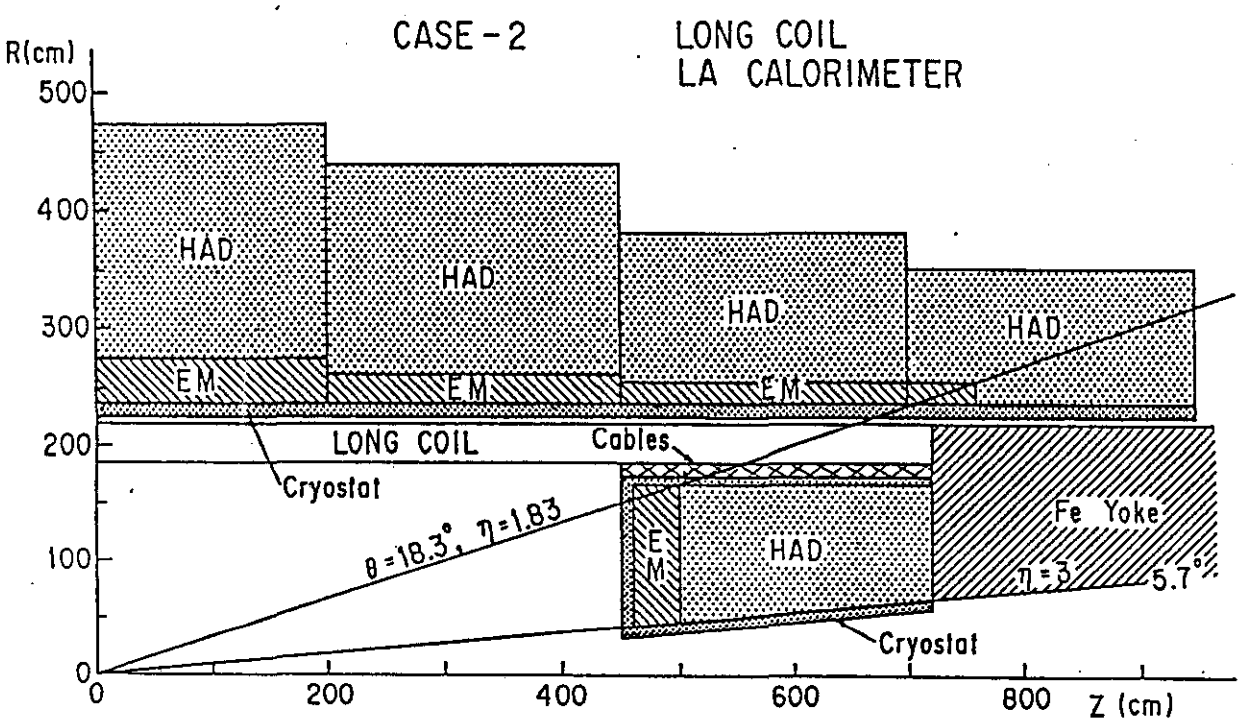

Fig.2-2 Configuration case-2 : long coil and liquid argon calorimeter.

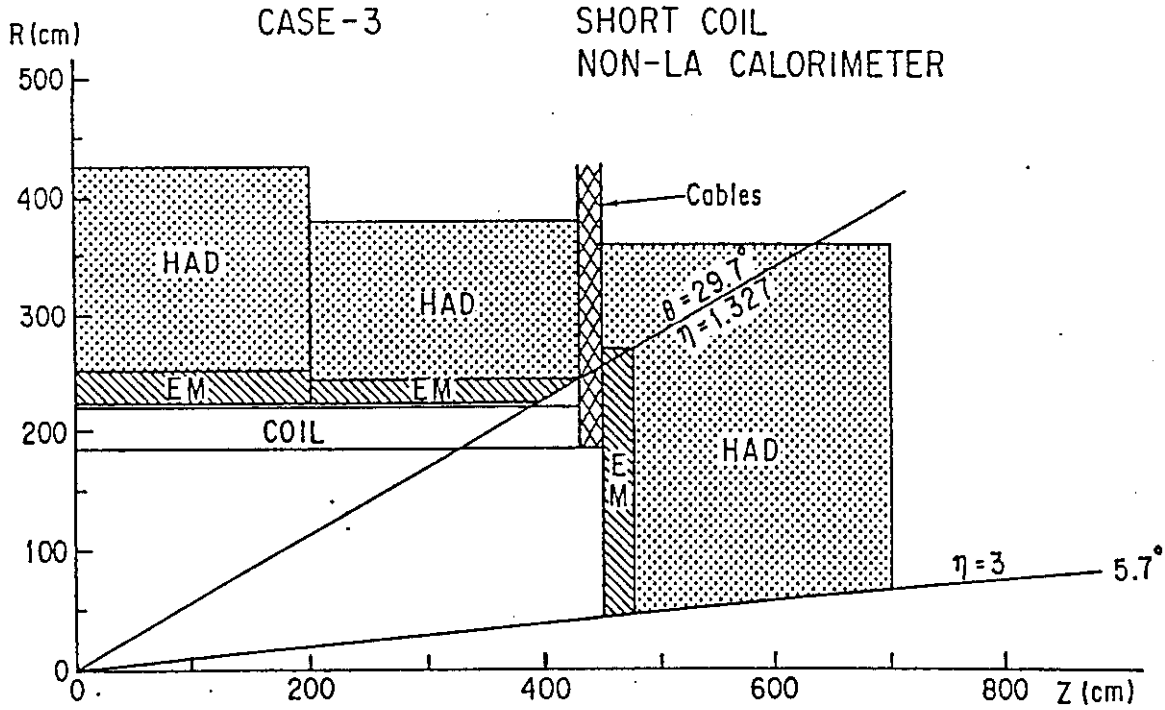

Fig.2-3 Configuration case-3 : short coil and non-liquid argon calorimeter.

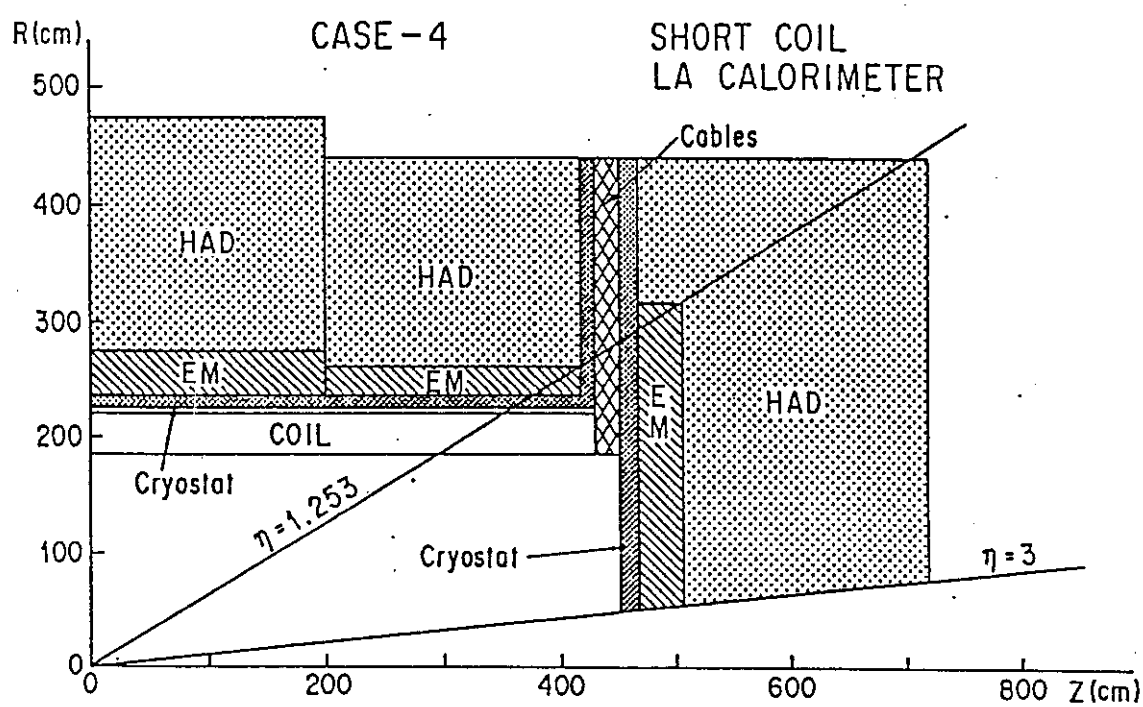

Fig.2-4 Configuration case-4 : short coil and liquid argon calorimeter.

To begin a comparison, we have calculated the weight of each calorimeter:

	Case-1	Case-2	Case-3	Case-4
Barrel Calorimeter	4194 T	4902 T	2742 T	2914 T
End Calorimeter	2 x 196 T	2 x 137 T	2 x 907 T	2 x 1100 T
Total Weight	4856 T	5176 T	4556 T	5114 T
Barrel::End	1::0.18	1::0.06	1::0.66	1::0.75

In spite of the stretched-out shape of the calorimeter for the long solenoid case, the total weight of the calorimeter is surprisingly close to that of short coil. The difference in the total weight is at most 300 tons. It is also notable that the ratio of the barrel to end calorimeter weight is very high in the long solenoid case.

Other geometrical features that manifest significant differences between two coil styles are as follows:

	Short Solenoid	Long Solenoid
1. Barrel Calorimeter	9 m long	17 m long
2. Endcap/Plug Calorimeter	~ 8 m high	small and compact
3. Barrel Muon System	~ 8.5 m long	~ 10 m long
4. Movement for Access	1 ~ 2m	5 m
5. Inner Tracker Support	short and radial	long & cylindrical
6. Cabling	radial at z = 4.5 m	axial along the coil

These differences arise from the calorimeter geometries. One can say that the short coil is favored in items 1,3,4,5 and 6, while the long type has advantages in item 2. In general, the short type is favored as far as calorimeter geometry is concerned.

2.2.3 Non-active materials

In order to evaluate the calorimeter performance, it is best to simulate EM and hadronic showers. However, these simulations require a fair amount of computing time. A much simpler method, ray-tracing, was introduced by M. Strovink et al.[2.2] This method is extremely useful to pin-point cracks, dead material as well as calorimeter depth. A ray-tracing program was developed in the framework of GEANT [1]. We have used this program to ray-trace the four calorimeter configurations stated above in order to evaluate the magnet style dependence on calorimetry.

Figures 2-5, 6, 7, 8 are the plots of the radiation thickness as a function of pseudorapidity. The plots indicate accumulated radiation length from the interaction point. As a measure for evaluation, we take a rapidity interval in which the thickness of front material exceeds 3 X_0 (gray EM area) and 5 X_0 (bad EM area).

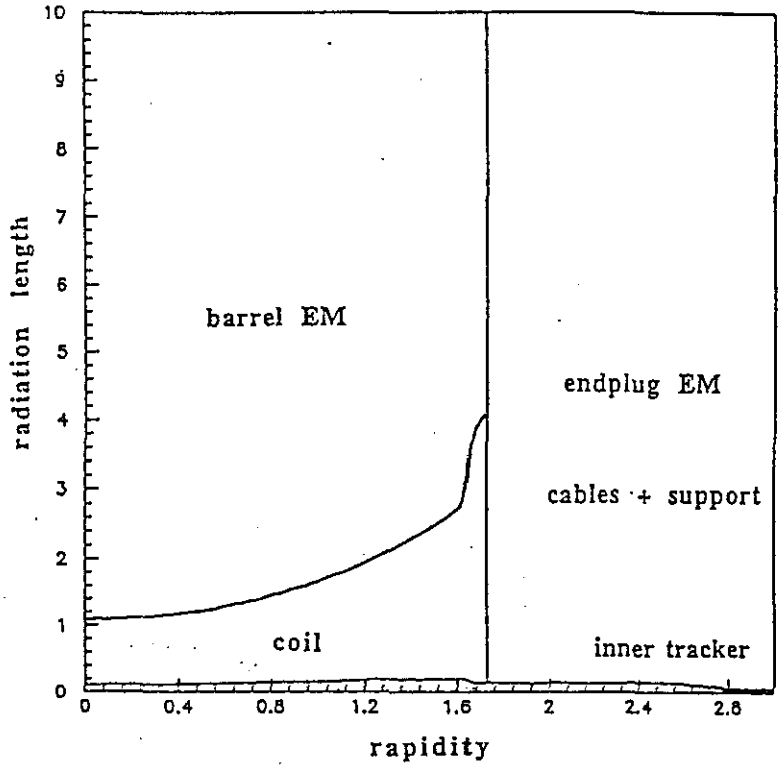

Fig.2-5 Rapidity dependence of radiation length for case-1.

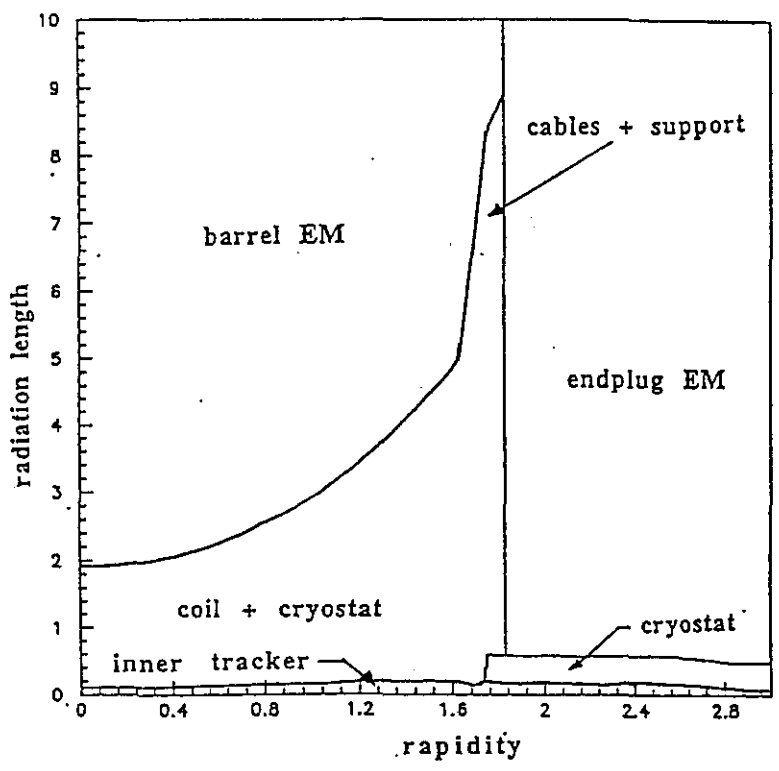

Fig.2-6 Rapidity dependence of radiation length for case-2.

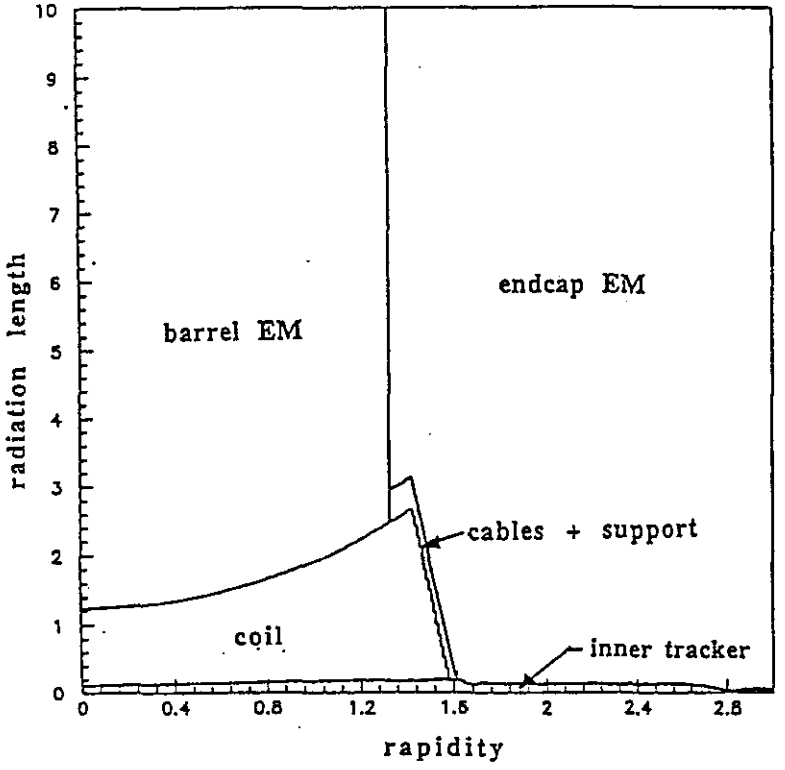

Fig.2-7 Rapidity dependence of radiation length for case-3.

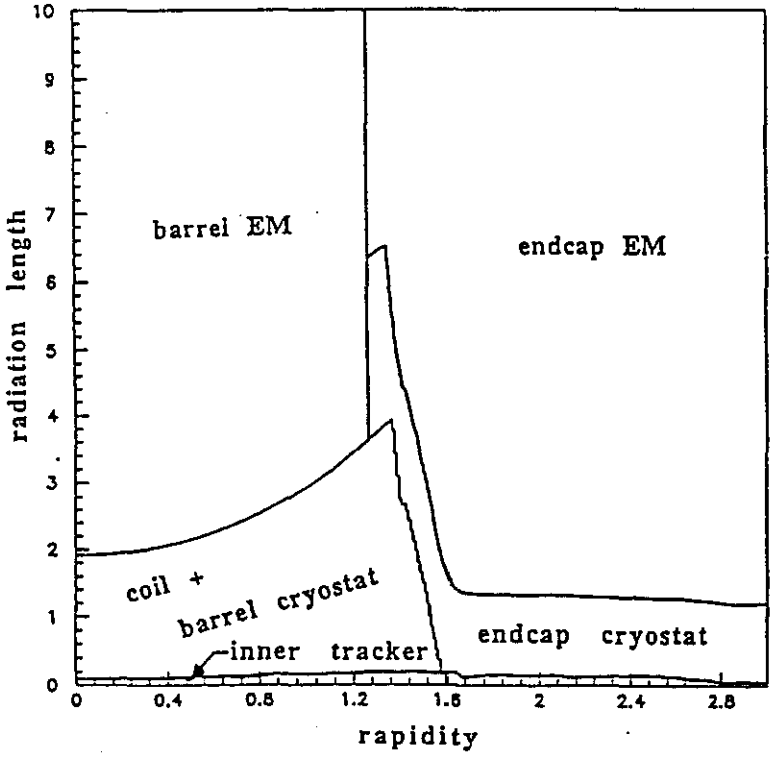

Fig.2-8 Rapidity dependence of radiation length for case-4.

	Case-1	Case-2	Case-3	Case-4
Type	long, nonLA	long, LA	short, nonLA	short, LA
Gray EM Area	0.1	0.8	0.1	0.45
Bad EM Area	0.0	0.2	0.0	0.15

Figures 2-9, 10, 11, 12 are similar plots in terms of interaction length. One can see distinct differences in the rapidity region in which the barrel to endcap (plug) transition occurs, eta ~ 1.2-1.4 for short magnet while ~ 1.7-2.0 in the case of long type. For the sake of evaluation, we take two measures: one is the total area of dead material (in unit of eta × lambda) in the first 5 interaction lengths; the other is the rapidity interval in which the total dead material exceeds 1 lambda inside the region of the first 5 interaction lengths

	Case-1	Case-2	Case-3	Case-4
Type	long, nonLA	long, LA	short, nonLA	short, LA
Dead Area*	0.85	1.91	0.69	1.23
Bad Region†	0.14	0.55	0.0	0.32

(* in unit of eta × lambda, † in unit of eta)

It is clear from these measures for EM as well as hadronic calorimetry that Case-2 is the worst and Case-4 is the second worst. In the present report, we are comparing not calorimeter types (LA vs. non-LA) but magnet styles (long vs. short). Therefore our conclusion on style preference is:

non-LA case: short magnet is preferred (case-3 better than case-1)
LA case : short magnet is preferred (case-4 better than case-2)

According to above criteria, whatever the calorimeter type is, a short solenoid is preferred.

2.2.4 Energy Resolution Degradation Effects

J. Hauptman has studied the coil effect more quantitatively [2.3, Appendix-C]. He has parameterized the effect of dead regions, both in front and also embedded within the calorimeter mass, using the energy resolution of the CCFR data. The resolution degradation is expressed as a multiplicative factor. The degradation of the energy resolution on a jet energy measurement is then calculated by evaluating the degradation factors as a function of rapidity. The transverse energy profile of a jet is convoluted in the calculation. Figure 2-13 shows these degradation factors, indicating the differences are not large (although the long coil is slightly worse). It is noted that Hauptman has assumed only the presence of the coil and calorimeter neglecting cables and supports in his calculation. Thus the actual differences are larger than shown here.

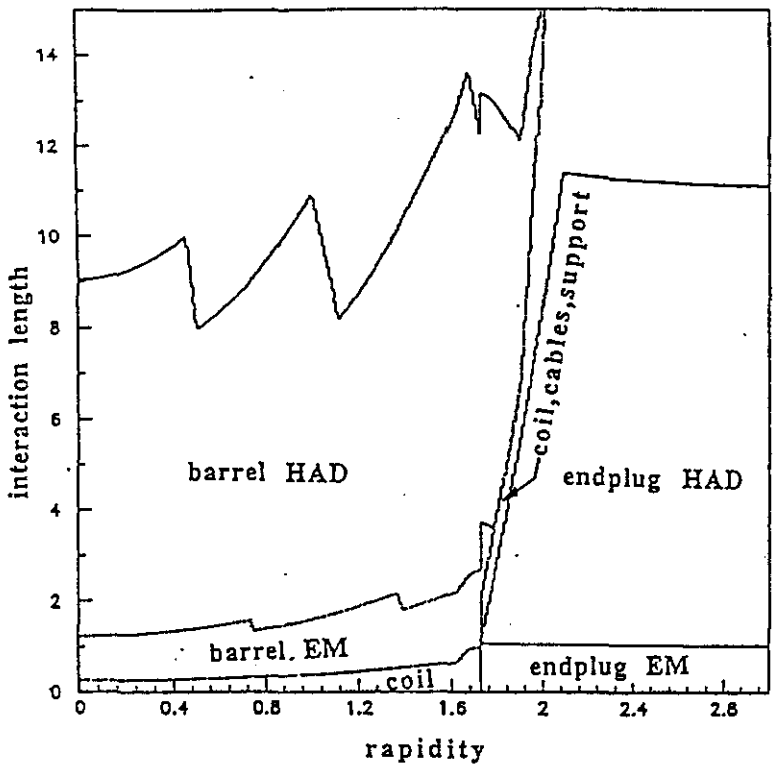

Fig.2-9 Rapidity dependence of interaction length for case-1.

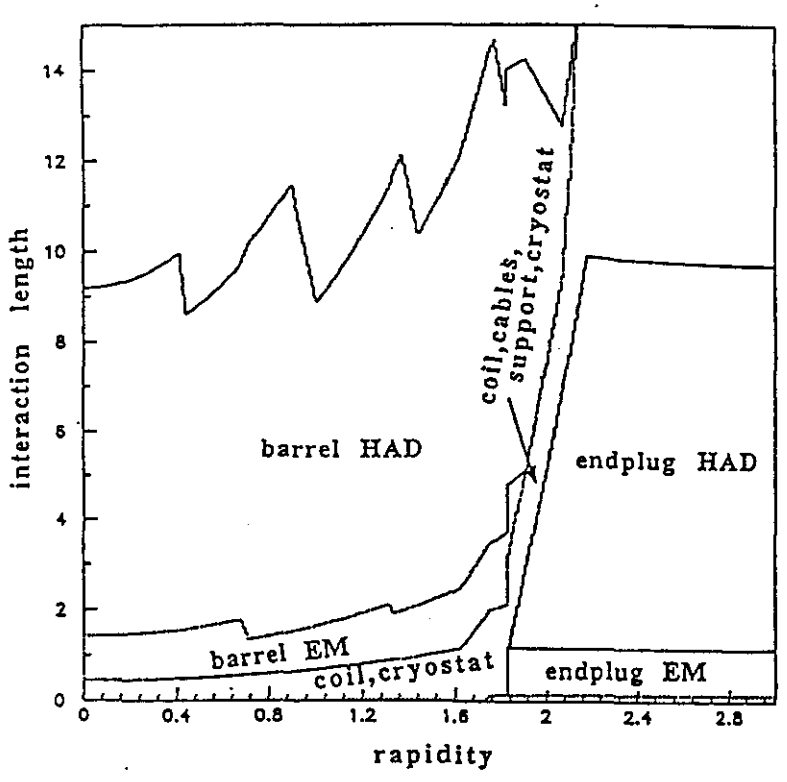

Fig.2-10 Rapidity dependence of interaction length for case-2.

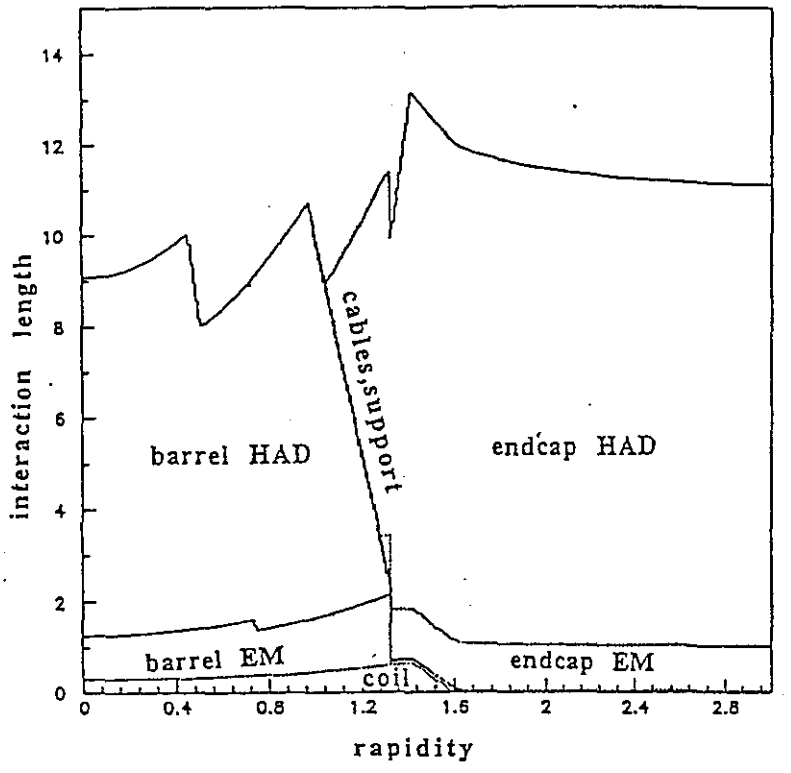

Fig.2-11 Rapidity dependence of interaction length for case-3.

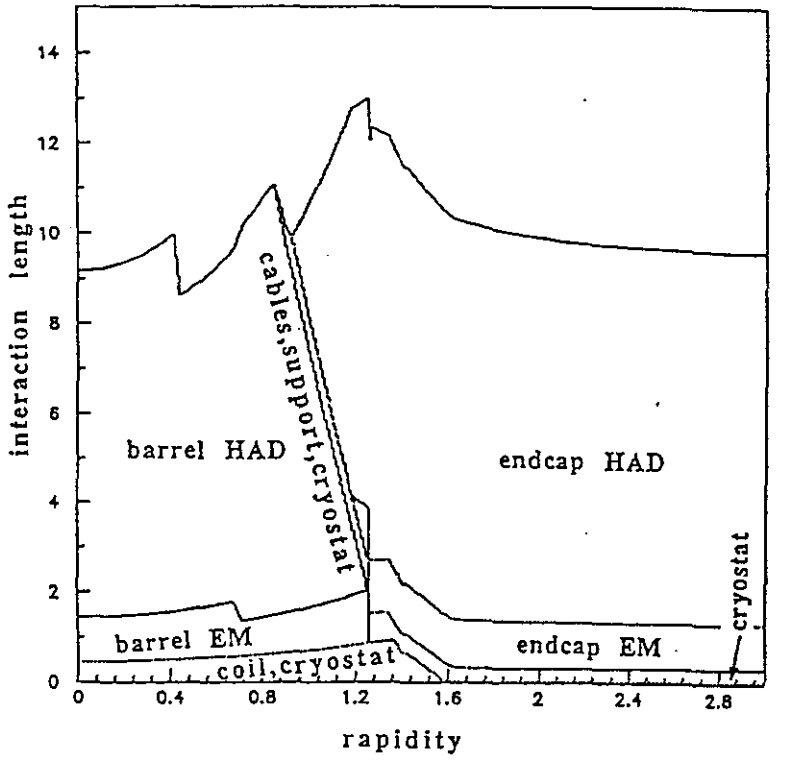

Fig.2-12 Rapidity dependence of interaction length for case-4.

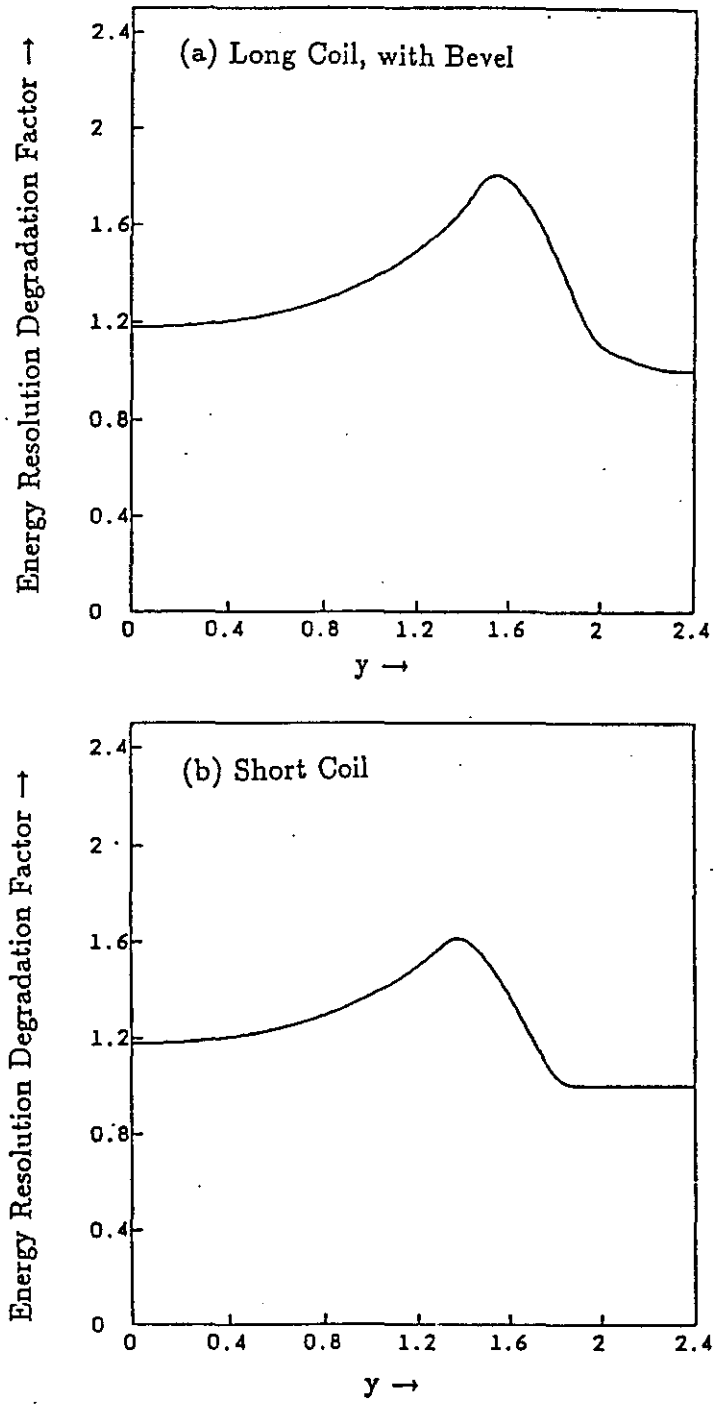

Fig.2-13 Energy resolution degradation due to the dead space of the coil for (a) the long coil with bevel, and (b) the short coil [4].

Mismeasurement of a jet energy may potentially cause a larger missing E_t trigger rate. J. Hauptman calculated the absolute missing E_t trigger rate at $L = 10^{33} cm^{-2} s^{-1}$ for the EHLQ single-jet cross section as a function of dead material in the calorimeter and as a function of the triggering threshold. Figure 2-14 shows the trigger rates per unit rapidity for the long coil case without a bevel and for the short coil. Again the short coil case is better. However, after introducing a bevel in the endplug calorimeter, the differences become smaller. As stated before, cables and supports are not included so actual performance will be worse.

2.2.5 Side Leakage in the Bevel of the Endplug Calorimeter

In the same article J. Hauptman pointed out that the beveled edge of the endplug calorimeter which is necessary for the long coil may raise a problem. Since the particles at shower maximum are low energy and nearly isotropic, many shower particles exit backwards into the tracking volume, and spiral through the outer layers of the straw tubes. This could disrupt the triggering layers, and augment the straw occupancy. This effect is demonstrated in Fig. 2-15 which shows a GEANT simulated event with 300 GeV incident π^+ mesons striking near the bevel.

2.2.6 Magnetic field related effects

Figure 2-16 shows the field map of the Type-S configuration. One sees a fringe magnetic field distributed in the area of the calorimeter. In the types I and L magnets, there is no field in the barrel calorimeter section, but the full 2 Tesla appears in the end calorimeter region.

In the following we discuss and evaluate calorimeter-related problems that arise from the presence of the magnetic field:

1. Magnetic forces on iron-loaded calorimeter

   If the calorimeter absorber is made of ferromagnetic materials like iron (Type-I), the magnetic field pulls the calorimeter toward the coil center. The force is calculated for the case of uniform magnetic field at the coil end:

$$F = \int B^2/(2\mu^o)^* \, dS = B^2 \pi R^2/(2\mu^o) = 1710 \text{ tons},$$

   where R is 1.85 m, the radius of solenoid. This can be compared with the magnetic force of 630 tons for the case of CDF. In the case of other types (Type L and S), non-magnetic calorimeter will be used and thereby the magnetic force is not on the calorimeter but on the flux return yoke. In Type-L, the force is the same 1710 tons, while in Type-S, it is much smaller. It is estimated to be an order of 100 to 200 tons. These magnetic forces must be taken into consideration in the structural design.

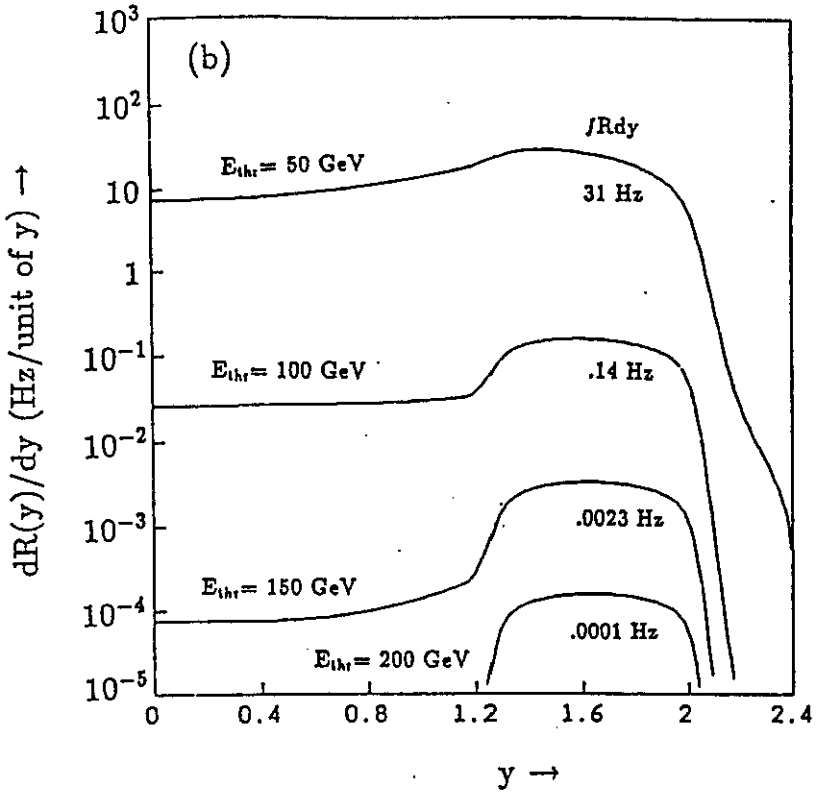

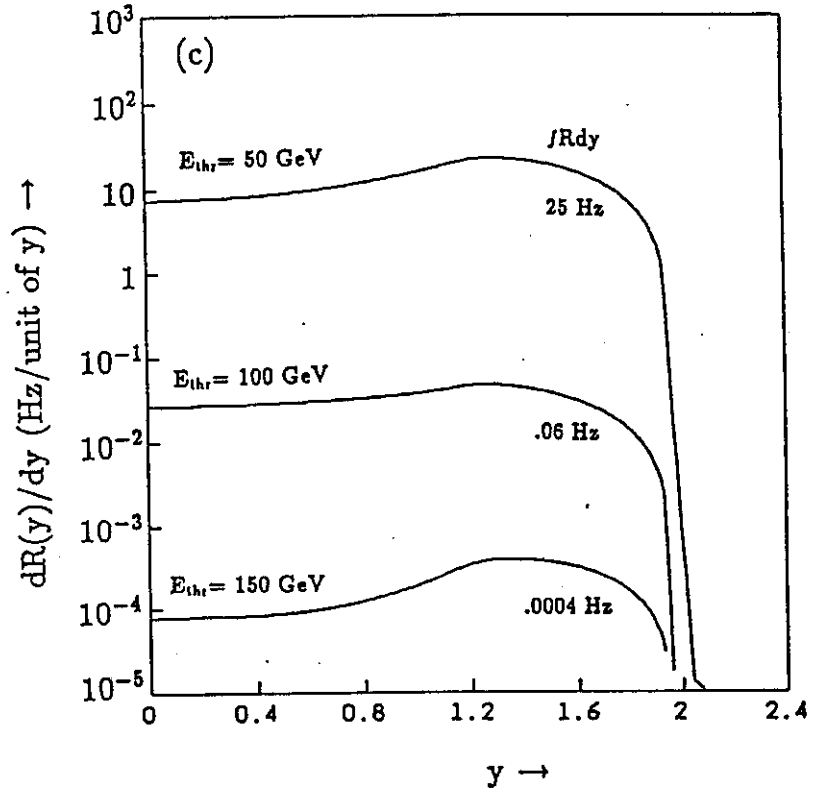

Fig.2-14 The trigger rate per unit of rapidity due to fake missing Et exceeding a specific triggering threshold, due to the dead space of (b) long coil without bevel, and (c) the short coil [4].

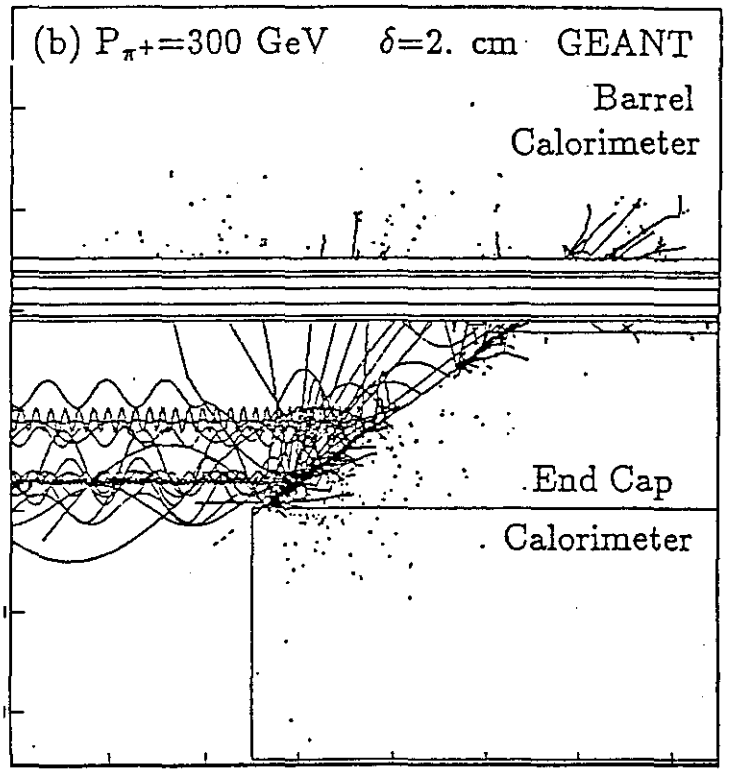

Fig.2-15 A Geant event with 300 GeV incident pion striking near the bevel.

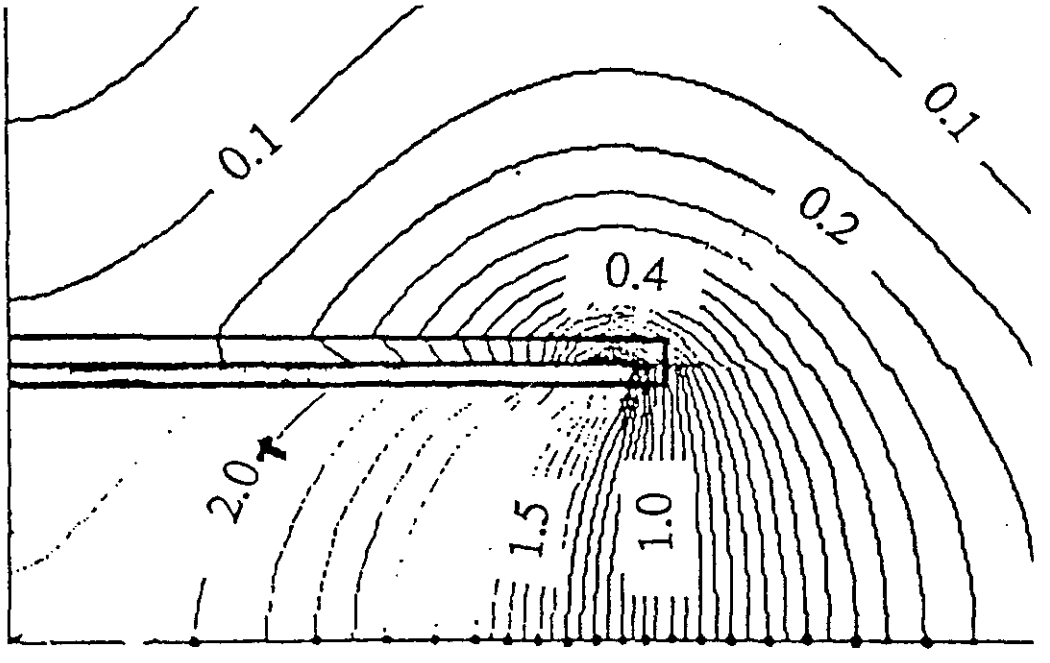

Fig.2-16 Magnetic field map of the Type-S.

2. Shield of magnetic transformer for liquid ionization calorimeters

It is necessary to utilize either a magnetic transformer or an electro-static transformer to obtain a high speed response in liquid ionization calorimeters. In the case of magnetic transformers, care must be taken to shield them in the presence of stray magnetic fields. A standard magnetic transformer works in an external field of up to about 0.02 T (parallel) and 0.10 T (normal) without any performance degradation even at liquid nitrogen temperature. Beyond 0.02 T, a magnetic transformer enters saturation and must be shielded.

F. Lobkowicz et al. have carefully investigated the problem of shielding magnetic transformers [2.5]. They have demonstrated that shielding by a steel cylinder works up to several tenths of a Tesla. Their conclusions are:

1) It is possible to shield transformers to a field of < 0.7 Tesla, while it is impossible in a field of > 1 Tesla.

2) The long or intermediate coil options with a field of 2 Tesla, makes it impossible to use magnetic transformers in the end plugs. The central barrel calorimeter has zero fringe field so no shielding is necessary there.

3) The short coil option (Type-S) makes it possible to use magnetic transformers in most places (with the exception of some of the EM section in the endcap) which is bathed ina field of > 1 Tesla.

If, on the other hand, an electro-static transformer is employed in the liquid calorimetry for noise reduction and for speed, there is no influence from the magnetic field. Hence the magnet style is irrelevant from this point of view.

2.2.7 Photomultiplier Shielding

The problem of stray magnetic fields affecting PMT based readout is a common one (a shield from the earth's magnetic field is required for a precision device) and the solution is well documented. Typically a shield consists of a soft iron ring surrounding the PMT and extending some distance in front of the photocathode. For shielding from fields up to 300 Gauss, an additional ring of mu-metal may be used. Such a shielding scheme, as used by the ZEUS collaboration is shown in Fig. 2-18. The resulting magnetic field at the photocathode for such a shielded PMT in a 300 Gauss axial magnetic field is shown in Fig 2-19.[2.6] This design of shield yields a magnetic field at the photocathode of less than 1 gauss (as required for proper tube operation) for external fields less than 170 Gauss. In addition to the operation of the PMT's, it is necessary to perform detailed calculations of the effect on the field itself as field non-uniformity and magnetic forces can be significant if much flux is passing through the non-homogeneous shield structure.

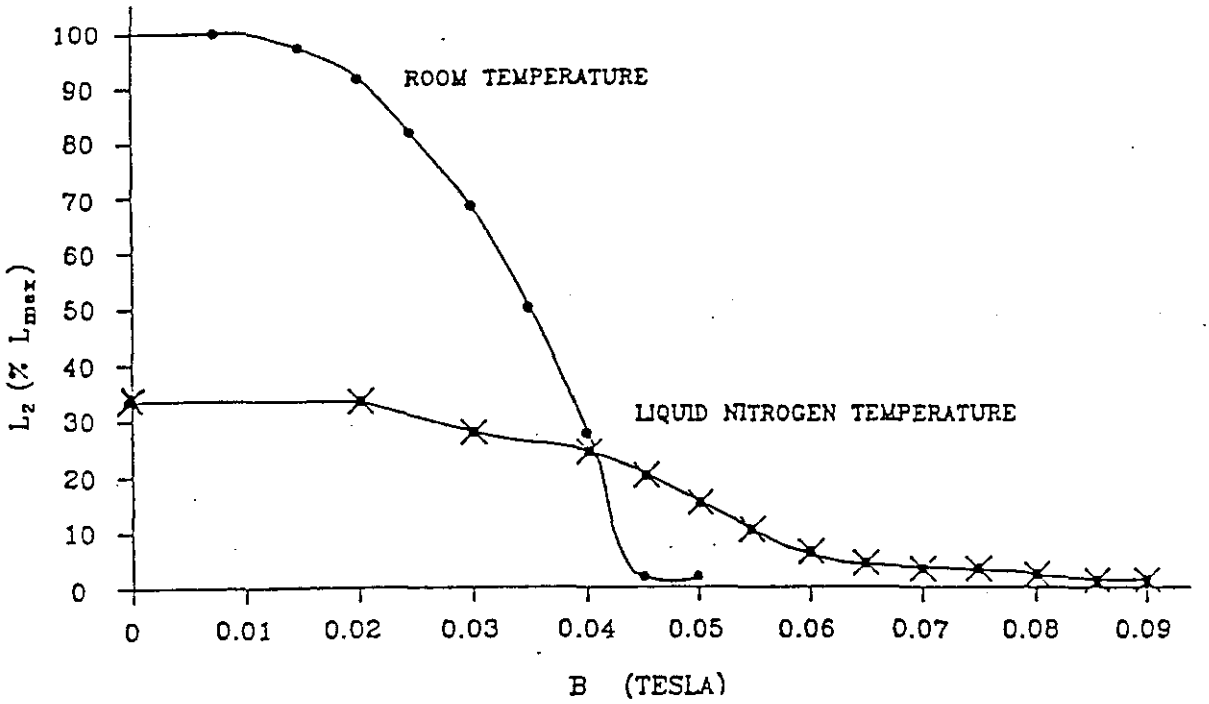

Fig.2-17 Response of a 3D3 toroid magnet to an external magnetic field lying in the plane of the torus.

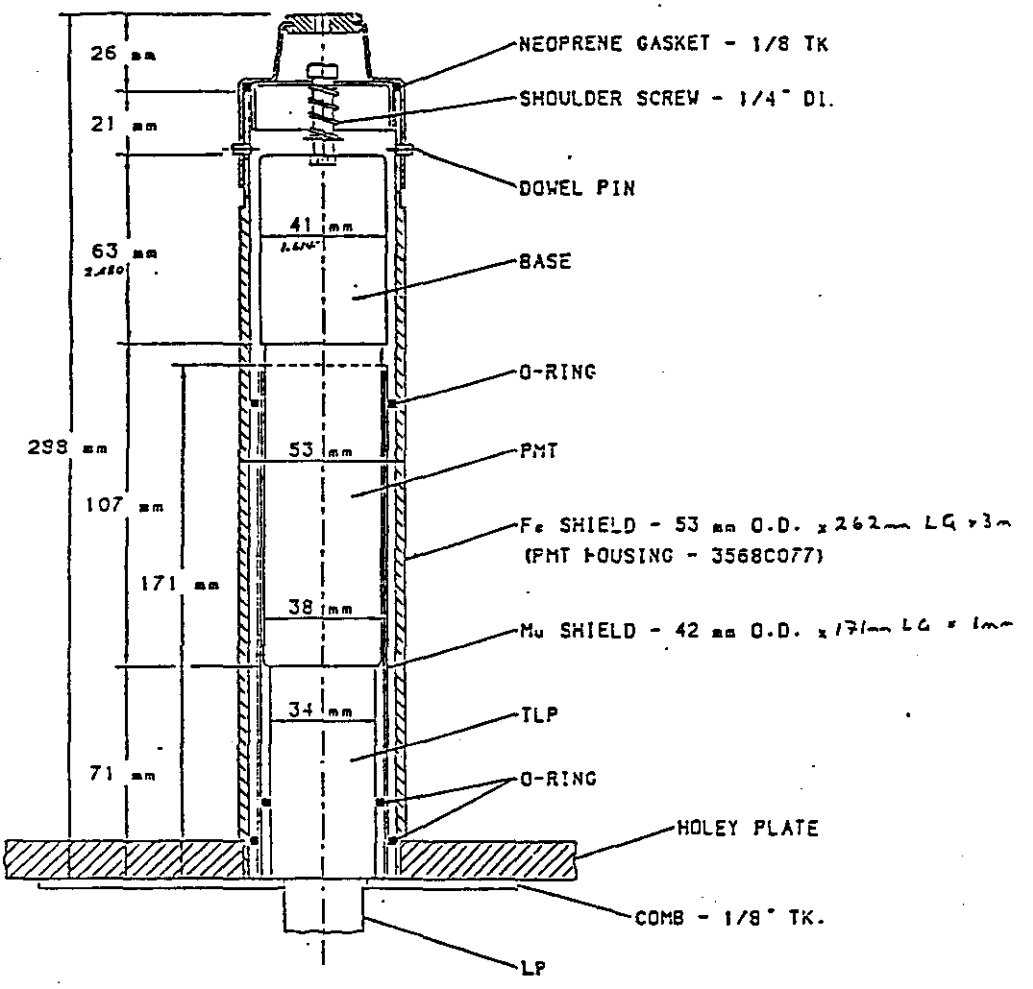

Figure 2-18. ZEUS PMT Magnetic Shield

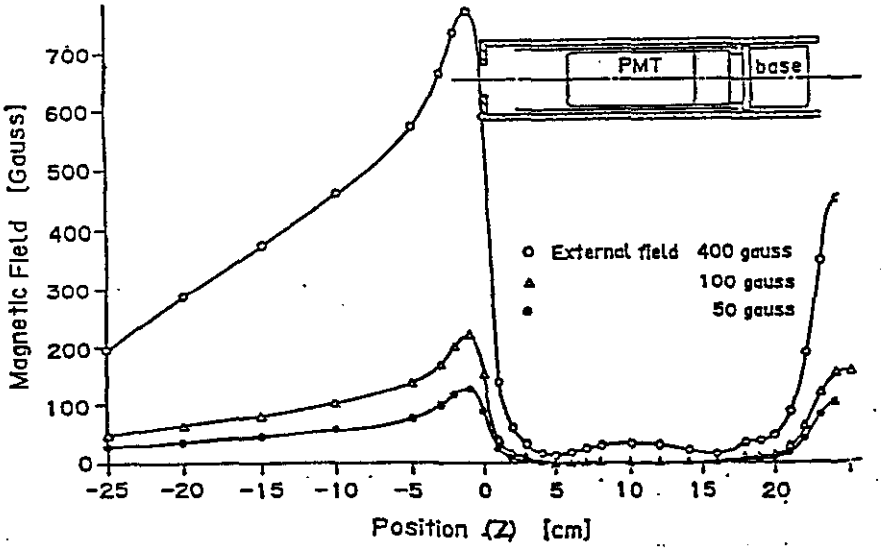

Figure 2-19. Magnetic field at photocathode for shielded PMT in 300 Gauss axial magnetic field

In conclusion, for PMT's to be usable, less than 1% of the magnetic flux from a 2 Tesla solenoid may be returned in the radial region containing the PMT's. Such a condition can be obtained by locating a thick iron flux return ring in front of the PMT's (as is already being considered in the "lead option"). For a pure lead design this thickness is of order 65 cm. However, its thickness can clearly be reduced by incorporating magnetic iron in the calorimeter.

2.2.8 Scintillator Light Yield

It is now well know in the HEP community that scintillator embedded in a high magnetic field produces more light than when in a field free region. The quantitative change is observed to be between 1% and 5%. The CDF group [CDF 443] observed a 1.3% increase in light yield in SCSN-38 at a field strength of 1.5 Tesla. 2.20). Measurements by Jeenicke et al. in organic scintillator, NE-235 [2.7], gave an increase of 1.8 % at 100 Gauss. The ZEUS collaboration report an increase in light yield in SCSN-38 of about 5% in going from 0 to 1000 Gauss magnetic field.[2.8] None of these changes is of serious concern to a calorimeter system with a precision calibration system which also has the capability of in-situ calibration.

Indeed, the typical variation in light yield from variation in scintillator thickness is also up to 5% and contributes only about 1% to the constant term. The sole area of concern for the active calorimetry volume for a scintillator-based calorimeter is the operation of ancillary equipment such as source drive motors. This aspect must be included in the design of such systems once the magnetic field distribution is known.

2.2.9 Compensation

It is desirable to have the e/h ratio close to 1.0 to provide a smaller constant term as well as for better linearity. Experimental evidence [2.8] has demonstrated that this performance can be met and potentially exceeded if either lead or depleted uranium is used as the passive absorber. In addition, it has been demonstrated that such compensating calorimeters achieve excellent resolution (35-45%/$\sqrt{E}$).

However, the best achieved in a calorimeter using iron as the passive absorber is e/h = 1.18.[2.9] Simulation studies carried out at Argonne in the last year confirm this result (Fig. 2-20). Beam tests of iron systems to determine the potential of degrading the electron response of the calorimeter to electromagnetic showers and thereby reducing e/h will be carried out in the spring of 1991 (simulation studies of this issue are presently in progress).

Compensation has not been observed experimentally in calorimeters using iron as the passive absorber. For many years, the best value reported was e/h = 1.18[2-9]. However, more recent work reports a value of e/h = 1.13 in a worse sampling hadron calorimeter using liquid scintillator as the sensitive medium[2-10].

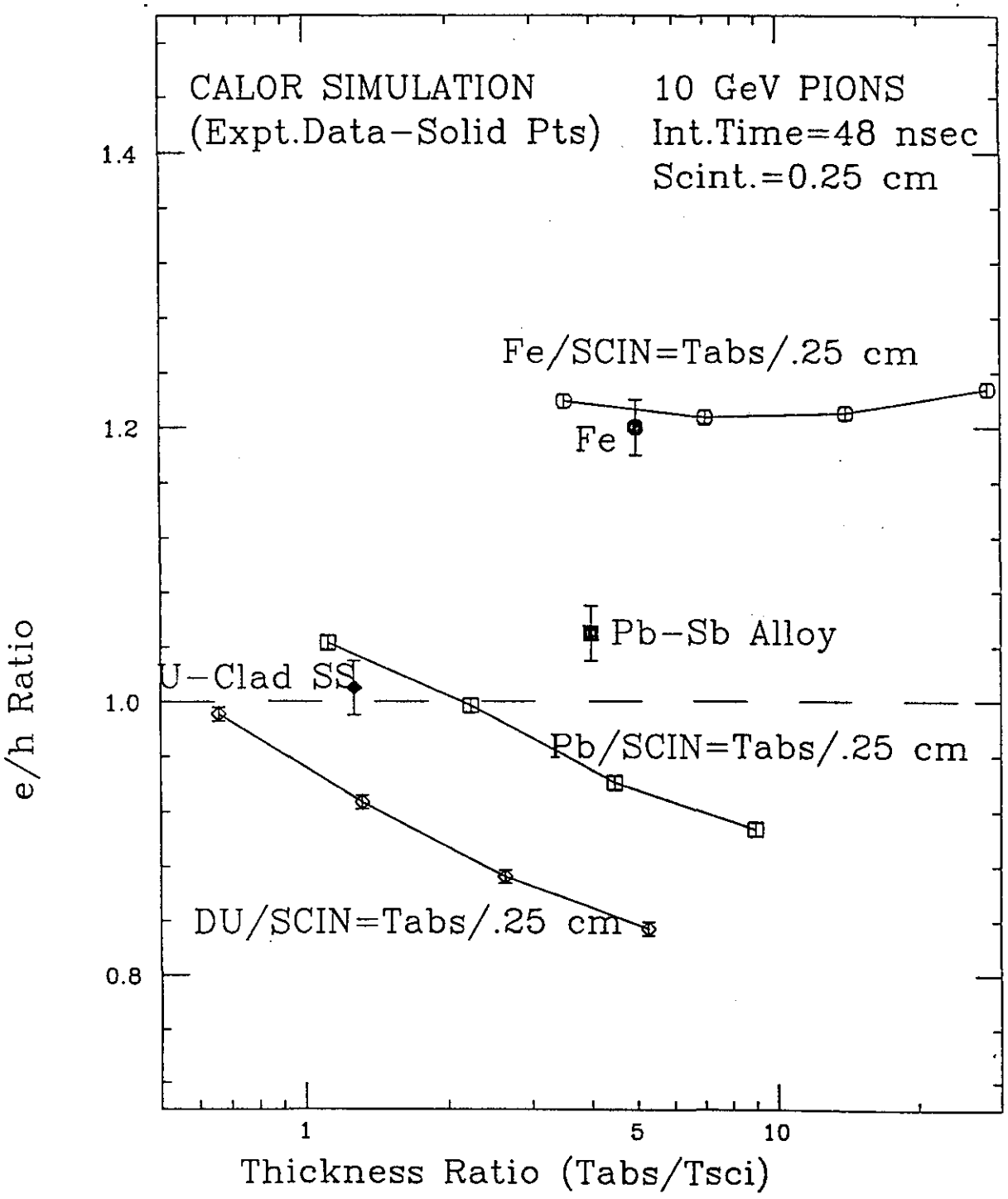

Relative response of electrons to pions (e/h) as a function of absorber thickness and composition for a fixed scintillator thickness of 0.25 cm.

Figure 2-20

2.2.10 Compatibility and Relative Performance

Now the compatibility of each calorimeter with magnet type can be qualitatively examined, case-by-case, taking into account the various effects described above. PMT stands for photomultiplier; MT stands for magnetic transformer; EST stands for electrostatic transformer.

1) Scintillating plate calorimeter with plate wave-length shifters

Barrel	Type-L	compatible, no magnetic field
	Type-I	compatible, no magnetic field
	Type-S	compatible but PMT must be shielded
End	Type-L	light guides difficult because PMT must be behind the flux return.
	Type-I	absorber must be iron, iron percentage?
	Type-S	compatible but PMT must be heavily shielded.

2) Scintillating plate calorimeter with fiber wave-length shifters

Barrel	Type-L	compatible, no magnetic field
	Type-I	compatible, no magnetic field
	Type-S	compatible but PMT must be shielded.
End	Type-L	compatible, PMT must be behind the flux return.
	Type-I	compatible (iron-loaded)
	Type-S	compatible but PMT must be shielded.

3) Scintillating fiber calorimeter

Barrel	Type-L	compatible, no magnetic field
	Type-I	compatible, no magnetic field
	Type-S	compatible but PMT must be shielded.
End	Type-L	difficult since PMT must be behind the flux return.
	Type-I	compatible (iron-loaded)
	Type-S	compatible but PMT must be shielded.

4) Liquid argon calorimeter

Barrel	Type-L	compatible, no magnetic field
	Type-I	compatible, no magnetic field
	Type-S	compatible but MT must be shielded.
End	Type-L	difficult due to cryostat edges, only EST readout,
	Type-I	incompatible due to magnetic force on iron absorber.
	Type-S	compatible

5) Warm liquid calorimeter

Barrel	Type-L	compatible, no magnetic field
	Type-I	compatible, no magnetic field
	Type-S	compatible with EST or shielded MT
End	Type-L	compatible with EST readout
	Type-I	compatible with iron absorber
	Type-S	compatible with EST or shielded MT.

Under the assumption that a single calorimeter technology is used for barrel AND end calorimeters, we can combine the above case-by-case evaluations as follows:

	Type-L	Type-I	Type-S
plate + plate readout	I	C	C
plate + fiber readout	P	C	C
scintillating fiber	I	C	C
liquid argon	I	P	C
warm liquid	P	C	C

(P = possible; I = impractical; C = compatible)

Although the table might be oversimplified, the trends are clear, namely:

1. if Type-L is chosen, the calorimeter technology is limited to two options: plate-fiber and warm liquid,
2. liquid argon calorimeter is compatible only with the Type-S coil,
3. Type-S can be compatible with all calorimeter technologies.

Besides the compatibility-incompatibility matrix, we compared effects of magnet-style dependent issues quantitatively to some extent. They can be summarized as follows :

	Type-L	Type-I	Type-S
calorimeter weight	RW	RB	RB
barrel calorimeter shape	RW	RB	RB
end calorimeter shape	RB	RW	RW
barrel muon system	RW	RB	RB
inner tracking support	RW	RB	RB
access to inner tracker	RW	RB	RB
cabling for inner tracker	RW	RB	RB
material in front of EM cal.	RW	RB	RB
dead space in hadron cal.	RW	RB	RB
magnetic force on calorimeter	RB	RW	RB
field strength in barrel cal.*	0T	0T	< 0.5T
field strength in end cal.*	2T	2T	< 1T

(RB = relatively better, RW = relatively worse)
(* : calorimeter technology dependent)

The table indicates the Type-I and/or Type-S is relatively better in expected performance.

2.2.11 Summary

It has been shown that the calorimeter technology and design is intimately related to the magnet style, and therefore it is difficult to provide any decisive preference on the magnet style at this stage without selecting calorimeter technology. Stated another way, only the choice of the Type-S magnet design leaves open all the potential calorimeter technology options. Type I compromises the choice of liquid argon and Type L is compatible only with plate/fibre scintillator and warm liquid technologies.

Calorimeter compatibility and relative performance were studied by: (1) drawing possible calorimeter configurations, (2) ray-tracing for the study

of inactive materials, (3) estimating resolution degradation, (4) a GEANT simulation and (5) shielding tests on magnetic transformers and phototubes.

Our conclusions can be summarized as:

1. Type-L is compatible with two options: plate-fiber and warm liquid,
2. liquid argon calorimeter is compatible only with the Type-S coil,
3. Type-S can be compatible with all calorimeter technologies,
4. Type-I and -S give relatively better performance than Type-L.

In summary, we recommend either Type-I or Type-S from the calorimetry point of view.

We also note that, in the course of magnet-calorimeter studies, W. Foster, and R. Kephart have noted an effect of magnet coil end of Type-I/S and support structures on the EM calorimetry. Their new proposal is for a variation of the Type-I geometry in which the coil end is placed behind the endcap EM calorimeter. The resulting corner structure is somewhat similar to that of CDF. The impacts on various calorimeter features have not been assessed here due to limited time the since introduction of this new geometry.

References

[2.1] T. Kondo and M. Asai, Ray Tracing Study for Magnet Style Selection, Appendix-C (to this report).
[2.2] M. Strovink, W. J. Womersley, and G. E. Forden, Invited talk at the Workshop on Calorimetry for the Super Collider, University of Alabama, SSC-SDC-14, 1989.
[2.3] Proceedings of the International Workshop on Solenoidal Detectors for the SSC, KEK, April 23-25, 1990, pp. 360-365, Appendix-2.
[2.4] J. M. Hauptman, Coil Effects on the Calorimeter, Proceedings of the International Workshop on Solenoidal Detectors for the SSC, KEK, April,1990, Appendix-C.
[2.5] I. Horvath et al., Magnetic Transformers for the SDC, SDC-1990-69.
[2.6] ZEUS 1989 Status Report.
[2.7] NIM 126, (1975) 459.
[2.8] ZEUS Status Report 1989.
[2.9] NIM 180 (1981) 429.
[2.10] Univ. of Rochester Preprint, UR-1142, 1990.

2.3 Magnet-Related Tracking Considerations

Momentum resolution and pattern recognition are the major items related to magnet types, since they are the primary role of the tracking system. A Type-L and Type-I magnet provides almost uniform magnetic field in the entire tracking volume, whereas the Type-S magnet has a non-uniform field. Therefore, here we discuss and evaluate the effect of a non-uniform field relative to a uniform field (Type-L) case.

There are several options for the tracking detector system, however, the non-uniform field effects on track finding and fitting are common to any tracking system, although the details of operation in a non-uniform field might depend on the detector. Therefore, we will discuss these two aspects with a simple model tracking system in the following sections. The results should apply for any type of detector. Some of the detector specific effects will be discussed in the section 2.3.3.

2.3.1 Momentum Resolution

The effect of a non-uniform field on the momentum resolution or track fitting is divided into two issues: A) Can the correct momentum be obtained by track fitting for a non-circular trajectory in an inhomogeneous field? B) How large is the degradation of resolution due to the lower magnetic field at edge of the coil?

A) It is possible to achieve accurate track fitting no matter how inhomogeneous the field is, once the magnetic field map is precisely known. This technique has been developed in bubble chamber and fixed target experiment data analyses. The procedure may be complicated and time consuming depending on the magnetic field and the precision one wants. In fact it is reported that the non-uniform field in ZEUS has resulted in an increase in software development time. However, it would appear that the increased CPU time required for track fitting would be small compared with pattern recognition and it would not increase the total CPU time much in the SSC case.

For the solenoid type magnet, a fast method used at TRISTAN by the AMY experiments called IMFIT[1] can be applied. Starting from a circular track, IMFIT refits the track with the trajectory function including a correction for the inhomogenious field which is written analytically with some approximation. The difference between a circle fit and the IMFIT result in the S-type magnet case is shown in Fig. 2.3.1-1. Not surprisingly, at large rapidity the non-uniformity will be important.

B) Even if the track fitting is done perfectly, the momentum resolution will be worse for the Type-S magnet than the uniform field case because of the lower magnetic field. The momentum resolution in the Type-S field has been calculated analytically for high P_t tracks using a parameterized magnetic field.[2] For a high momentum particle with initial direction in x-z plane (take z-axis along beam direction), the y position at a given x is written as follows

by solving an equation of motion;

$$y = \frac{q}{p} \int_0^x dx' \int_0^{x'} dx''(B_z - B_x \cot(\theta))$$

where q is the charge of the particle, and θ is the polar angle of the particle. Note that the y position is proportional to the double integral of the magnetic field. Allowing the trajectory to have a non-zero y and y' at x=0, one can fit measured hit points by

$$y = \delta + \phi x - \frac{1}{2} cI(x,\theta)$$

$$I(x,\theta) = \frac{2}{B_0} \int_0^x dx' \int_0^{x'} dx''\left(B_z - B_x \cot\theta\right)$$

where ϕ and c are the parameters to be determined by the fit. c is the curvature at x=0 and related to P_t by $c = qB_0/P_t$. B_0 is the magnetic field at x=0. Since the fit function is linear in the parameters, the fit can be done by matrix calculation and the error of the parameter is given by the error matrix which is written using measured positions, position resolutions, and $I(x,\theta)$. The double integral $I(x,\theta)$ is calculated by parametrizing the Type-S field as

$$Bz(r,Z) = B_0[1 + a(r^2 - 2z^2) + b(r^4 + 8z^4/3 - 8r^2z^2)]$$

$$Br(r,z) = B_0[2a\ rz + b(-16z^2/3 + 4r^2)rz]$$

$$a = 6.91 \times 10^3,\ b = -3.29 \times 10^4$$

This parametrization reproduces a Type-S magnetic field within a few percent over the entire tracking volume as shown in Fig. 2.3.1-2. and is good enough for the present study. The pixel/Silicon-strip/wire-chamber system is chosen as a model for the calculation. The length in the z direction is (artificially) extended to cover the intermediate tracking region (up to $\eta = 2.5$) listed in Table 2.3-I.

Table 2.3-I: Geometry of the tracking device used in calculation.

Element	r_{in}(m)	r_{out}(m)	Z max	Layers	Sigma resolution (μm)
Pixel	0.05	0.10	0.4	2	10
Silicon	0.21	0.42	3.0	8	15
wires	0.71	1.81	4.5	64	150

The results are shown in Fig. 2.3.1-3 and they are summarized in the following table.

Table 2.3-II. Resolution effects of nonuniform field.

Element	Vertex Constraint	dp/p2 (%/TeV) (|h| >1.5)	Type-S/Uniform
Pixel/Silicon/wire	No	9- 63	1.2-1.3
Silicon/wire	No	15-120	1.3-1.4
Wire only	No	57-200	> 2.0
Pixel/Silicon/wire	20 mm	9- 60	1.2-1.3
Silicon/wire	20mm	10- 64	1.2-1.3
Wire only	20 mm	16-200	1.3-2.0

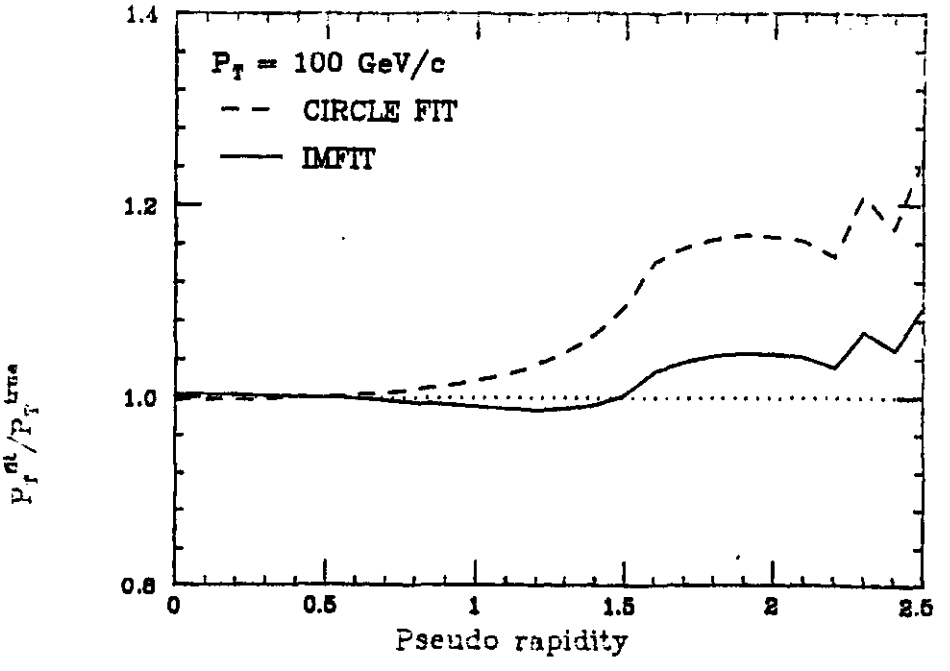

Fig. 2.3.1-1 The difference between a simple circular fit and the IMFIT result. The dashed line is the circle fit.

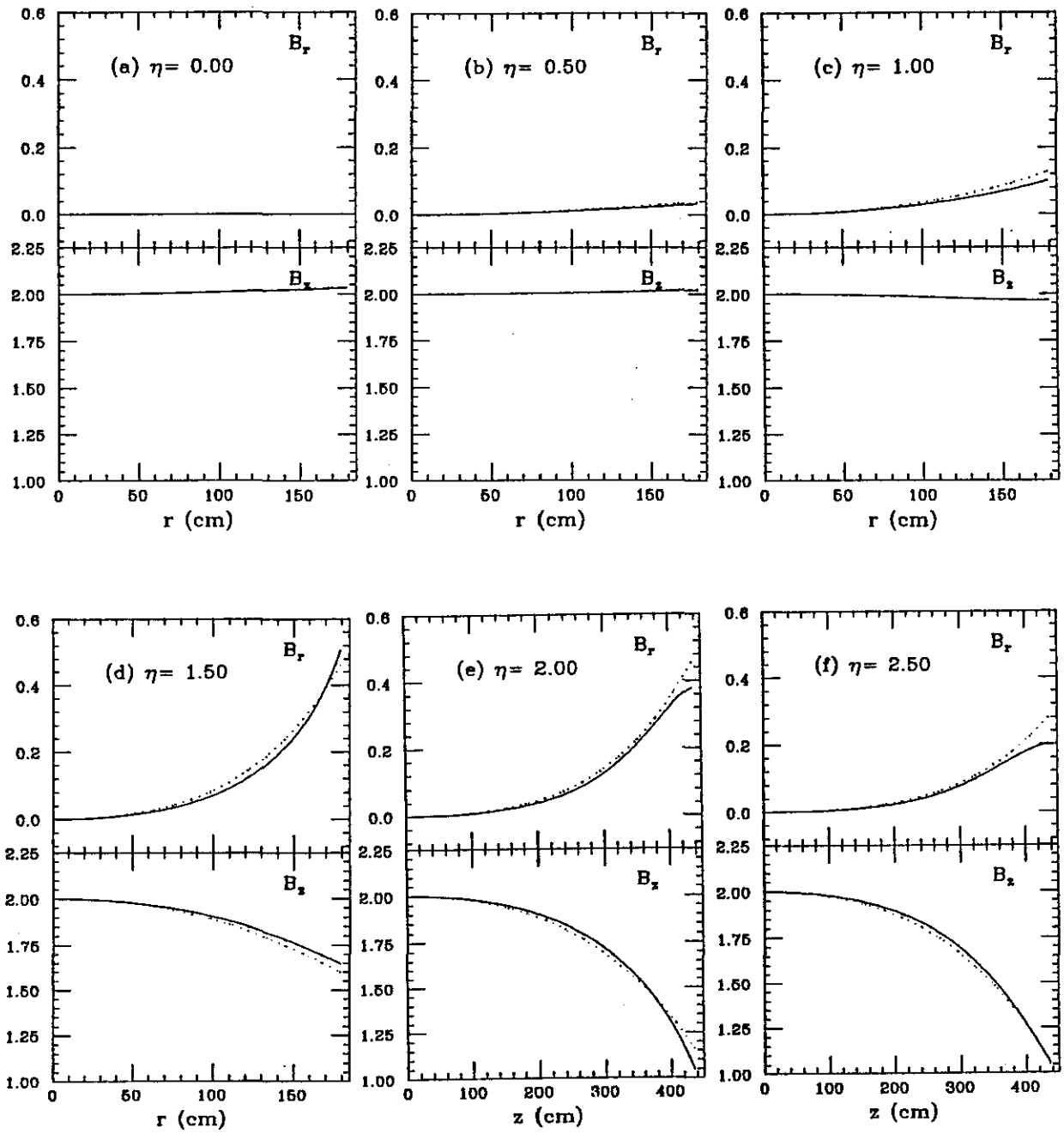

Fig. 2.3.1-2 Comparison between the parameterized global fit and the S-Type field (dots).

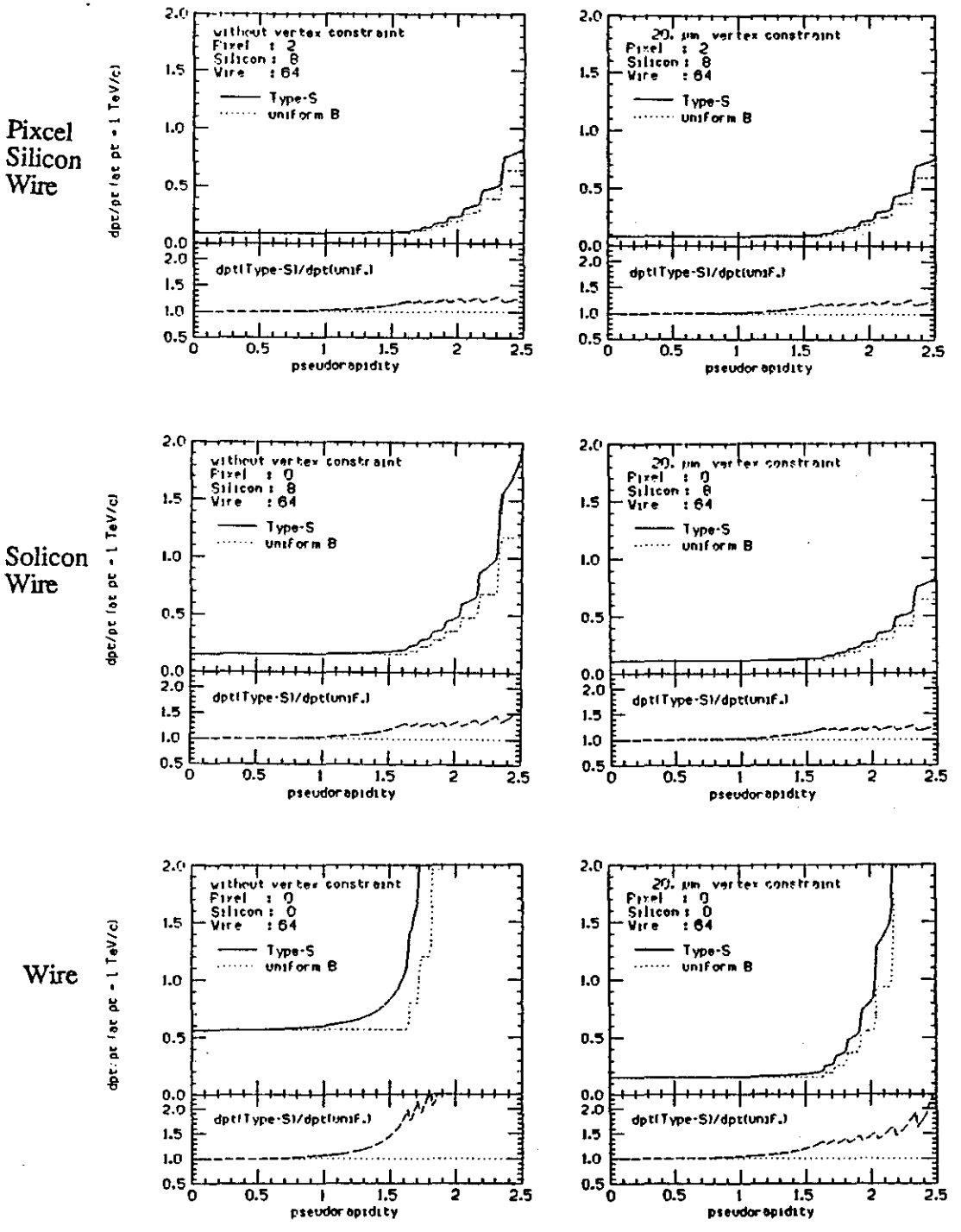

Fig. 2.3.1-3 The momentum resolution in the S-Type coil obtained with three different tracking configurations. The vertex constrained fits are on the right. The lower plot in each figure compares the resolution to that obtained in the L-type coil.

2.3.2 Pattern Recognition

Pattern recognition in the tracking system will be one of the challenges at SSC since very high multiplicity and density of tracks are expected. Most of proposed options for SDC tracking system have a super-layer structure. To take advantage of the super-layer structure, most commonly used algorithms find track segments (vectors) within super-layers and then link them into tracks. No difference is expected in track segment finding between Type-S and uniform field cases since the effect of non-uniformity in a small local area is negligible. The effect of the non-uniformity would appear in the linking and fitting stage of track finding. The simplest segment linking algorithm is to calculate the curvature C and initial azimuthal angle, ϕ, for each track segment assuming circular tracks (i.e. in uniform field) coming from origin, and then finding clusters of segments in the c-ϕ plane. Fig. 2.3.2-1 shows the deviation of ϕ calculated from a vector at position r in the Type-S field for P_t = 10 GeV tracks with various η. Systematic deviations are seen for large eta as expected, however, these are small or at most comparable to the errors due to the position resolution of the detector as shown in the figure. These deviations are proportional to $1/P_t$, therefore this is not a problem for high P_t tracks, but could be a problem for very low P_t tracks. If one uses a more clever algorithm, for example, linking segments with one in adjacent super-layer in turn, then the effect of non-uniform field will be even smaller.

The pattern recognition with straw tubes in the Type-S field has also been studied using a simulation program[3] for track finding. The ACE[4] program used in TRISTAN AMY detector is applied to SDC straw tubes. For this study, only the first stage of the ACE program is applied, i.e. finding tracks in r-phi plane using axial layers only. In order to apply ACE directly, 4 axial super-layers (#1,3,5,7) are reassigned as 8 super-layers with 4 layers each, since the AMY CDC has only 3-5 layers in one super-layer. ACE uses the same algorithm described above. Fig. 2.3.2-2(a) shows the hits in straw tubes and reconstructed tracks for a top-pair event in the Type-S magnet. In Fig 2.3.2-2(b) the correspondence of original and reconstructed tracks in c-phi plane is shown. The reconstructed track points are shifted from the original because the tracks are fitted with a circle, but it does not appear to be a substantial problem for track finding. This shift can be corrected by a further elaborate fit as discussed in the previous section. Fig. 2.3.2-3 shows the corresponding plots for the Type-L case. As can be seen, the effects are comparable to measurement errors. The comparison of CPU time and number of reconstructed tracks is shown in Fig. 2.3.2-4 for the Type-S and Type-L magnet case for top-pair events where one top decays into e + ν + jets. No significant difference is seen. Fig. 2.3.2-5 compares the reconstruction efficiency for Type-S and Type-L cases. Again, no significant difference is seen.

The pattern recognition in the silicon system has been studied by J. Matthews.[5] In a similar manner to the previous pattern recognition study, he examined a two-dimensional scatter plot of track parameters to look for clustering of superlayer information from each track. In this study the forward region was examined by calculating the helical track parameters f' and k/tan λ As in the previous study the superlayer structure of the forward silicon system allows an independent calculation of the two parameters, which should then

cluster for the same track. The nonuniform field, multiple scattering and intrinsic measurement resolution will spread these clusters for any one track. These effects are shown in Fig. 2.3.2-6a,b,c,d. It is hard to tell the difference between the effects of the type-S coil (b) and multiple scattering (d). In order to make this more quantitative the spread of points for each track has been calculated as a function of momentum in Fig. 2.3.2-7a,b,c,d. For each momentum the rms spread of the parameters for each track has been normalized to s_k, the intrinsic measurement error. The figures also show the effects of shifting the interaction point by 500 microns. It appears that above 10 GeV the effects of nonuniform field on pattern recognition are small. However, for 2 Gev tracks the pattern recognition broadening is twice the size of multiple scattering effects.

Our conclusion is that one would not be seriously handicapped by the non-uniform field of the Type-S coil, however, it is clear that the capability of the detector has been reduced. Momentum resolution will be worse by 20%-30% for η greater than about 1.2, pattern recognition will be harder at low momentum, and detailed work on field mapping and track fitting would be needed.

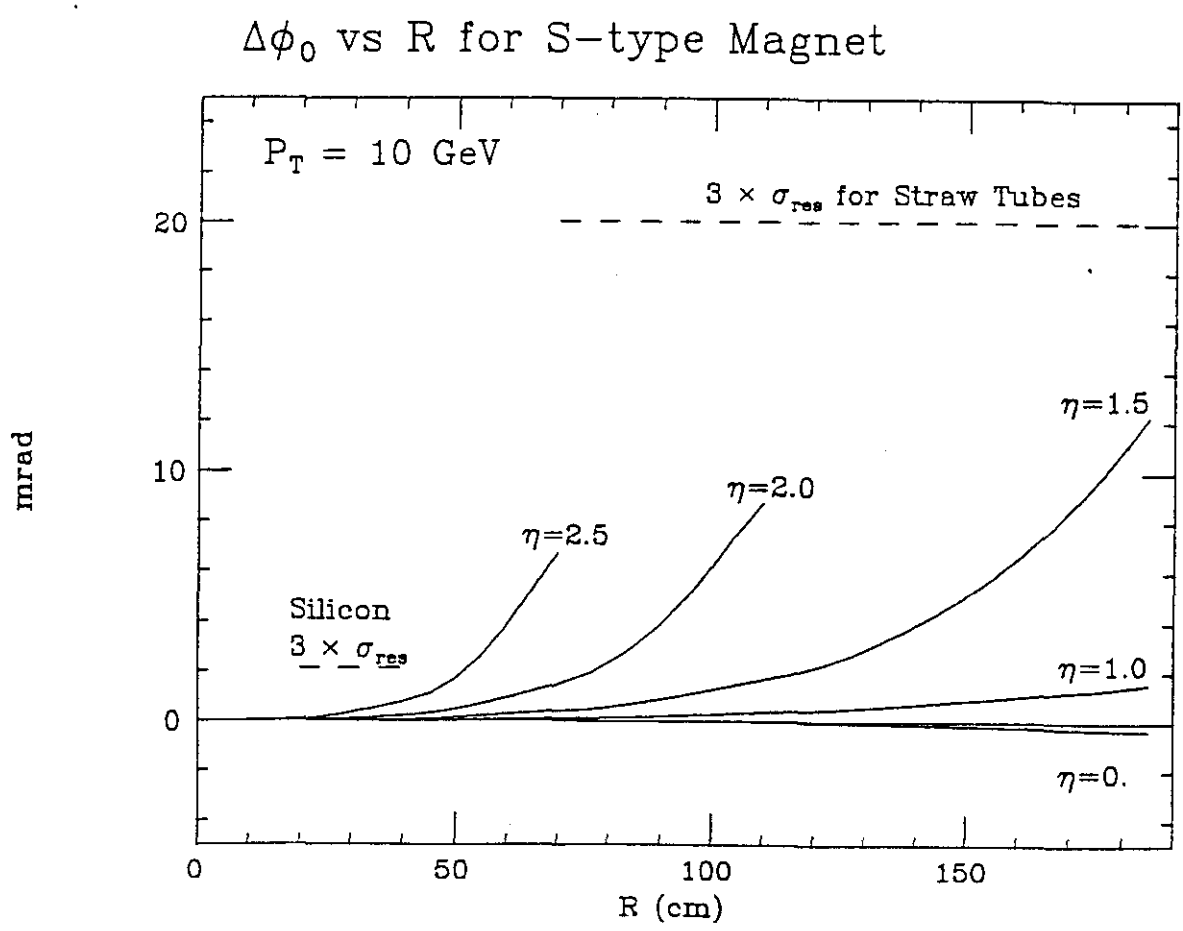

Fig. 2.3.2-1 The error in calculating the initial azimuthal angle of a track as a function of the radius and eta of the super layer for a nonuniform Type-S coil.

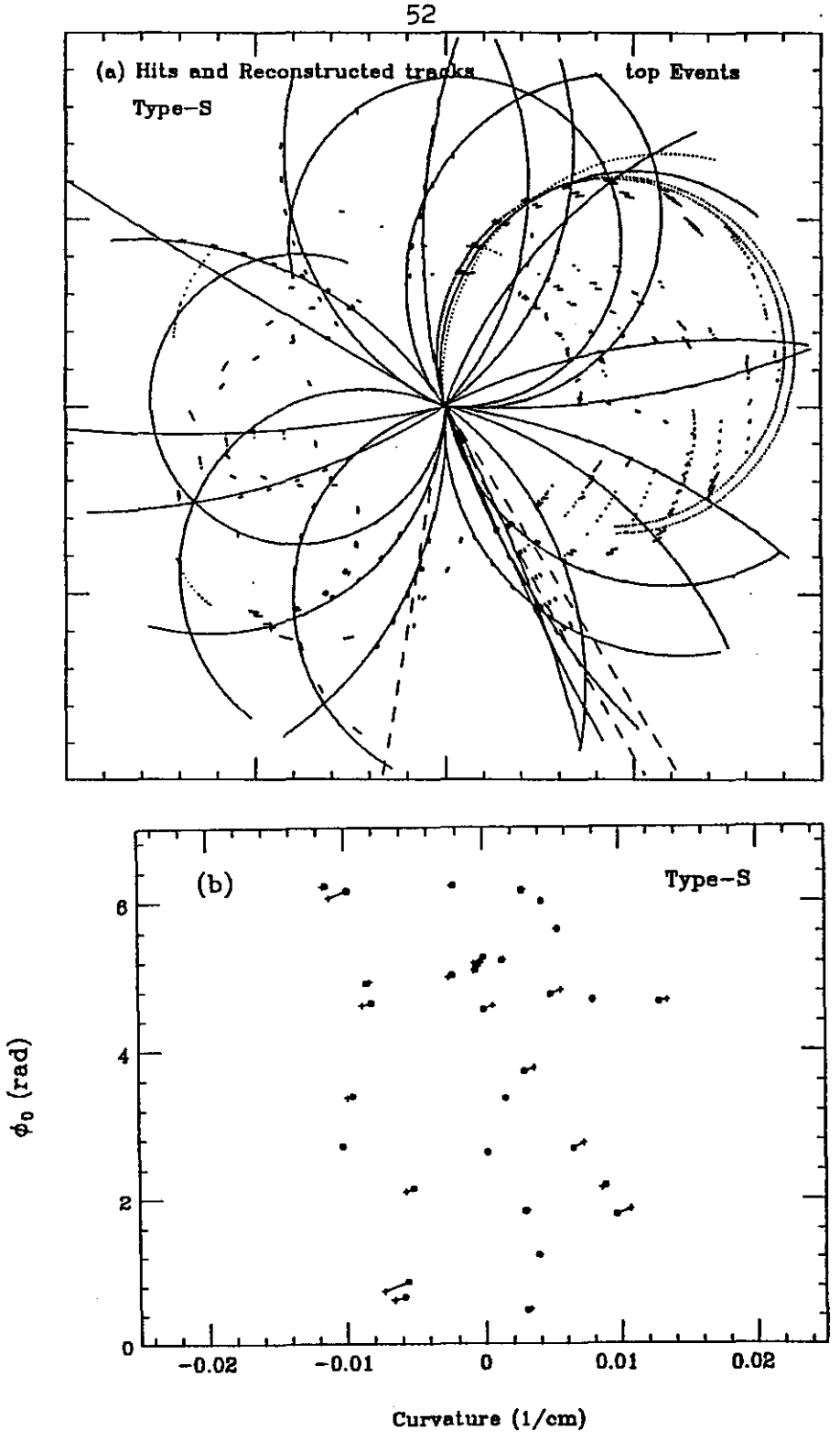

Fig. 2.3.2-2 a) An event in the Type-S magnet. b) The shift of the track points from the original to the reconstructed is shown in this two-dimensional plot of ϕ, curvature.

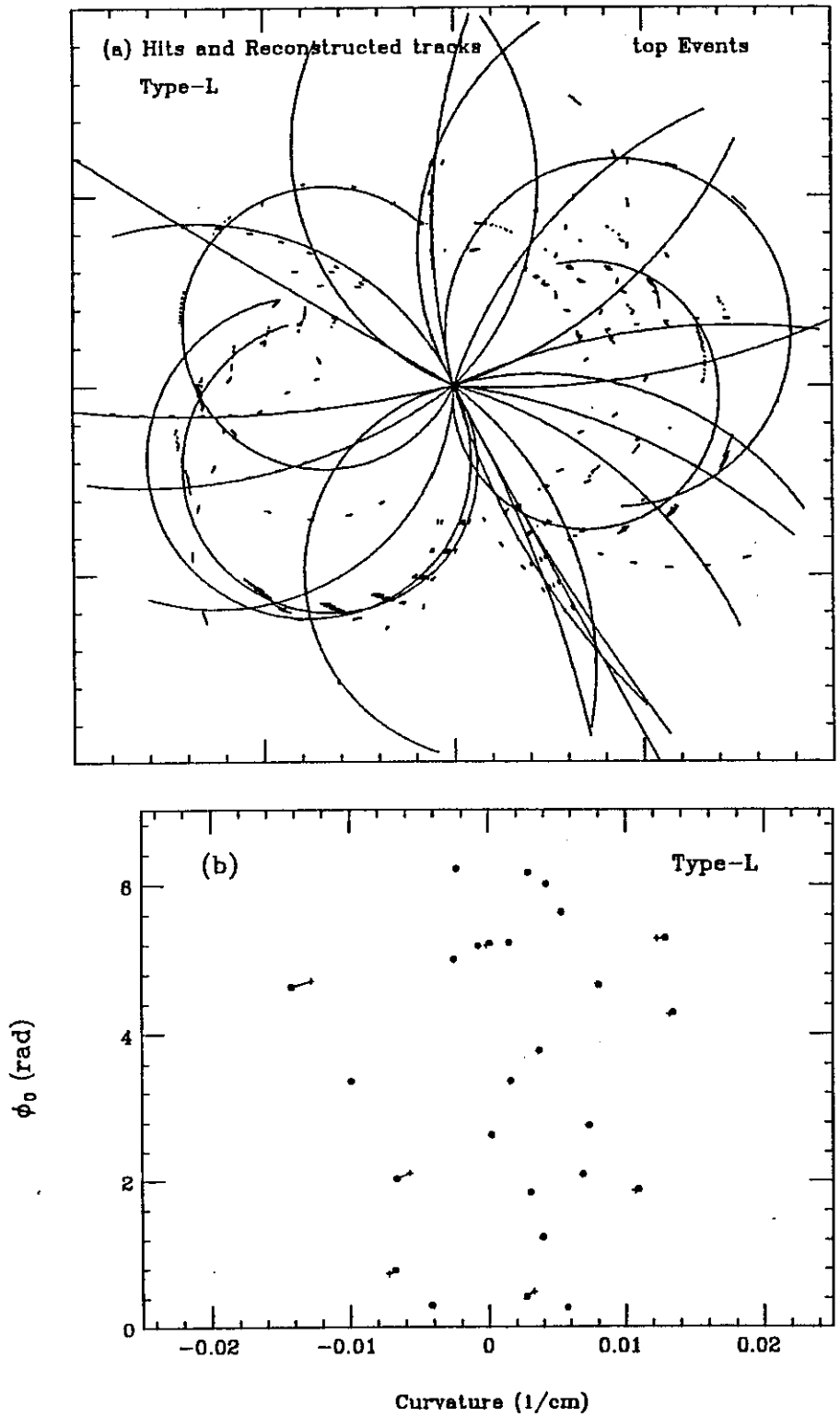

Fig. 2.3.2-3 a) An event in the Type-L magnet. b) The shift of the track points from the original to the reconstructed is shown in this two-dimensional plot of ϕ, curvature.

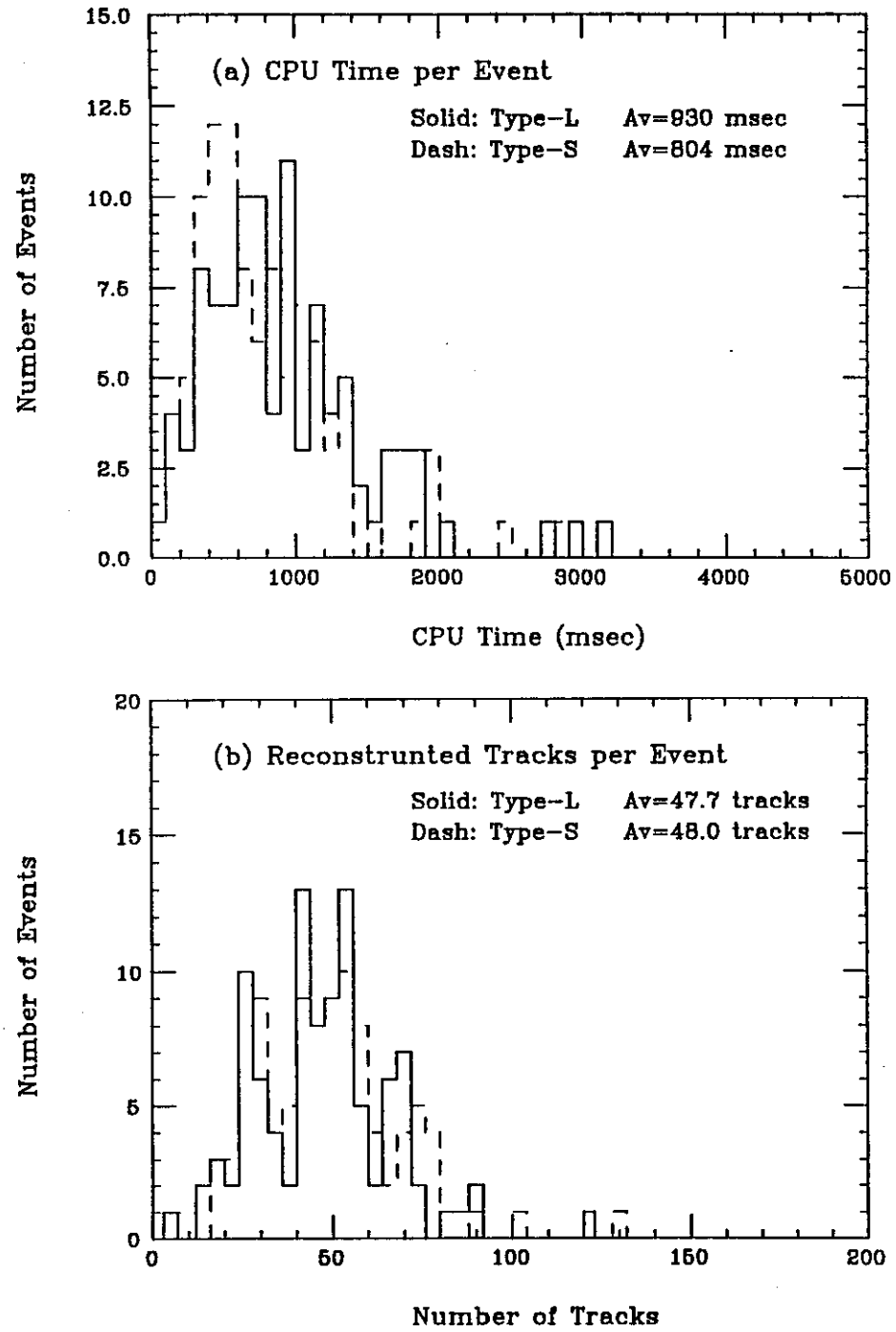

Fig. 2.3.2-4 A comparison of CPU times and numbers of reconstructed tracks for the Type-L and Type-S coils.

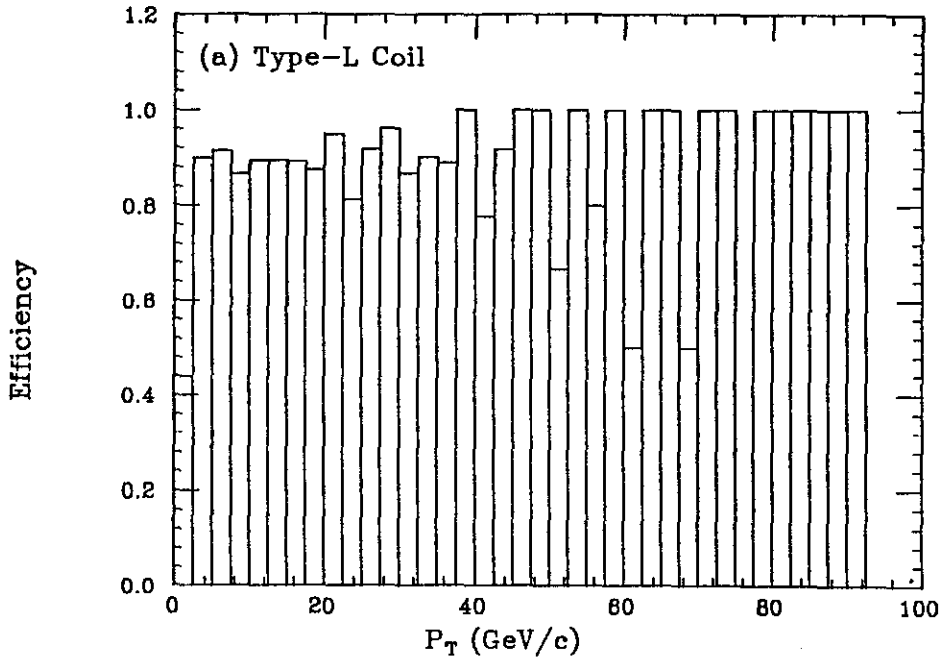

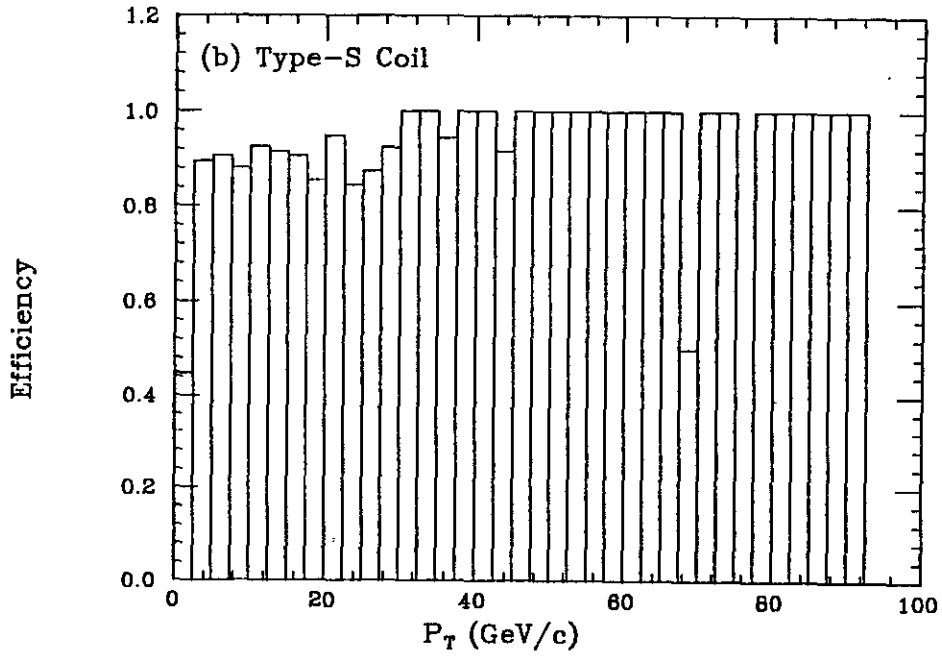

Fig. 2.3.2- 5 A comparison of reconstruction efficiency: (a) for the Type-L coil and (b) for the Type-S coil.

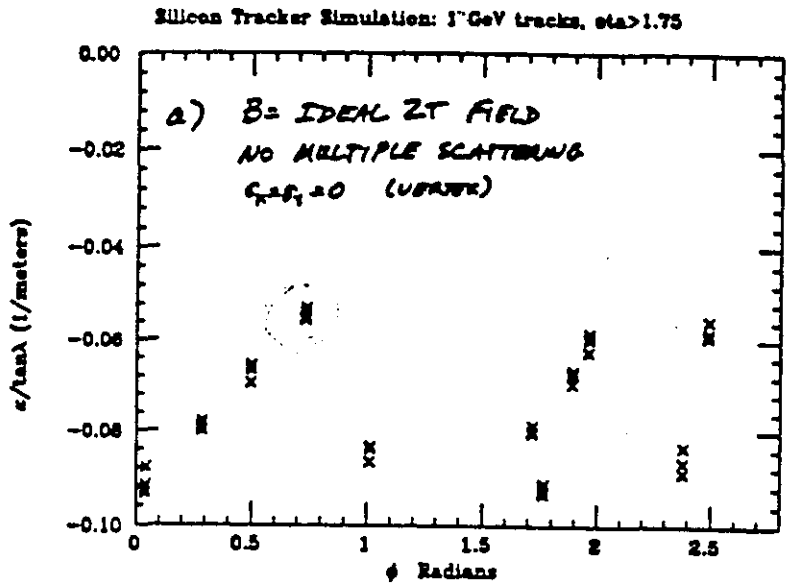

a

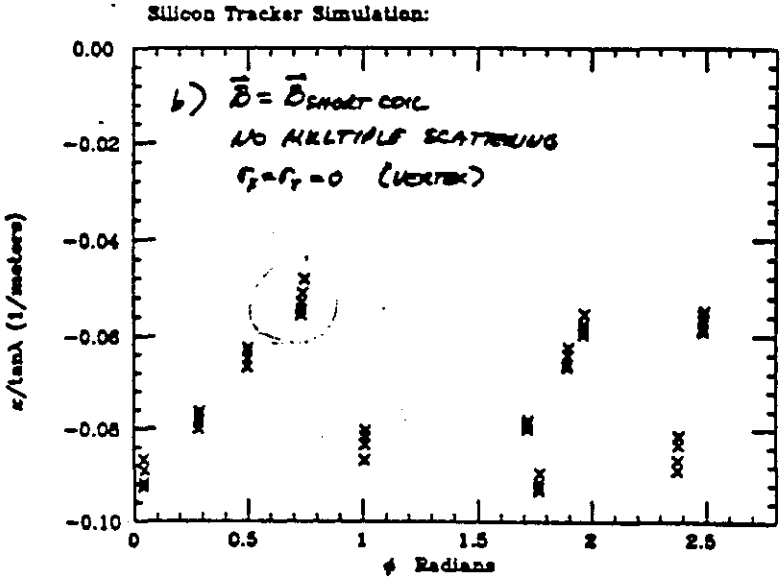

b

Fig. 2.3.2.-6 a,b Silicon superlayer measurements of k/tanλ versus φ for P_t = 1 GeV tracks with h > 1.75 as simulated in the forward silicon planes: a) an ideal magnetic field with not multiple scattering, b) Type-S coil with no multiple scattering.

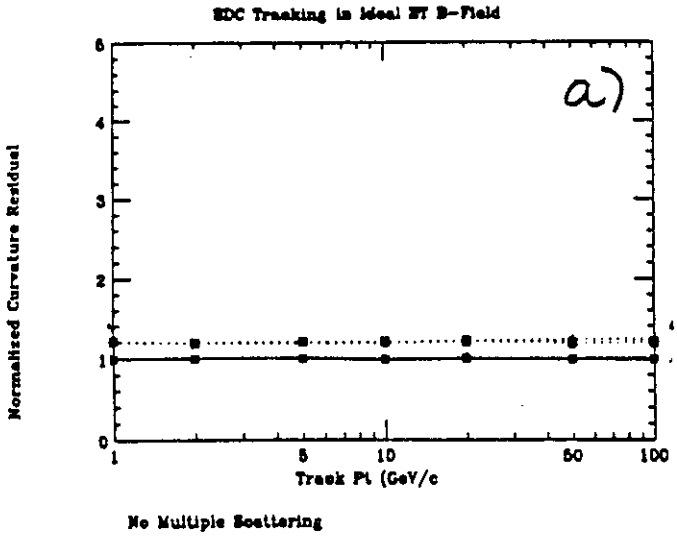

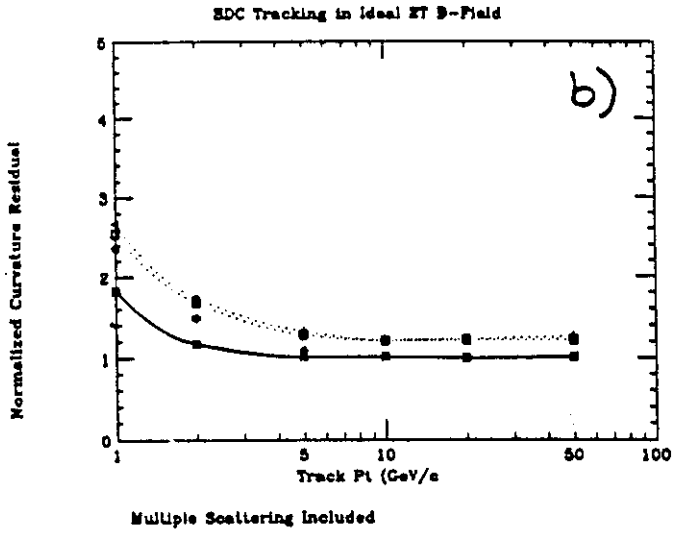

Fig. 2.3.2-7a,b Super layer measurements of (k(simulated)-k(true))/S_k shown as a function of the track P_t as simulated in the SDC tracking system. The dotted line connects the results for the forward silicon planes in the intervals $1 < \eta < 1.75$ and $1.75 < \eta < 2,5$; the solid line connects the results for the axial large radius tracking system $0 < \eta < 1.75$. The unconnected points are from the axial silicon system for $0 < \eta < 1$. a) Ideal magnetic field with no multiple scattering. b) Ideal magnetic field with multiple scattering.

2.3.3 The Judgement Matrix

In order to quantify our judgment of the effects on tracking of the different coil options, there are detector specific items that should be mentioned.

a) Nonuniform field effects on detector elements.

The silicon and sci fi systems are inherently insensitive to the magnetic field nonuniformities. However the straw tubes will be affected by field variations. The drift time of the straw cell will vary as the field changes, however, given the z position of the track, this can be corrected for in the track fitting. A potentially more serious problem which turns out to be negligible, however, is a change in the electronic trigger due to the variation of the drift time at different positions along the straw. This is shown in Fig. 2.3.3-1. The field at z = 0 is 2.0 T, while at the end of the outer straw system (z = 4.0 m, r = 1.85) the field components are Br = 0.8T, Bz = 1.6T, |B| = 1.8 T.

At z = 0 the drift time contours are circles, and the maximum drift time is 30 ns. In the nonuniform region near the end of the straw, the drift time contours varies from 25 to 28 ns at the 2mm radius. These are shown in Fig. 2.3.3-2 . However, this will have only a small effect on the trigger for reasonably stiff tracks since they will be entering nearly radially and the worst case shift of maximum drift time will be about 2 ns. This should have little effect on the trigger electronics.

b) Cable space.

All the potential tracking systems will have cables or fibers that must exit from the tracking volume. The possible cable routes have been shown in Fig. 2.3.3-3 a,b. The long coil presents the longest cable runs. The sci fi system would possibly suffer the most degradation from these longer runs, but all systems would like to keep cables short in order to maintain signal risetime. The parameters are shown in Table 2.3.3-I.

Table 2.3.3-I Cabling requirements for detector elements.

Detector	Area of Cabling Each End	Minimum Size Constraint	Type-L Cable Length	Type-S,I
Silicon	about 1130 cm^2	10 cm diameter pipe	10m-14m	6m-8m
Sci Fi	2500 cm^2	2 cm thick ring at 185 cm radius	8m-11m	3m-6m
Straws	900 cm^2	1 cm ring at 185 cm radius	8m-12m	4m-6m

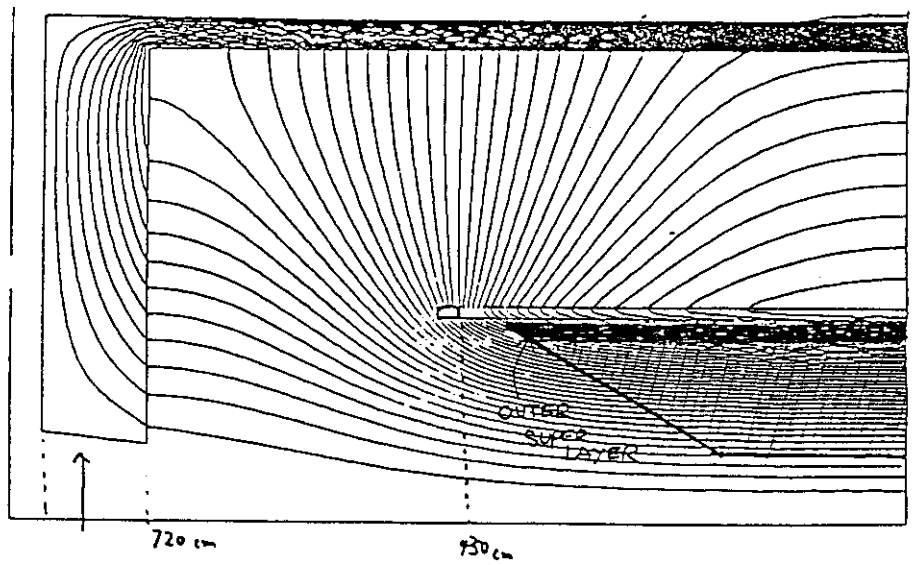

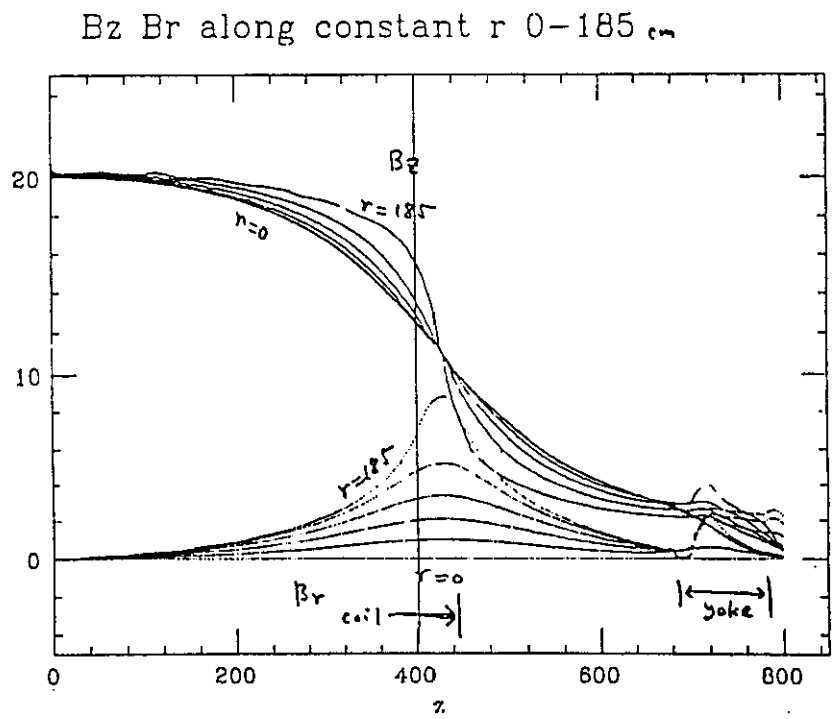

Fig. 2.3.3-1 a) The S-Type coil field configuration in the region of the outer super layer. b) The radial and z field components as a function of r and z.

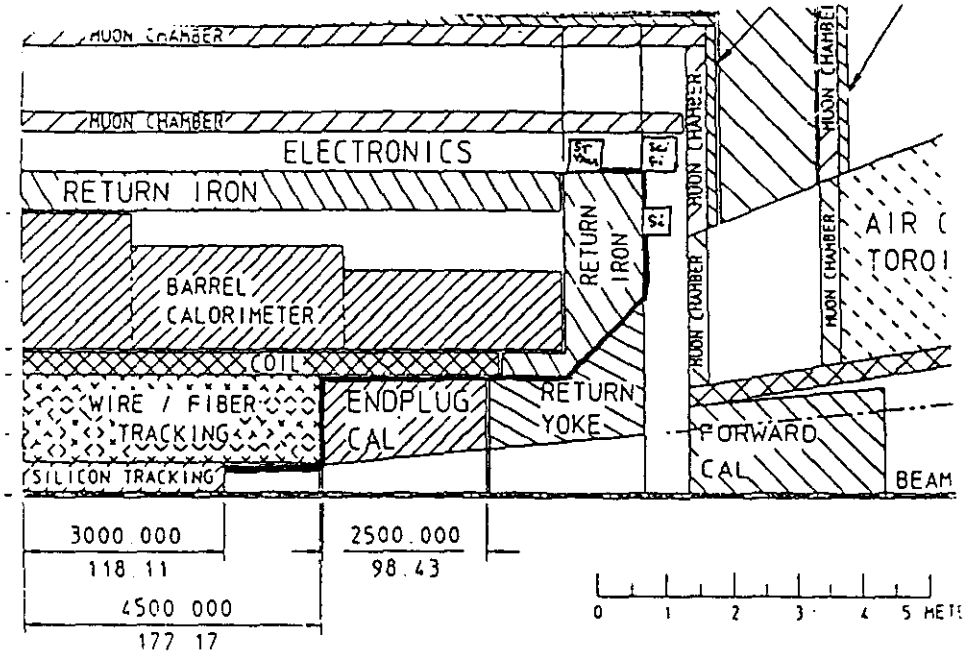

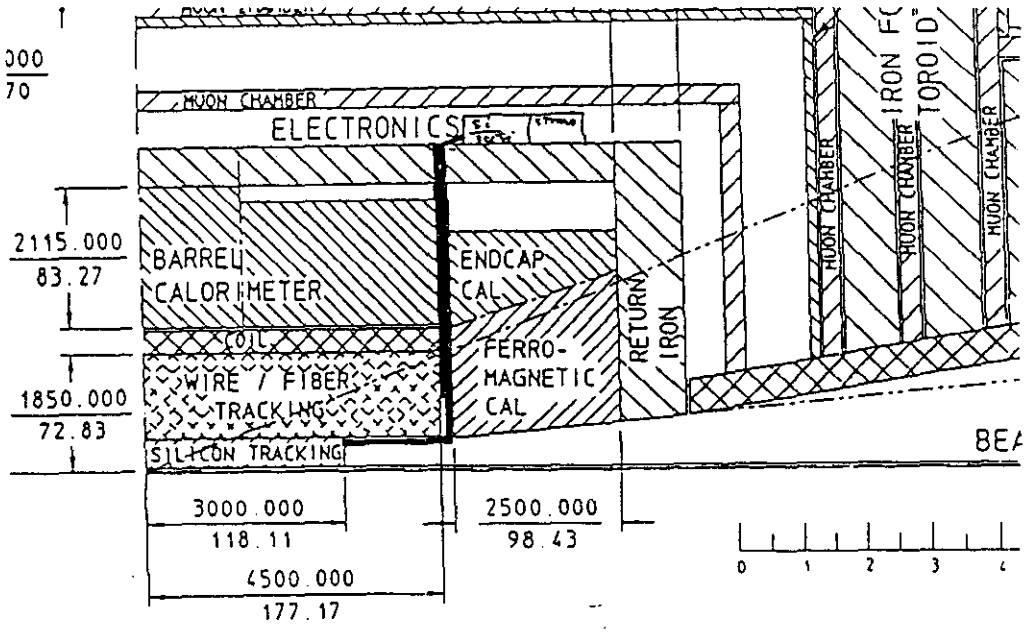

Fig. 2.3.3-3 Possible cable routes for the tracking system for a) the Type-L coil and b) the Type-I or Type-S coil.

1 K. Ueno, 'Tracking in an Inhomogeneous Solenoid', submitted to NIM; Y. Takaiwa, in Proceedings of the International Workshop on Solenoidal Detectors for the SSC, p164, KEK Report 90-10 (1990)}

2 H. Iwasaki, JSD Note 1990-48.

3. Takaiwa, JSD Note 1990-49.

4 ACE (AMY CDC Event Analysis) is a first stage tracking program which gives track seeds to a subsequent elaborated track finding/fitting program called DUET adopted from CLEO. See T.Mori, Ph.D Thesis, Univ. of Rochester (1988).

5 J. Matthews, "Effects on Non-uniform Magnetic Fields on SDC Central Tracing SNOWMASS- 1990.

2.5 Magnet-Related Muon System Considerations

The precision measurement of muon momentum is done with the use of the inner tracker in the barrel region. Therefore effects due to magnet style are the same for the inner tracker. However, in the end region (1.5 < eta < 2.5), one cannot expect high momentum resolution from the inner tracking system in any of the magnet styles due to insufficient field integral traversed. Thus the muon momentum measurement depends solely on the forward muon toroid system; here the solenoid style has little effect regardless of the specific details of the muon toroid system in the endcap region.

It has been pointed out by G. Feldman that the muon momentum can be much improved if the central solenoid trackers and the outer muon trackers are used simultaneously for track fitting[1]. This is due to the presence of a long field free region between two tracker systems which provides a useful geometrical lever arm in the measurement that strongly improves the resolution at high momentum. In the case of the Type-S solenoid, however, some percentage of the magnetic field returns in the "field free" region, and as a result, some of the momentum resolution benefit could be lost.

S. Odaka has examined the magnitude of this resolution degradation with the use of a semi-analytic[2, Appendix 1]. Under the high energy approximation, he uses a matrix inversion method of 13 parameters to calculate the momentum resolution. The multiple scattering effects in the calorimeter as well as flux return yokes are included in this calculation. A magnetic field of 1.8 T in the muon iron toroids is taken into account in the calculation. G. Feldman's results are reproduced with this method. The estimate of momentum resolution is separately done for two rapidity regions in order to avoid complications due to the existence of many detector edges.

Figure 2.5-1 shows the estimated momentum resolution for P_t = 1 and 5 TeV/c muons. We can see that the degradation due to non-uniform magnetic field in the Type-S solenoid is very small and practically negligible (~ 10%) in the central region. In the forward region, the magnitude of degradation is ~ 20% for 1 TeV/c and ~ 60% for 5 TeV/c muons. However, P_t = 5 TeV/c at eta ~ 1.5 corresponds to an absolute momemtum of ~ 10 TeV/c, this represents an extremely rate case even at SSC.

In summary, the possible degradation of the muon momentum resolution due to Type-S non-uniform magnetic field is small in the central rapidity region. In the forward region, it is an order of ~ 30% at 1 TeV/c.

[1] G. Feldman, talk at Snowmass '90.
[2] S. Odaka, Momentum Resolution for Muons Using the Full Tracking System of SDC, SDC-90-00074 and Appendix 1 (included here as Appendix E).

COST CONSIDERATIONS

3.1 General Remarks

The cost considerations associated with choosing among the three coil styles discussed in this report can be conceptually divided up into three categories:

1) costs specifically connected to the coil and its cryogenic system;
2) cost of systems strongly affected by the magnet style choice (calorimetry);
3) costs of systems weakly affected by the choice of magnet style (tracking muon system, triggering).

Of these, the costs in category 1) are the only ones that are well enough known that specific cost comparisons can be made and used to decide among the style choices. In the case of calorimetry, a useful comparative model has been made for a scintillator plastic calorimeter, but equivalent comparative models for the liquid argon-based calorimeters are not not available. Likewise, specific comparative cost models for central and intermediate trackers or for muon trackers are not available yet. In both these cases, it is expected that the cost dependences will be relatively weak but will slightly favor the shorter Type-S or Type-I models over the Type-L arrangement.

3.2 Magnet Coil and Cryogenic Support System

The costs of superconducting solenoids built to date can be roughly scaled by the 3/4 power of their stored energy. A useful normalization point is the 30 MJ CDF solenoid built by Hitachi Ltd. of Japan in 1984 for a price of ¥ 600 M. Accounting for translation into U.S. dollars and for relevant inflation factors, this would give a cost of $4.0 M in 1990 dollars.

In Table 3-1, we compare the stored energy and estimated costs of the three magnet types presently under consideration for the SDC solenoid. Note that significant R&D costs are associated with each of the magnet styles, but that these represent only about 10% of the magnet cost in the case of Types I and L, but rise to nearly 40% in the case of Type-S, reflecting the technical uncertainty associated with the much stronger compressive forces in the S-coil and the need to demonstrate a safe coil/bobbin locking design.

$18K/Ton for LA calorimetry to characterize the magnitude of the costs and cost differentials in this type of comparison.

Table 3-2
Comparative Calorimeter Weights and Costs*
for 4 Models of SDC Coil Types

Case	Weight (Tons)	Cost/Ton ($K/Ton)	Total Cost ($M)
1 - Type-L/non-LAC	4856	18	87
2 - Type-L/LAC	5176	22	114
3 - Type-S/non-LAC	4556	18	82
4 - Type-S,I/LAC	5114	22	112

*these costs do not include electronics costs but do include return yoke steel.

Several comments can be made about the contents of Table 3-2:

1) the unit costs per Ton for liquid argon calorimetry are significantly higher, reflecting the cost of dewars and cryo-plumbing plus cryogenic supports and signal penetrations;

2) the total mass of the calorimeter in each case is roughly constant although the barrel/end weight ratio varies strongly;

3) there is no significant difference in this cost estimating method between Type-S and Type-I;

4) Type-L calorimetry systematically costs more in this cost estimating method than Type-S or I.

These conclusions are based on only the crudest cost estimating basis. In the near future, better bottom-up estimates will become available, but the basic comparative offsets of Table 3-2 are likely to persist.

In order to make a more detailed comparison between the costs of calorimetry for Type-S and Type-I coils, a bottom-up estimate was made by T. Kirk[3-1] for the models G and H shown in Figure 1-1. These models had as their goal to explore the details of cost differences between the S and I magnetic configurations while holding calorimetry performance constant (to the extent allowed by the intrinsic differences). A scintillator plate/fibre model was chosen as the basis for this exercise.

The results of the cost estimating exercise for Model G (Type-I) and Model H (Type-S coil) are displayed in Table 3-3.

Likewise, the muon tracker geometry and layout are independent of the Type-S/Type-I choice. Again, the direct differential costs do not differ for the muon tracking subsystem.

The trigger system may need to be increased in complexity if the Type-S coil is chosen. This result is related to the more complex magnetic field (hence charged particle bending) circumstances. The full impact of the Type-S field on the trigger is not yet clear, but it should be noted that both the tracking and muon triggering systems must already cope with particles exiting the magnet before reaching the outer radius (hence experiencing a variable transverse momentum magnet kick). In addition, the intermediate angle muons pass through the iron flux-return yoke which subjects them to a complex field path integral.

References

[3-1] T. Kirk, "Scintillator Plate Calorimeter Costs", Version: September 18, 1990.

APPENDIX A

SDC Magnet Task Force Members

G. W. Foster	- Fermilab
R. Hollebeek	- University of Pennsylvania
R. Kephart	- Fermilab
T. Kirk*	- Argonne National Laboratory
T. Kondo	- KEK, National Laboratory for High Energy Physics
S. Mori	- University of Tsukuba
H. Ogren	- Indiana University
J. Proudfoot	- Argonne National Laboratory
Y. Sakai	- KEK, National Laboratory for High Energy Physics
A. Yamamoto	- KEK, National Laboratory for High Energy Physics

*Chairman

APPENDIX B

CHARGE TO THE SDC SOLENOID MAGNET TASK FORCE

The solenoid magnet for the SDC detector design has been envisioned in one of two basic forms:

a) "short" coil with a non-magnetic field termination or with iron plate calorimetry to partially guide the magnetic field;

b) "long" coil with full iron flux termination at the end of the coil.

The first coil geometry can provide partial magnetic termination if the endcap calorimeter is iron loaded. If the calorimetry is not ferromagnetic, the flux is allowed to spread out at the end of the coil and return through a suitable iron flux return path placed outside the calorimetry. In the second coil geometry, the field is fully terminated in iron, but the coil penetrates the calorimetry, giving rise to the need for an end plug calorimeter inside the coil.

The purpose of the task force is:

1) to assemble appropriate data to allow critical technical and cost comparisons to be made among the two general coil designs;

2) to evaluate and organize these data in such a manner that a rational magnet design choice can be made for the SDC detector.

The goal is that a final magnet choice for SDC can be made with full confidence that all significant decision factors have been properly taken into account. Among the most significant factors to be considered are the design constraints that each magnet coil geometry places upon the calorimetry and the central tracking system, as well as the specific technical feasibility of each of the two coil designs.

The size and character of the solenoid magnet has very significant interactions with all the technical subsystems of the detector (tracking, calorimetry, muon system, triggering, etc.). The physics measurement capability of the whole detector as well as its cost are also determined to a significant extent by the detailed magnet parameters. Overall safety and reliability of the magnet design is a relevant characteristic for the Task Force's evaluation.

APPENDIX C

TECHNICAL COMPARISON OF THREE DESIGN OPTIONS FOR THE SDC SOLENOID

August 13, 1990

Akira Yamamoto (KEK)

This note describes comparisons of three solenoidal coil design options: Type-L (Long); I (Intermediate); and S (Short). All have a common design basis as discussed during the last SDC magnet subcommittee meeting at Snowmass (July 1990). The subgroup agreed that the parameters and dimensions in the following tables are for inter-comparison of models and not necessarily to be considered fixed in the final design.

The design basis and boundary conditions for the solenoid design are summarized in Table 1. This table is based on the following consensus achieved during the last meeting of the Magnet Subcommittee:

- use of Aℓ-based superconductor with:
  RRR(pure-Aℓ) = 750
  Max. allowable hoop stress = 4.5 kgf/mm^2 (6,400 psi)
  Max. allowable stress intensity = 6 kgf/mm^2 (8530 psi)
  (within elastic limit)

- nominal operating conditions consisting of:
  B_0 = 2.0 Tesla
  I = 8,000 A (50% Ic on the load line)

- quench characteristics estimated using conductor material only, no quench back and:
  V-max across terminals after quench = 500 V
  T-max after quench = 100 K

- the following design basis for the vacuum vessels:
  Minimum collapse pressure in outer wall = 2 atm.
  Minimum collapse pressure in inner wall = (0.05 atm)

Results of the calculations satisfying these boundary conditions and this design basis are given in Table 2. In order to compare the designs appropriately with one another in terms of mechanical safety, the allowed maximum combined stress vector sum has been kept below 4.5 kgf/mm^2 in each design. The shear strength between the coil and the outer support cylinder is kept below the various experimental results which show successful performance up to 1.5 kgf/mm^2.

Table 1
Boundary Conditions of the Coil Design for
Three Solenoid Design Options of the Type L, I and S

Items		Type-L	Type-I	Type-S
Boundary conditions:				
Inner radius of cryostat	:mm	1,850	1,850	1,850
Outer radius of cryostat	:mm	2,200	2,200	2,200
Total length of cryostat	:mm	15,000	9,000	9,000
Mean coil radius	:mm	1,970	1,970	1,970
Total length of coil	:mm	14,600	8,600	8,600
Central magnetic field	:Tesla	2	2	2
Nominal operating current	:A	8,000	8,000	8,000
RRR of Aℓ stabilizer		750	750	750
Iop/Ic on load-line	:%	50	50	50
Max. hoop stress	:kgf/mm2	4.5	4.5	4.5
Max. stress intensity	:kgf/mm2	6	6	6
Max. shear str. at epoxy		0.5	0.5	0.5
T-max after quench	:K	< 100	< 100	< 100
V-max after quench	:V	< 500	< 500	< 500

APPENDIX D

RAY TRACING STUDY FOR MAGNET STYLE SELECTION

T. Kondo
KEK, National Laboratory for High Energy Physics
and
Makoto Asai
Hiroshima Institute of Technology

September 7, 1990

1. Introduction

In order to evaluate the calorimeter performance, it is best to simulate EM and hadronic showers and eventually relate the simulation results to the physics goals. However, these simulations require fair amount of computing time. A much simpler method, ray-tracing, was introduced by M. Strovink et al.[1] This method is extremely useful to pin-point cracks, dead material as well as calorimeter depth, all of which are intimately related to the calorimeter performance. One of us (Asai) has developed a program of ray-tracing in the framework of widely-used GEANT. Once one enters input parameters for any kind of detector geometries according to the GEANT, the program calculates integral and differential radiation length as well as absorption length on a straight line specified by eta and phi. We have used this program to ray-trace four possible calorimeter configurations in order to evaluate the magnet style dependence on calorimetry.

2. Calorimeter Configurations

In the present study, four different cases are considered depending on calorimeter types and magnet styles:

Solenoid style	Calorimeter Type	
Case-1	long	non-LA
Case-2	long	LA
Case-3	short	non-LA
Case-4	short	LA

where LA stands for liquid argon calorimeter and non-LA includes rest of calorimeter types, warm-liquid, scintillating plate and scintillating fiber calorimeters. This is because it is known from on-going design studies on liquid argon calorimeter that non-negligible amount of space and material is required in front of active calorimeter region for cryostat. It is not clear

	Case-1	Case-2	Case-3	Case-4
Barrel Calorimeter	4194 t	4902 t	2742 t	2914 t
End Calorimeter	2 x 374 t	2 x 137 t	2 x 907 t	2 x 1100 t
Total Weight	4856 t	5176 t	4556	5114 t

It is noted that, in spite of the stretched shape of the calorimeter for a long solenoid, the total weights of the calorimeter are surprisingly close to those of a short coil. The difference is at most 300 tons. Other features that manifest significant differences between two styles are as follows:

	Short Solenoid	Long Solenoid
1. Carrel Calorimeter	9 m long	17 m long
2. Endcap/Plug Calorimeter	~ 8 m high	small and compact
3. Barrel Muon System	~ 8.5 m long	~ 10 m long
4. Movement for Access	1 ~ 2 m	5 m
5. Inner Tracker Support	short and radial	long & cylindrical
6. Cabling	radial at z =4.5 m	axial along the coil
7. Magnetic Field (barrel)	0 or < 1T	0
8. Magnetic Field (endcap/plug)	2T or < 1T	2T

These differences arise from the calorimeter geometries and the geometry of the magnetic flux return. Although it is difficult to make any "definitive" preference from the list shown above, especially since details depend on calorimeter technology, one can say that the short coil is favored in items 1, 3, 4, 5 and 6, while the long type has advantages in items 2 and 7. Therefore in general, the short type is favored as far as calorimeter geometry is concerned.

4. Ray-tracing Results

By inserting all the relevant input parameters into GEANT, we get GEANT pictures as shown in Fig. 5 for Case-3. The inner tracking part is based on silicon-wire EoI configuration. Intermediate angle trackers are assumed to consist of 6 straw superlayers. One of the immediate results from the present ray tracing program is the radiation thickness of the inner tracking system as shown in Fig. 6. Note that tracker support structure is yet to be included in this calculation.

Figures 7-10 are the plots of the radiation thickness as a function of pseudorapidity. The plots indicate accumulated radiation lengths from the interaction point. It is better to have less radiation thickness in front of the active EM calorimeter for better energy resolution and for better electron identification. Qualitatively, however, it is known that there is no significant degradation of energy resolution even with a few radiation lengths in front of the EM calorimeter. With special massless gaps, it is possible to apply a correction to recover energy lost in the front materials up to about 5 X_0 with moderate energy resolution[2]. As a measure of evaluation, we take a rapidity interval in which the thickness of front material exceeds 3 X_0 (gray EM area) and 5 X_0 (bad EM area).

calorimeter shape. Although it is difficult to make any "definitive" preference from these differences, the short magnet appears to count more favored points as far as the calorimeter geometry is concerned.

We have displayed the results on GEANT ray-tracing for all four cases as a function of rapidity. Among others, the radiation thickness of materials in front of EM calorimeter, as well as the non-active hadronic part up to 5 interaction lengths, are taken as measures for evaluating each calorimeter's performance. For both cases (liquid argon and non-liquid argon), short magnets are preferred by these measures.

[1] M. Strovink, W. J. Womersley, and G. E. Forden, Invited talk at the Workshop on Calorimetry for the Super Collider, University of Alabama, SSC-SDC-14, 1989.

[2] H. Hirayama, Proceedings of the International Workshop on Solenoidal Detectors for the SSC, KEK, April 23-25,1990, pp. 360-365.

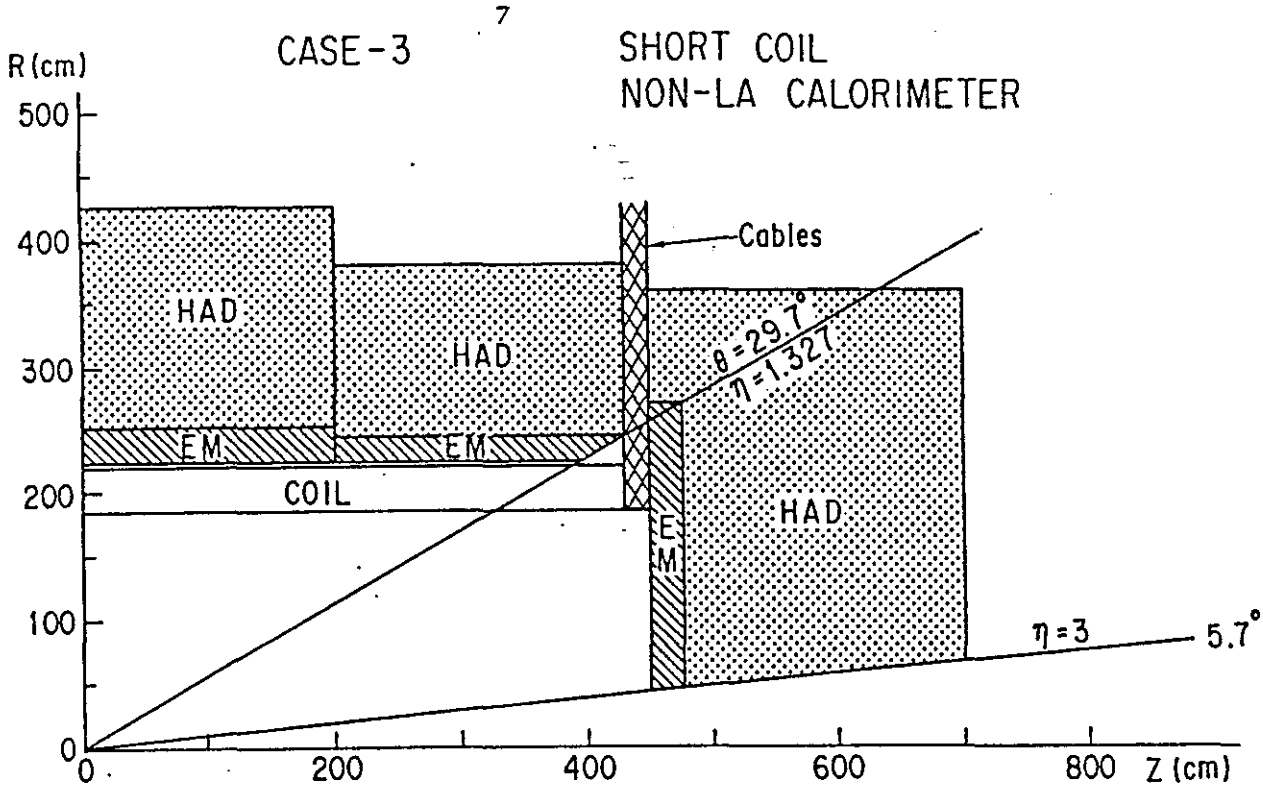

Fig. 3 Configuration of case-3 : short coil and non-liquid argon calorimeter.

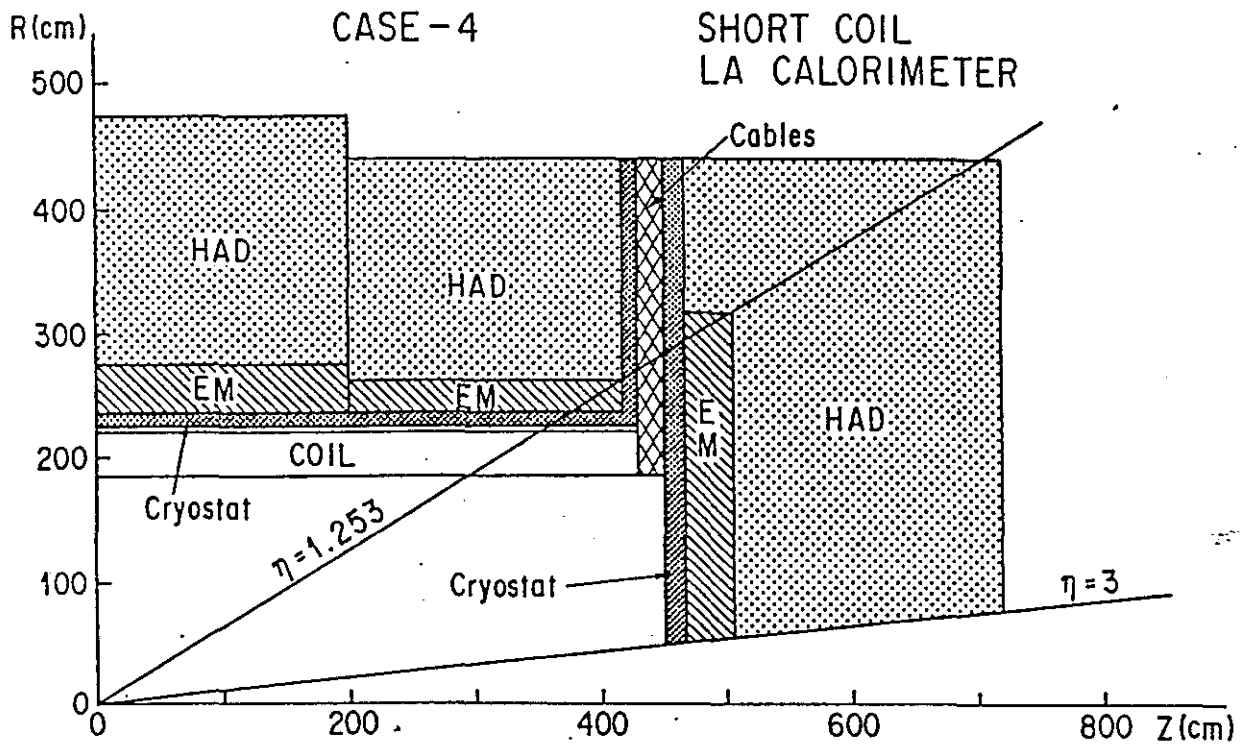

Fig. 4 Configuration of case-4 : short coil and liquid argon calorimeter.

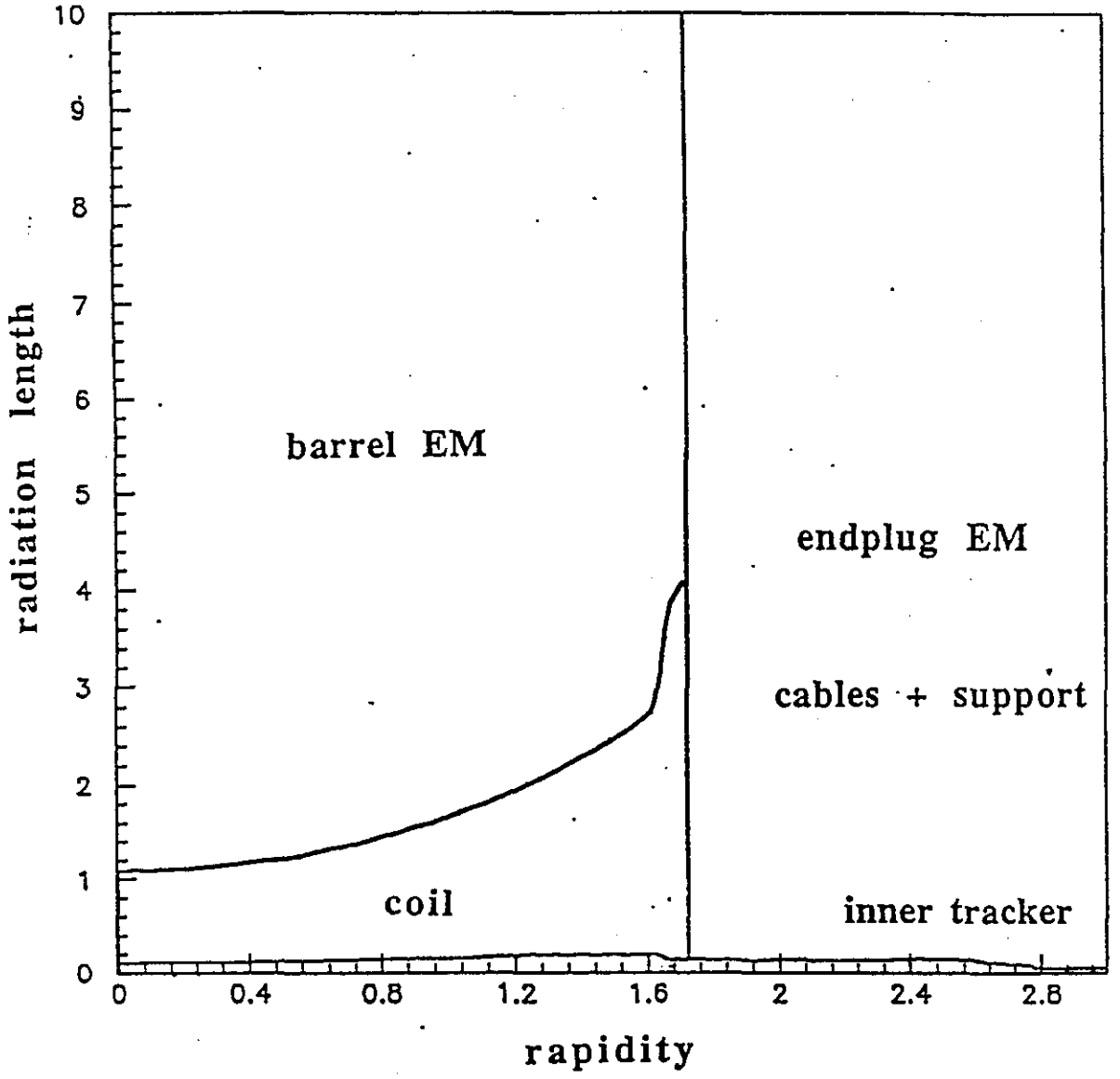

Fig.7 Rapidity dependence of radiation length for case-1 (long coil + non-liquid argon).

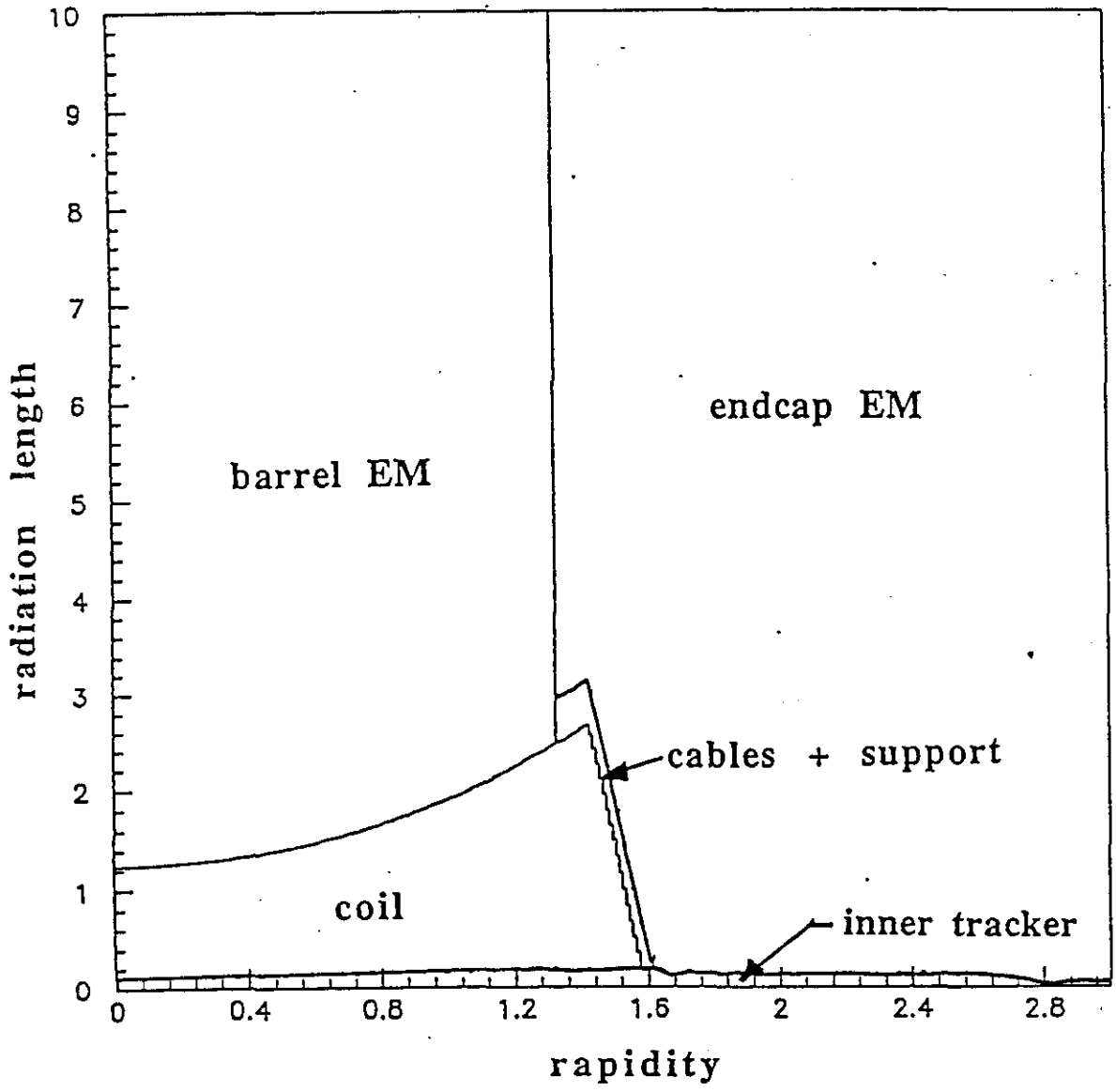

Fig.9 Rapidity dependence of radiation length for case-3 (short coil + non-liquid argon).

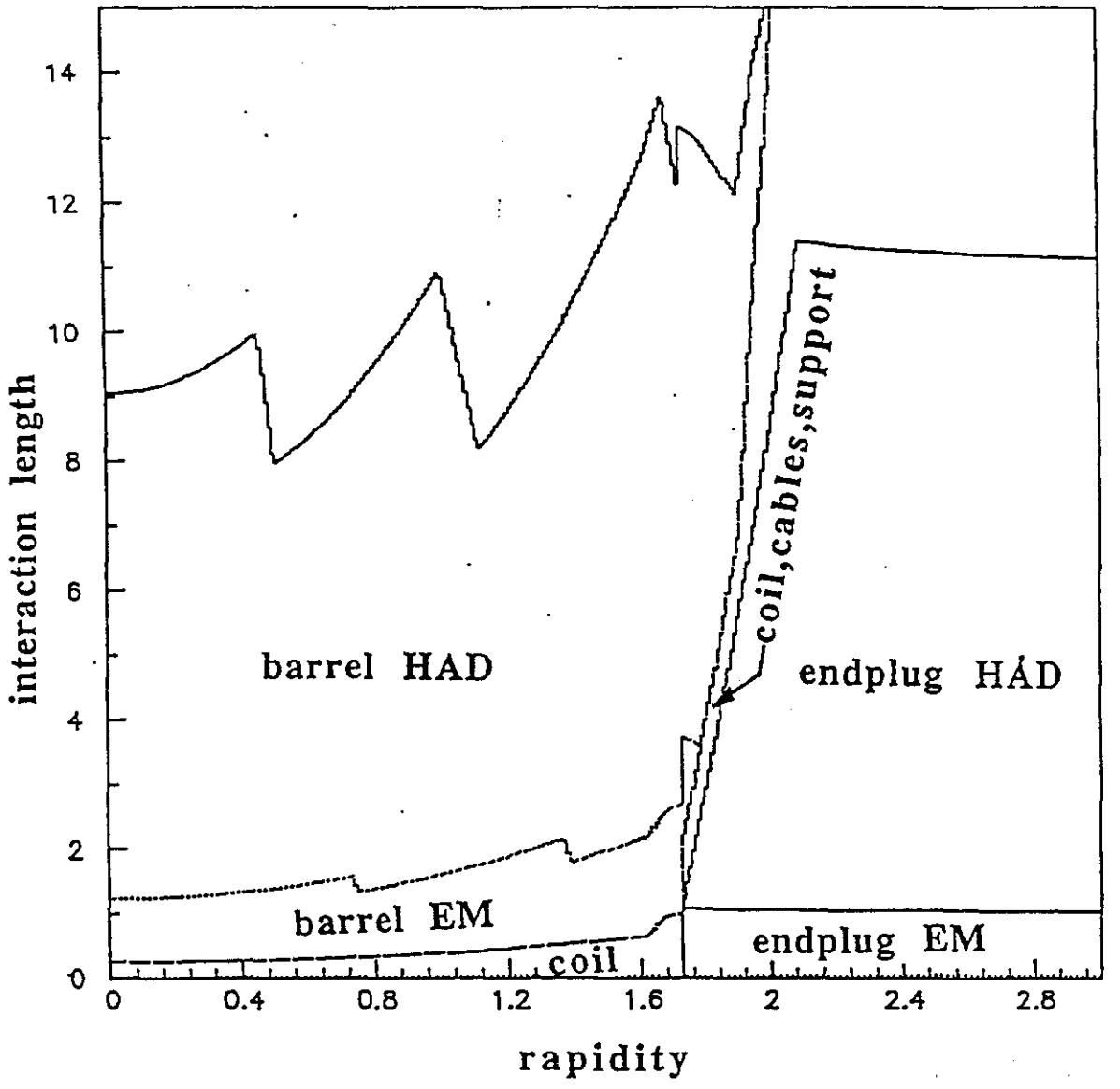

Fig.11 Rapidity dependence of interaction length for case-1 (long coil + non-liquid argon).

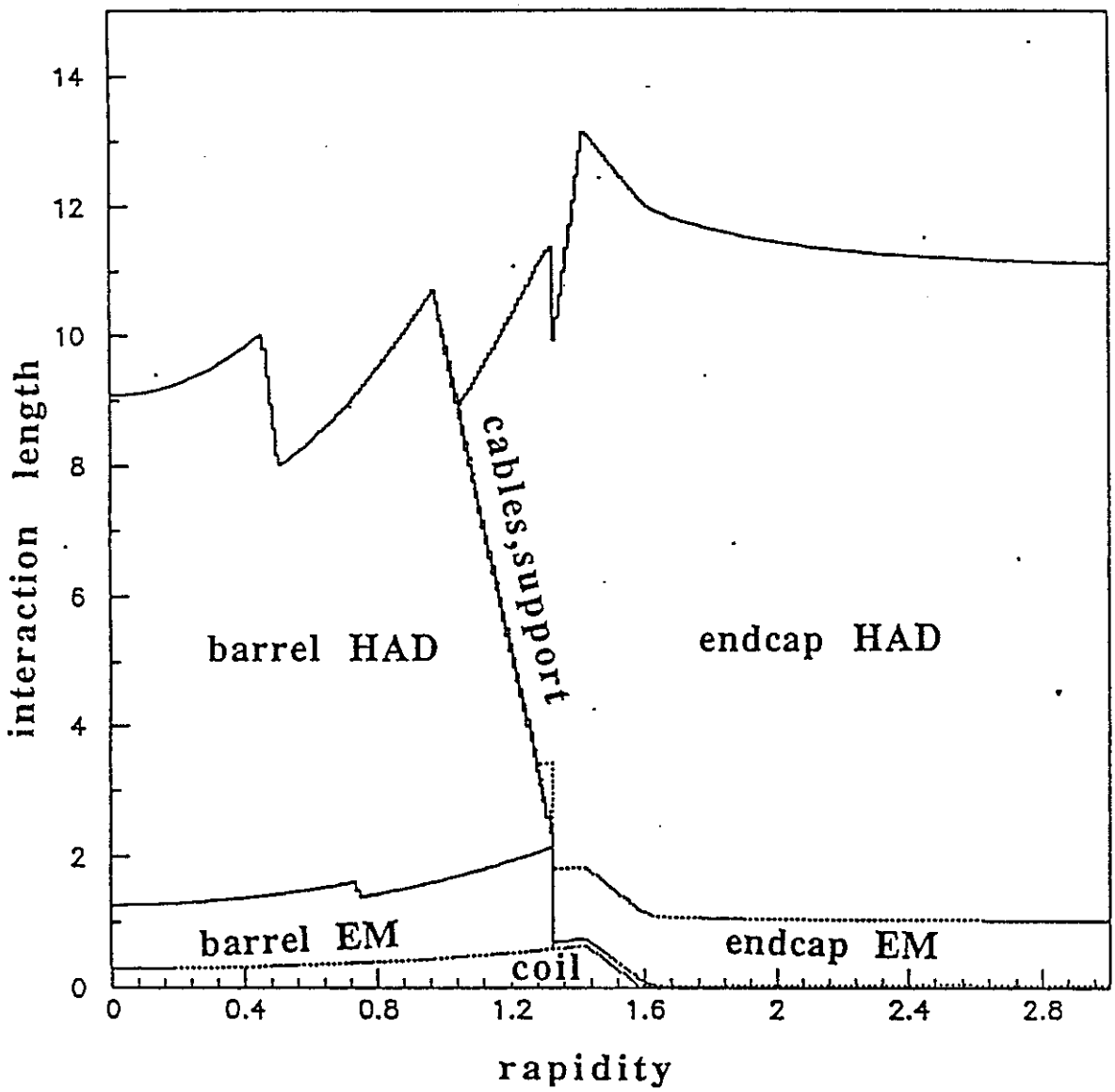

Fig.13 Rapidity dependence of interaction length for case-3 (short coil + non-liquid argon).

JSD-NOTE-1990-47
SDC-90-00074

APPENDIX E

MOMENTUM RESOLUTION FOR MUONS USING THE FULL TRACKING SYSTEM OF SDC†

Shigeru Odaka

KEK, National Laboratory for High Energy Physics
1-1 Oho, Tsukuba-shi, Ibaraki-ken, 305 Japan

Abstract

The momentum resolution of the SDC detector for high momentum muons was estimated assuming that the full tracking system is available for track fitting. The result of G. Feldman shown at Snowmass '90 was independently reproduced, and a comparison was done between the Type-S and the Type-L magnet configurations presented in the EoI. The non-uniform field and the return field in the calorimeter area of the Type-S magnet do *not* significantly degrade the momentum resolution.

†Talk given at the 1st JSD Workshop, KEK, August 8-9, 1990.

The parameters of the inner trackers are chosen so as to give a momentum resolution of $\sigma_p/p = 0.2\ p_T(\mathrm{TeV}/c)$. We follow this setup in this section.

2-2 Methodology

The χ^2 of a hypothetical function $f(x;\vec{\alpha})$ against independent measurements y_i at the points $x_i (i = 1, 2, \ldots, n)$ is defined as

$$\chi^2 = \sum_{i-1}^{n} \frac{1}{\sigma_i^2}\left[f(x_i;\vec{a}) - y_i\right]^2 \quad , \tag{1}$$

where σ_i is the estimated measurement error, and $\vec{\alpha}$ symbolically denotes a set of parameters $\alpha_\mu (\mu = 1, 2, \ldots, m)$ characterizing the function. When the parameter set $\vec{\alpha}$ is unknown, their optimum values can be estimated from the measurements by searching the parameter set that minimizes χ^2, and the errors of the optimized values of the parameters can be estimated from the second derivatives of the χ^2. Defining the matrix G as

$$G_{\mu\nu} = \frac{1}{2}\frac{\partial^2\chi^2}{\partial\alpha_\mu\partial\alpha_\nu} \quad , \tag{2}$$

the error matrix $E_{\mu\nu}$ of the parameter $\vec{a}$ can be obtained by inverting the matrix G; i.e., $E = G^{-1}$. The diagonal component of E is defined as the square of the error of the corresponding parameter, $\sigma(\alpha_\mu)^2 = E_{\mu\mu}$, and the error $\sigma(\alpha_\mu)$ is usually a good approximation of the resolution of α_μ.

Further, by using expression (1), the second derivative in eq. (2) can be written as

$$\frac{1}{2}\frac{\partial^2\chi^2}{\partial\alpha_\mu\partial\alpha_\nu} \cong \sum_i \frac{1}{\sigma_i^2}\frac{\partial f\ (x_i;\vec{\alpha})}{\partial\alpha_\mu}\frac{\partial f(x_i;\vec{\alpha})}{\partial\alpha_\nu} \tag{3}$$

if $\partial^2 f/\partial\alpha_\mu\partial\alpha_\nu \cong 0$. This is a good approximation unless the function is quite exotic, and the equality is exact when the function is linear. Therefore, if the derivatives $\partial f/\partial\alpha_\mu$ are given at each measured point, the matrix G can be calculated by eq. (3). Though this is a good method for some simple cases, the calculation may become very complicated when we have to treat a large number of parameters or a complicated setup.

The most easy-going and flexible way to calculate a derivative in computer programs is the finite-difference method; taking a finite difference $\Delta\alpha$, a derivative is approximated as $df(a)/da = [f(\alpha+\Delta\alpha) - f(\alpha]/\Delta\alpha$. The matrix G is evaluated with this technique in the subroutine HESSE of the widely-used optimization program MINUIT[4]. We borrow the algorithm of HESSE in the following estimations.

where ϕ is the deviation in x-y projection from the straight line drawn approximately along the track direction at the production point, and $\alpha = 0.3$ (GeV/c)/(T•m). The trajectory in the iron toroid is also approximated with similar functions but the deflection is along the z-axis.

In addition to the above five parameters, we treat the parameters z_1 and z_2 of the multiple scattering as track parameters. Since we have to consider two directions for each material an we have two thick materials, the number of parameters becomes $5 + (2\times2\times2) = 13$ in total.

The parameters p and α_0 are given as inputs in our calculation. At the first step, the ideal hit point are left at all measured points according to eq. (6) and other functions for free spaces and for the iron toroid, where we set $d_0 = \phi_0 = z_0 = 0$. Then the 13×13 matrix G given by eq. (2) is calculated by means of the finite difference method. The matrix G is inverted by using the utilities in the FACOM's scientific subroutine library SSL II, to obtain the error matrix E. And then we take $\sigma(1/p)/(1/p)$ to be the estimated momentum resolution σ_p/p.

2-5 Results

The resultant momentum resolution is shown in Fig. 2 as a function of the transverse momentum p_T. We obtain the resolution of ~ 12% for p_T = 1 TeV/c and ~ 30% for 5 TeV/c. These are in good agreement with the results shown by G. Feldman (Fig. 1). The resolutions when the inner and the outer trackers are separately used are shown for references.

The dotted line in the figure shows the resolution when the multiple scattering is ignored. We can see a reasonable behavior of the full resolution; it is almost identical to the inner only resolution up to a few 100 GeV/c and gradually approaches the full (no MS) resolution as p_T increases.

3. Effects of the Non-uniform Field of Type-S Magnet

3-1 Method of Estimation

The magnetic field of the Type-S magnet is illustrated in Fig. 3, which was calculated by S. Terada according to the geometry shown in the EoI. A non-uniformity of the field is apparent. For such non-uniform magnetic field, the approximated trajectory of high momentum particles, eq. (6), is modified to be

$$\delta = d_0 + \phi_0 r + \frac{\alpha}{p_T} I_B(r) \quad , \tag{7}$$

where

$$I_B(r) = \int_0^r dr' \int_0^{r'} \left[B_z(r'',z) - B_r(r'', z)\cot\theta\right]dr'' \tag{8}$$

the SDC detector can be used for track fitting and the spatial resolution of 250 μm can be achieved in the outer trackers.

We examined the possible degradation of the resolution due to the non-uniform magnetic field of the Type-S magnet configuration comparing with the Type-L configuration. In consequence, the degradation is not significant: practically negligible ($\lesssim$ 10%) in the central rapidity region $|\eta| < 1.0$, and at most ~ 30% even at $|\eta| \sim 1.5$.

References

[1] G. Feldman, talk at Snowmass '90.
[2] H. Iwasaki, talk at Snowmass '90.
[3] Y. Takaiwa, talk at Snowmass '90.
[4] F. James and M. Roos, Comput. Phys. Commun. 10 (1975) 343.
[5] See p. 65 of: Review of Particle Properties, Phys. Lett. 204B (1988) 1.

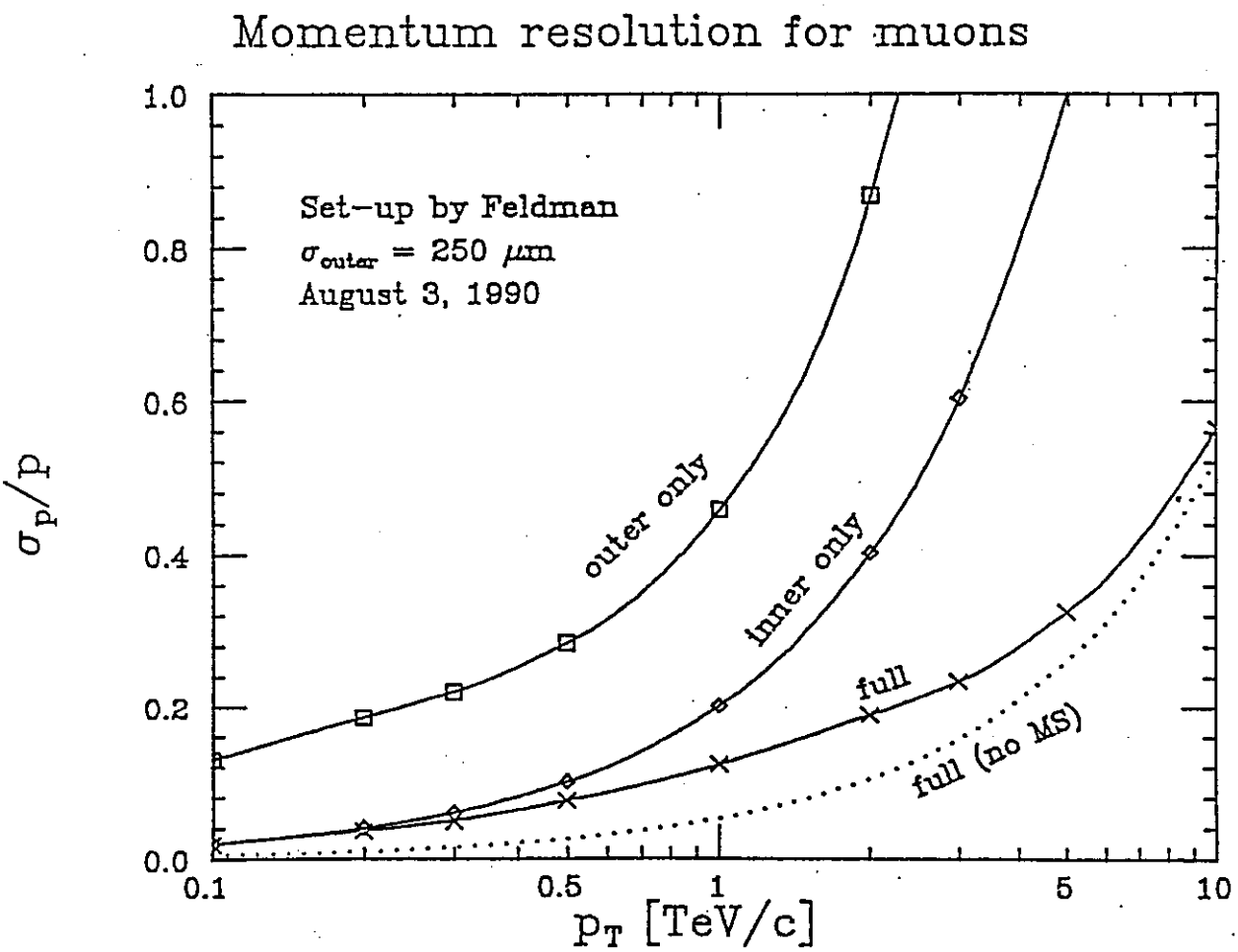

Fig. 2 Our estimation of the momentum resolution for high momentum muons. The detector setup is the same that G. Feldman used to derive the results shown in Fig. 1 (see the text).

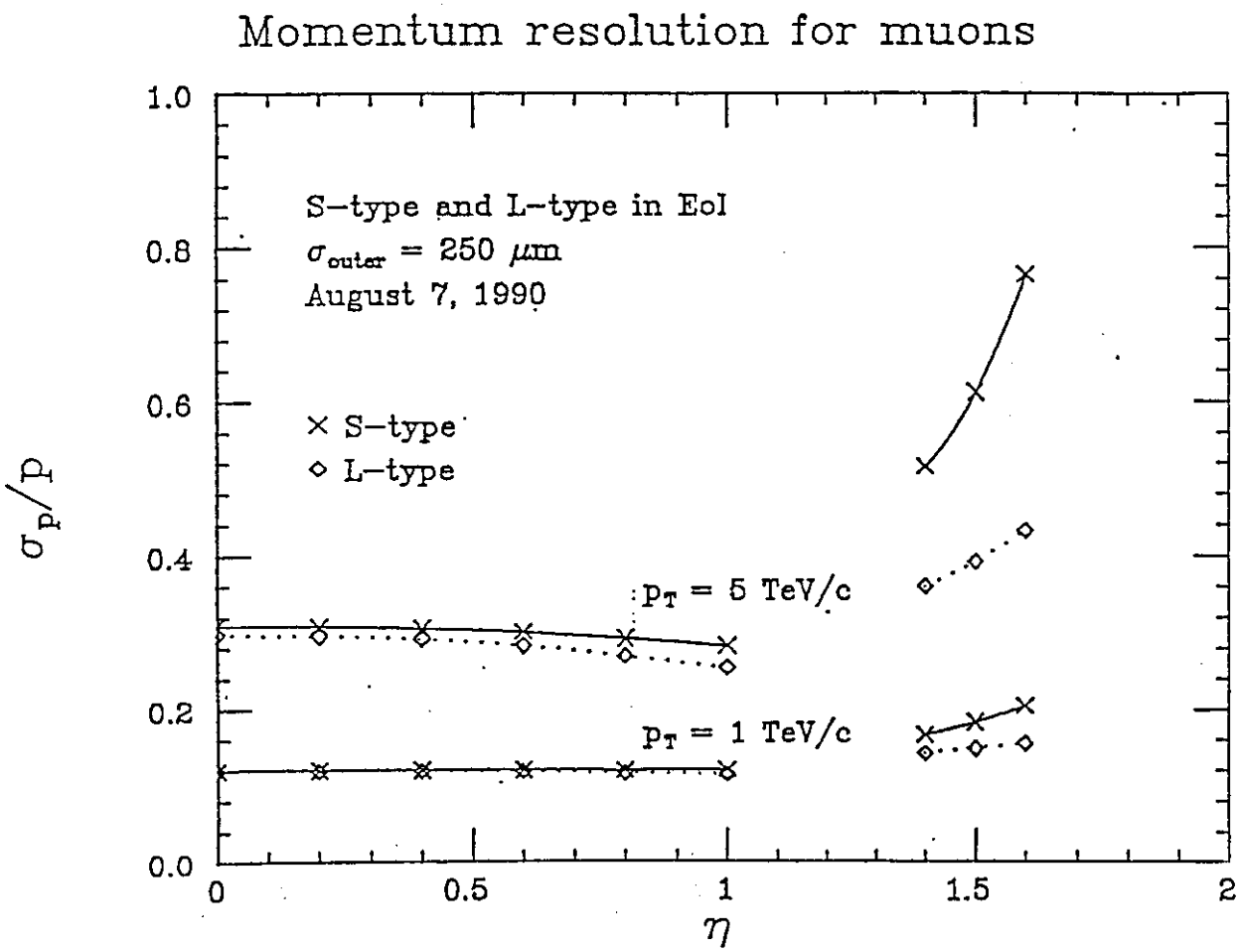

Fig. 4 The results of our estimation. The momentum resolution is shown for p_T = 1 and 5 TeV/c, and Type-S and Type-L, as a function of rapidity.